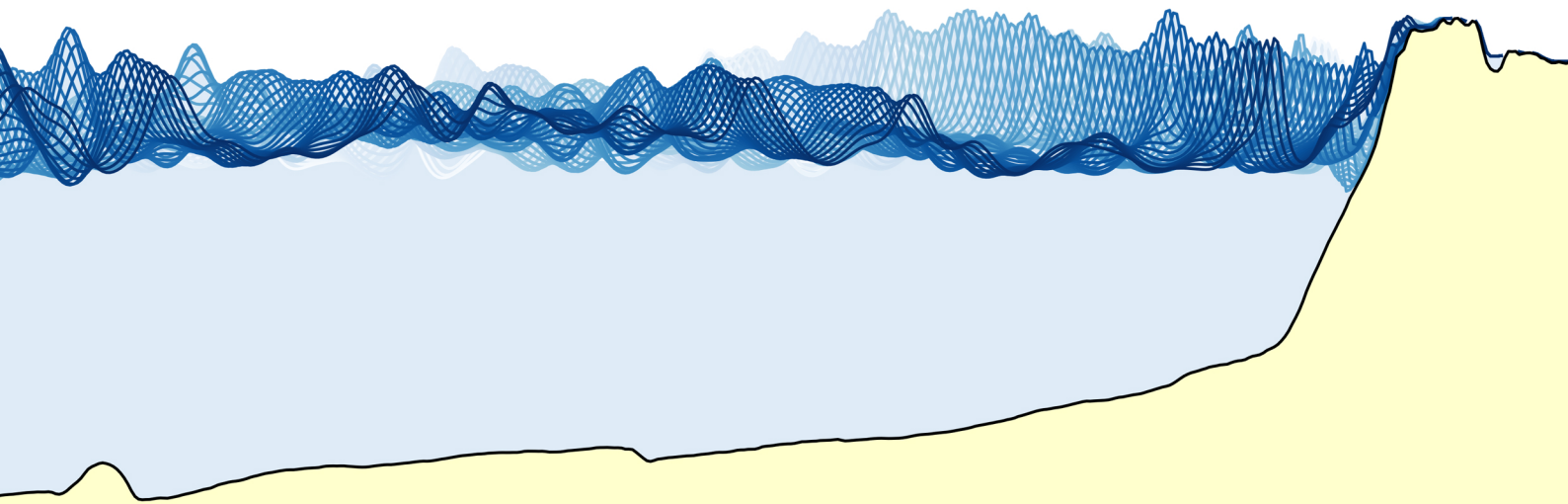


Comparing flood susceptibility estimation methodologies

A case study of Eastbourne

Ian Mullens

July 2021



DELFT UNIVERSITY OF TECHNOLOGY
&
IMPERIAL COLLEGE LONDON

Final MSc Thesis:
**Comparing flood susceptibility estimation
methodologies**

Author: Ing. Ian Mullens
Date: Monday 5th July, 2021
Course: Civil engineering double track:
Hydraulic Engineering & Watermanagement
Cover: A snapshot of a SWASH overtopping estimation simulation,
in which the water elevation darkens as time progresses.

Graduation committee:

Prof.dr.ir. A.J.H.M. Reniers	Delft University of Technology
Dr.ir. R.J. Labeur	Delft University of Technology
Dr. Markus Hrachowitz	Delft University of Technology
Dr. Ioannis Karpadakis	Imperial College London
Dr. Athanasios Paschalis	Imperial College London

An electronic version of this research is available at
<http://repository.tudelft.nl/>.

The scripts made by the author for the application of the various methodologies are available at
<https://github.com/IansGithubAcc/Thesis/>



Preface

This MSc thesis completes a three-year long civil engineering double track degree in hydraulic engineering and watermanagement at Delft University of Technology. This research has been executed as a collaboration between Delft University of Technology and Imperial College London.

First of all, I would like to thank both Imperial College London and Delft University of Technology for allowing a MSc thesis with supervision from two universities. It was a great experience which I will never regret.

I would like to give special thanks to my main supervisors Ioannis and Ad. Thank you Ioannis, for listening to me when I barged into your office unannounced and enquired about thesis opportunities, and for all the support you have given me since. Thank you Ad, for all your advice and your positive and sober attitude.

I would like to thank the members of my graduation commission for their interest, their support, and there time. Thank you Athanosios, for your guidance regarding the inundation modelling. Thank you Robert-Jan, for being critical but fair. And thank you Markus, for your great attitude and the insightful questions. I am grateful for such a well-rounded graduation commission.

I would like to thank my family, for always encouraging education, even after 9 years of it. I would like to thank my girlfriend, for listening to my many pointless questions regarding sentence structure, and the less pointless questions regarding mathematics. And lastly, I would like to thank my friends at Delft and at London, for the amazing time I had during my MSc. Working and relaxing together as students made the years fly by.

Ian Mullens
Delft, July 2021

Summary

Recent studies have shown that flood risk contributes to a major part of the total risk caused by natural hazards in Western Europe. Especially in the United Kingdom, flood risk has been identified as a substantial threat, which is likely to continue to grow due to (coastal) urbanisation, sea level rise and climate change. A separate study has shown that common analysis practice may underestimate flood risk due to the exclusion of compound flood events. These are flood events with multiple flood causes, such as a combined coastal and pluvial flood event.

Floods are often caused by a complex system of multiple dependent flood driving mechanisms, which vary and interact as time progresses. Various fundamentally different methodologies have been developed to estimate the susceptibility of an area to floods. There is no singular best methodology which can be applied to every problem. Due to the complex nature of flood events, it is vital to understand these methodologies and their characteristics to represent the susceptibility to flooding correctly. Misrepresentation of flood susceptibility can lead to inefficient decision making, or worse, insufficient flood safety.

The goal of this research is to compare several flood susceptibility estimation methodologies (including coastal, pluvial, and compound flooding), to observe the results and clarify notable differences in outcomes. A case study is conducted on the coastal town of Eastbourne, which has various common, but non-trivial characteristics. The flood susceptibility of Eastbourne is estimated using various estimation techniques, such as statistical analysis and numerical modelling. Not only did this give insight into the flood susceptibility of Eastbourne, but it also illustrated the capabilities of the selected methodologies.

Eastbourne has a history of coastal and pluvial/fluvial flooding. In order to include the physical mechanisms of these flood types, it was decided to use relatively computationally expensive flood susceptibility estimation methodologies. Hence, use was made of sensibly chosen storm scenarios, based on extreme value analysis.

The statistical analysis started with a general exploratory data analysis in order to find notable dependence structures between variables. Afterwards, two variants of extreme value analysis on reanalysed historical data were used to create "smart" scenarios. First of all, the peak over threshold approach (POT) was used to create scenarios in which a singular flood type was dominating. Secondly, the conditional approach was applied to create compound storm scenarios. In total, 8 different scenarios were created. These scenarios gave the input conditions for the models.

At the coastal boundary, a spectral action balance resolving wave model (SWAN) was used to estimate close shore conditions based on offshore scenario input. These nearshore conditions were then used to estimate overtopping rates into the inundation domain via three different overtopping methodologies. First of all, an empirical equation (the "new" overtopping formula of the EuroTop manual) has been applied. Secondly, a Gaussian process emulator (Bayonet GPE), an approach similar to a neural network, has been applied. And lastly, use was made of a numerical hydrodynamic model (SWASH) to simulate wave transformation and overtopping. This last approach is especially interesting since numerical models have the ability to improve upon spectral action balance resolving wave models. Numerical models can implicitly account for infra gravity waves, a physical mechanism that is known to impact overtopping rates, something that spectral action balance resolving models struggle with.

The numerical hydrodynamic model HEC-RAS, is used for the simulation of inundation caused by the storm scenarios. All 8 scenarios are calculated twice, in order to compare simulations made with two sets of governing equations: The diffusive wave approximation of the shallow water equations (DSW) and the full shallow water equations (SWE), also known as the Saint Venant equations. The DSW approach has the advantage of being relatively computationally efficient, whilst SWE approach has the benefit of including a more accurate representation of physics. Since the DSW approach is more computationally efficient, it allows for solving on a higher spatial resolution. The model was applied to the part of Eastbourne, which is deemed to have the highest flood risk. It was then fed with overtopping discharges at the coastal flood defences and used precipitation events as defined by the respective scenarios. After the simulation, flood maps have been generated to compare the inundation patterns. Inundation curves have been made as well, for a more objective and apprehensible comparison of the severity of the flood events.

The overtopping results showed that all three approaches agreed reasonably well, and were able to estimate plausible overtopping rates. There were no overtopping measurements for validation purposes, but the overtopping magnitude does agree with the coastal flood history of Eastbourne. The numerical method is more advanced than the empirical formula and the GPE. However, the results also showed a large sensitivity with regards to the (vertical) discretisation. Furthermore, the numerical approach, as applied in this research, did require explicit inclusion of refraction and fitting of breaking behaviour based on computationally expensive simulations, in order to give reasonable estimations. The numerical approach is promising and has the potential

to become more accurate than the other methods considered. However, in its current state the method does seem as uncertain as the other considered approaches, whilst being more complex to implement.

Lastly, regarding the comparison of governing equations for the estimation of inundation, it was found that the low spatial resolution SWE approach systematically underestimated inundation severity with regards to the high spatial resolution DSW approach. In addition to this, it was found that the times between the storm peaks and the inundation peaks was systematically lower for the SWE simulations than for the DSW simulations. Both these phenomena can be explained as a consequence of using a different spatial discretisation. When using the same spatial discretisation these effects disappear and the inundation curves agree well. There are, however, still some smaller local differences between simulations visible on the inundation maps. In the case of Eastbourne, modelled as described in this report, it is thus more important to accurately include topological features than to accurately represent the flow physics. This could, however, be different when considering higher spatial resolutions.

Contents

Preface	I
Summary	II
List of acronyms and symbols	VI
Definition of key terms	VIII
1 Introduction	1
1.1 Problem definition	1
1.2 Research goal	2
1.3 Research demarcation	2
1.4 Report structure	3
2 Methodology	4
2.1 General approach	4
2.2 Location	5
2.2.1 Case study selection	5
2.2.2 Case study characteristics	6
2.3 Statistical analysis	7
2.3.1 Data sources	7
2.3.2 "Smart" scenario methodology	8
2.3.3 Data analysis	9
2.4 Nearshore wave model (SWAN)	12
2.5 Overtopping estimation techniques	15
2.5.1 General overtopping estimation approach	15
2.5.2 Empirical overtopping equation (EurOtop)	16
2.5.3 Gaussian Process Emulator (Bayonet GPE)	18
2.5.4 Numerical modelling of the surfzone and beach (SWASH)	18
2.6 Inundation modelling	21
2.6.1 Numerical approach	21
2.6.2 The inundation domain	22
2.6.3 Overtopping boundaries	23
2.6.4 Precipitation boundary	24
2.6.5 River boundaries	25
2.6.6 Flood severity comparison	26
3 Results	27
3.1 Statistical analysis and model scenario selection	27
3.1.1 Exploratory data analysis	27
3.1.2 Scenario creation	30
3.2 Nearshore wave model (SWAN)	32
3.3 Overtopping results and comparison	34
3.3.1 Correcting the numerical approach for refraction and breaking	34
3.3.2 Overtopping estimations	36
3.4 Inundation modelling	37
3.4.1 Inundation severity estimation	38
3.4.2 Comparison of governing equations	39
4 Discussion	42
4.1 Evaluation of applied method	42
4.2 Clarification of results and comparison with previous studies	43
4.3 Potential implications	44

5	Conclusion	46
5.1	Representative storm scenario generation	46
5.2	Overtopping estimation comparison	46
5.3	Governing equations of inundation modelling	47
5.4	Recommendations	47
	References	49
A	Summarising current flood susceptibility assessment practice	54
A.1	General	54
A.2	Spatial scale	54
A.3	Accurate representation of the physical mechanisms	54
A.4	Compound effects	55
A.5	Discussion on current common practice methodologies	56
B	The conditional approach for multivariate extreme values	57
B.1	The peak over threshold approach (POT)	57
B.2	Conditional POT	57
B.3	Complete joint distribution sampling	58
B.4	Creating scenarios using the conditional approach	59
	B.4.1 Primary variables	59
	B.4.2 Secondary variables	60
C	Typical SWAN input file	61
D	Typical SWASH input file	63
E	Figures	64
E.1	Correlation matrix	64
E.2	Refraction coefficients	65
E.3	Surf zone cross sections	66
E.4	SWAN output: Shore normal cross sections	68
E.5	SWAN output: SWASH wave spectrum input	73
E.6	Maps of Eastbourne	74
E.7	Boundary summary plots	76
E.8	Inundation maps of Eastbourne	78

List of acronyms and symbols

Acronym	Description
ANN	Artificial Neural Network
CoCC	Committee on Climate Change (UK)
DNV	Det Norske Veritas group
DSW	Diffusive wave approach of the shallow water equations
ELM	The Eulerian-Lagrangian method used for solving the SWE
EM	The Eulerian method used for solving the SWE
ERA5	The fifth generation ECMWF atmospheric reanalysis of the global climate
GPD	Generalised Pareto distribution
GPE	Gaussian process emulator
HPC08	High performance computing cluster of hydraulic engineering at TUD
IDF	Intensity duration frequency
I#	Intermediate location number #
loc#	Location number #
MSC	Multivariate conditional Spearman's correlation coefficient
MSL	Mean sea level
M2	Principal lunar semi-diurnal tidal constituent
PDF	Probability density function
POT	Peak over threshold approach
R	A programming language for statistical computing
SWE	Shallow water equations
TUD	Delft University of Technology
UK	The United Kingdom of Great Britain and Northern Ireland
1DH	One dimensional in the horizontal direction
2DH	Two dimensional in both the horizontal x and y direction

Greek symbol	Description	Unit
α	Beach slope angle	[°]
α_{break}	The range of maximum steepness a parameter used by the BREAK command in SWASH	[-]
α_g	The grade (smoothness restriction) of the Oceanmesh2D mesh	[-]
β	Wave obliquity, (mean wave angle relative to the shoreline)	[°]
β_{break}	A reduced range of maximum steepness for active breaking cells used by the BREAK command in SWASH	[-]
γ	Overtopping formula influence factors	[-]
γ_{bi}	Breaker index, ratio of wave height over still water depth	[-]
$\gamma_{jonswap}$	JONSWAP peak enhancement factor	[-]
ζ	Elevation of water level with respect to the mean water level	[m]
θ	Wave direction	[rad] _N
θ_{peak}	Wave direction of the peak of the wave spectrum	[rad] _N
θ_{wind}	Mean wind direction	[rad] _N
$\xi_{m-1,0}$	Iribarren parameter (surf similarity parameter) defined using the $m-1,0$ spectral moment	[-]
σ_E	Wave spectral directional width a dimensionless variable ranging from 0 to $\sqrt{2}$ indicating whether waves come from a wide range of directions or from similar directions. A value of 0 indicates a unidirectional spectrum (all waves travel into the same direction), whereas a value of $\sqrt{2}$ indicates a uniform spectrum.	[-]
ω	Angular frequency ($\omega = 2\pi/T$)	[rad/s]

Roman symbol	Description	Unit
b	Conceptual width of a wave ray	[m]
c	Wave celerity	[m/s]
c_f	Dimensionless friction coefficient	[-]
c_g	Group wave celerity	[m/s]
c_θ	Turning rate of the waves	[rad/s]
D_r	Rainfall event duration	[h]
d	Water depth from bottom to mean water level	[m]
f	Wave frequency	[s ⁻¹]
g	Gravitational acceleration (9.81)	[m/s ²]
H	Wave height	[m]
H_{m0}	Significant wave height formulated using the $m0$ spectral moment	[m]
h	Height of the water coulomb, from bottom to elevation ($h = \zeta + d$)	[m]
I_r	Rainfall intensity	[mm/h]
K_{ref}	Dimensionless refraction coefficient	[-]
K_{sh}	Dimensionless shoaling coefficient	[-]
$L_{m-1,0}$	Mean wave length defined via $m - 1, 0$ spectral moment	[m]
n	Ratio between group celerity and higher phase celerity ($n = c_{group}/c$)	[-]
R	Number of triangles to resolve coastline features with when using the Ocean-Mesh2D package	[triangles]
R_c	Crest height (defined as the height difference between the SWL and the crest top)	[m]
RP	Return period	[y]
P	Probability	[-]
p	The non-hydrostatic pressure in water (normalised by the density)	[Pa m ³ /kg]
Q	Discharge	[m ³ /s]
q	Overtopping discharge per running meter	[l/s/m]
\mathbf{q}	Mass flux vector ($\mathbf{q} = \mathbf{u}h$)	[m/s]
S	Spectral energy density (the source term, representing all effects of generation, wave-wave interactions and dissipation per unit time per unit surface area)	[m ² /Hz/°]
T	Wave period, the amount of time between arrival of consecutive wave crests at a fixed location	[s]
$T_{m-1,0}$	Mean absolute wave period defined via $m - 1, 0$ spectral moment	[s]
t	Time	[s]
u	Flow velocity in x direction	[m/s]
u_{10}	Vector of average x and y wind velocities at 10m above ground	[m/s]
\mathbf{u}	Flow velocity vector ($\mathbf{u} = [u, v]$)	[m/s]
v	Flow velocity in y direction	[m/s]
x	Location in x direction of a Cartesian coordinate system	[m]
y	Location in y direction of a Cartesian coordinate system	[m]
z	Location in z direction of a Cartesian coordinate system	[m]

Definition of key terms

Term	Description
Compound flooding	A flood resulting from two or more physical flood driving mechanisms. Recently more attention is given to the concept of compound flooding due to the realisation that strong location varying dependencies between flood driving mechanisms can exist. This report researches for example the dependency between an extreme sea state and precipitation, which are flood driving mechanisms regarding coastal and pluvial flooding.
Flood driving mechanism	A flood driving mechanisms is a physical mechanisms that can lead to or affect the severity of a flood. For example intense precipitation can be a flood driving mechanisms resulting in pluvial flooding, or a large storm surge can be a flood driving mechanism resulting into coastal flooding.
Hydrodynamic model	A hydrodynamic model numerically describes the flow of water over space and time by resolving simplified versions of the incompressible Navier-Stokes equations. Examples of such models applied in this research are SWASH (The SWASH team, 2019) and HEC-RAS (US Army Corps of Engineers, 2021)
Iribarren number	Denoted by ξ , also known as the surf similarity parameter and breaker parameter, is a dimensionless parameter expressing the seabed steepness relative to the steepness of the breaking waves.
Precipitation intensity	Denoted by I_r , is the discharge of precipitation per unit with of area, often expressed in mm/h . An average value for the precipitation intensity per unit of time can be calculated by measuring the cumulative rainfall per unit of area over than unit of time. One can for instance measure the amount of rainfall fallen in an hour to calculate the hourly rainfall intensity.
Primary variable	"Primary variable" refers in this research to a variable used to define a storm scenario. In this research all scenarios are based on combinations of H_{m0} and I_r . These are the primary variables of this research.
Return period	Denoted by RP , also known as a recurrence interval, is the expected/average time between events.
Secondary variables	Secondary variables refer to variables which are not directly used for scenario definition. Variables such as the wave period and the wind direction are necessary for the simulations, but they are not required for scenario definition. Instead these variables are chosen based on their dependence structure with the primary variables.
Significant wave height	Denoted by H_s or if using the spectral definition H_{m0} . Historically the significant wave height is defined as the average height of the highest one-third of waves in a sea state ($H_{1/3}$). However, these days the formal spectral definition using the M0 moment is used more often. The significant wave height is a parameter directly linked to the potential energy of a sea state.
Spectral action balance resolving models	A numerical wave model solving the spectral action balance is fundamentally different from a hydrodynamic wave model. The spectral action balance equation describes the motion of wave energy over space and time and does not resolve individual waves. An example of a spectral action balance resolving model used in this research is SWAN (The SWAN team, 2020b).
Spectral analysis of ocean waves	These days, spectral analyses is often used instead of wave by wave analyses in order to describe sea states. The concept is the following: A time series of water elevation is Fourier transformed into a sum of sine waves. The amplitudes and frequencies of those sines can than be related to the potential energy of the waves in their respective frequency bands. This is most commonly expressed via a wave height variance spectrum (wave spectrum). Integration of this spectrum times the frequency to the power of n gives the n 'th moment. Moments are often used for spectral definition of parameters such as the significant wave height (H_{m0}) or the mean wave period ($T_{m-1,0}$). Further information regarding the representation of waves in oceanic waters can be found in Holthuijsen (2007) .

1 Introduction

1.1 Problem definition

A recent study by the European Commission Joint Research Centre (JRC) on multihazard assessment in Europe concluded that Western Europe is especially susceptible to coastal and river floods compared to other natural hazards (Forzieri et al., 2016). Similarly, the (United Kingdom) Committee on Climate Change (CoCC) conducted research on future challenges regarding coastal protection (Russell, 2018). They concluded that coastal areas are already facing relatively large threats from coastal flooding, which will most likely increase even further in the future. This increase in risk is mainly driven by climate change and the growth in coastal urbanisation.

Accurate estimation of an areas susceptibility to different types of floods, is an essential tool for effective risk management. Misrepresentation of flood susceptibility could result in the derivation of skewed conclusions, which in turn can lead to ineffective or even insufficient flood risk reduction measures. Three specific difficulties within the estimation of flood susceptibility are outlined here.

1. A phenomenon that has gained much attention in research recently is compound flooding. Compound floods are flood events with multiple co-occurring flood causes. An example of this is a flood event caused by both a high river discharge and a high storm surge. Various studies have shown that compound flooding can have a significant impact on the flood susceptibility (Couasnon et al., 2020) (Hendry et al., 2019) (Paprotny et al., 2018). These studies state that not accounting for compound storms in susceptibility analysis often leads to misrepresentation and underestimation of flood risk. Another recent study (Eilander et al., 2020) found that around 19.7% of the coastline of the world is "compound-dominated", meaning that compound flooding is the governing flood type. Hence, not including compound flooding in risk analyses may in many cases lead to underestimation of the flood susceptibility. Compound flooding is, however, not accounted for by many traditional methodologies. One reason for this exclusion is that flood drivers were often assumed to be independent in the past. Another reason is because capturing the complex physical interactions of different flood types requires computationally intensive hydrodynamic modelling techniques using relatively high spatial resolutions (Paprotny et al., 2018).
2. Overtopping is the concept of waves flowing or splashing over a flood defence structure. Overtopping can lead to severe inundation of the hinterland and can thus induce flooding. There are various fundamentally different methodologies for the estimation of overtopping discharges. Methodologies usually use a parametric representation of the nearby sea state and the geometry of the flood defence as input for their estimations. Overtopping is a known source of uncertainty in flood susceptibility analyses. Most methodologies admit to this, by stating a relatively high uncertainty in their original publications (van der Meer et al., 2018) (Pullen et al., 2018) (Suzuki et al., 2017). Overtopping discharge estimations are usually within a factor of 3 of the actual overtopping discharge, meaning this value may be up to 3 times higher or lower in reality. For the sake of simplicity it is often preferred to use a singular estimation methodology. However, the effect of choosing one method over the others on the results is often unclear for the person performing the susceptibility assessment.
3. A common methodology of representing inundation is by using a numerical hydrodynamic model. Such models are regarded as accurate tools, since they are based on the motion of viscous fluids describing Navier-Stokes equations, in contrast to, for example "bathtub method"-type models, which are known to overestimate inundation (Gallien et al., 2014). Integration of the full Navier-Stokes equations in a general manner is, however, one of the open Clay Mathematics Institute millennium problems*. For the foreseeable future, hydrodynamic modelling will need to make use of simplified versions of these equations. There are various versions with different gradations of simplification and accuracy available for hydrodynamic modelling. Generally, in hydrodynamic modelling, one has to make a trade off between accuracy and computational efficiency. There are, however, no set rules regarding the required accuracy of governing equations when modelling flood susceptibility. Specifically inundation modelling of urban areas requires relatively high spatial resolutions (Asselman, 2009), which is why using very accurate governing equations may not always be computationally feasible. Conversely, using too much simplification could lead to misrepresentation of the flood susceptibility.

Flood events in coastal urban areas are in many instances caused by a complex system of multiple dependent flood driving mechanisms, which vary and interact as time progresses. The term "flood driving mechanisms" refers to the physical mechanisms that affect the severity or probability of a flood event. Many different

*All 7 Clay Mathematics Institute millennium problems can be found at <https://www.claymath.org/millennium-problems>

methodologies and combinations of methodologies have been developed to estimate the flood susceptibility of coastal areas. However, no perfect flood susceptibility estimation method exists and some simplification will always be required. It is often unclear what effect choosing one methodology over the other will have on the end result. Even after doing the assessment it is often unclear whether the method accurately represents reality. Validation of flood estimation methodologies is difficult to execute since data regarding the severity of floods is hard to come by. Reliable inundation data is scarce because extreme meteorological events such as coastal storms or intense rainfall usually coincide with heavy clouds, which obscure the inundation pattern for satellites.

It is vital to understand the differences between various flood susceptibility estimation methodologies to choose the one that suits the problem at hand best. Furthermore, even after selecting the most suitable methodology, it is still vital to understand which processes are well captured by the used method and which are not. Knowing and understanding when a method is conservative and when not, is essential to correctly interpret the results.

1.2 Research goal

This report aims to compare several flood susceptibility estimation methodologies to each other within an coastal urban context, to observe the results and clarify possible differences in outcome. Three specific methodology concepts are considered. Firstly, the necessity of including compound flooding in flood susceptibility assessment is researched. Secondly, the differences between three different types of overtopping discharge estimation methodologies are investigated. Finally, the numerical representation of inundation estimations via hydrodynamic modelling is researched. This research goal is achieved by addressing the following questions:

Research question:

How do different modelling techniques influence the overall flood susceptibility estimation?

Sub-questions:

1. How to generate representative storm scenarios?
2. How do different overtopping estimation methodologies compare to each other?
3. What set of governing equations should be solved when using numerical inundation modelling for the estimation of flood susceptibility?

The approach used to answer these questions is by conducting a case study research on the British coastal town of Eastbourne. Why specifically Eastbourne has been chosen for the case study, is further addressed in section 2.2. The flood susceptibility of Eastbourne will be estimated based on various estimation techniques, such as statistical analyses and numerical modelling, which were found using literature research. The results of these methodologies will then be compared to each other. Note that the flood estimation methodologies are not compared to measured data, since such data is not available. Not only will this approach give insight into the flood susceptibility of Eastbourne regarding different flood types, but it also serves as a case study to compare the different methodologies in practice.

1.3 Research demarcation

First of all, comparing all different methodologies developed to estimate flood susceptibility would be an enormous task. A task too large for a single MSc thesis. Hence, only several specific methodologies are actually included and compared in this research (see figure 2 in section 2.1).

Secondly, it is important to note that this paper discerns between flood risk and flood susceptibility. Flood risk is most commonly defined as the probability of floods occurring times the consequences of those floods. Flood susceptibility, as defined in this report, is the probability of floods occurring times the inundation severity of those floods. This paper on flood susceptibility does thus not include any damage estimation techniques.

Thirdly, in order to estimate the flood susceptibility of Eastbourne, some assumptions need to be made to make the research feasible. These assumptions are listed below.

- It is assumed that the flood susceptibility of Eastbourne is driven by either coastal flooding, fluvial flooding or flash flooding. Other (less common) types of flooding, such as groundwater flooding, are assumed to be negligible in the Eastbourne case study. Tidal effects are taken into account, however tidal flooding has not been treated specifically.

- The effect of the urban drainage system on the inundation is difficult to represent without the dimensions and layout of the system. This is why a worst case scenario, in which the urban drainage system is full, is assumed.
- The topography of the foreshore, (natural) sea defences and the coastal town of Eastbourne itself are assumed constant in time.
- The effect of evaporation and infiltration is assumed to be negligible on the inundation for short time scales. The effect of wind on the inundation process within the inundation domain is also assumed to be negligible (wind is however accounted for in the estimation of the sea state).

1.4 Report structure

In order to answer the research question, various flood susceptibility estimation techniques are implemented and compared. The report starts by introducing and describing these methodologies and how they are applied in this research in chapter 2. The subsequent results yielded from the implementing these techniques are given and compared to each other in chapter 3. The application of the techniques, the results they yielded, and potential implications are further discussed in chapter 4. Last of all, conclusions regarding the three sub-questions are drawn and recommendations are given in chapter 5.

Appendix A gives a small summary of common flood susceptibility estimation practice. Appendix B gives an in-depth description of the scenario creation procedure based on the conditional approach. Appendix C gives an example of the input scripts used for SWAN wave modelling. Appendix D gives an example of the input scripts used by SWASH for the numerical overtopping estimation approach. Lastly, appendix E gives additional figures which are referred to throughout the report.

2 Methodology

Since not all flood susceptibility estimation techniques can be compared, is this research focusing on a single case study and only a selection of flood susceptibility estimation methodologies. This chapter will go over the case study and the implementation of the various used techniques.

Firstly, the general overarching approach, explaining which and how various methodologies are addressed, is given in section 2.1. Secondly, the choice of location for the case study (Eastbourne), is elaborated in section 2.2. Thirdly, the used data and the statistical methodology which has been implemented to handle this data, is discussed in section 2.3. Fourthly, the concept of wave modelling (spectral action balance modelling) is introduced in section 2.4, which also discusses its implementation. Fifthly, various overtopping methodologies and their implementation are given and explained upon in section 2.5. Lastly, section 2.6 explains the techniques and implementation of the inundation estimation.

2.1 General approach

There are various approaches one can use to estimate flood susceptibility as is elaborated upon in appendix A. Which approach should be used, depends on the scale of the area, the complexity of the flood driving mechanisms, and the available computational power. The area of interested of this research is the coastal town of Eastbourne. Eastbourne is a relatively complex case since it is susceptible to both coastal and pluvial/fluviol flooding. Therefore, more computationally expensive methodologies representing physical mechanisms will be used and compared (instead of e.g., fully statistical approaches). Figure 2 shows the phases and various approaches, which will be used and compared in this research.

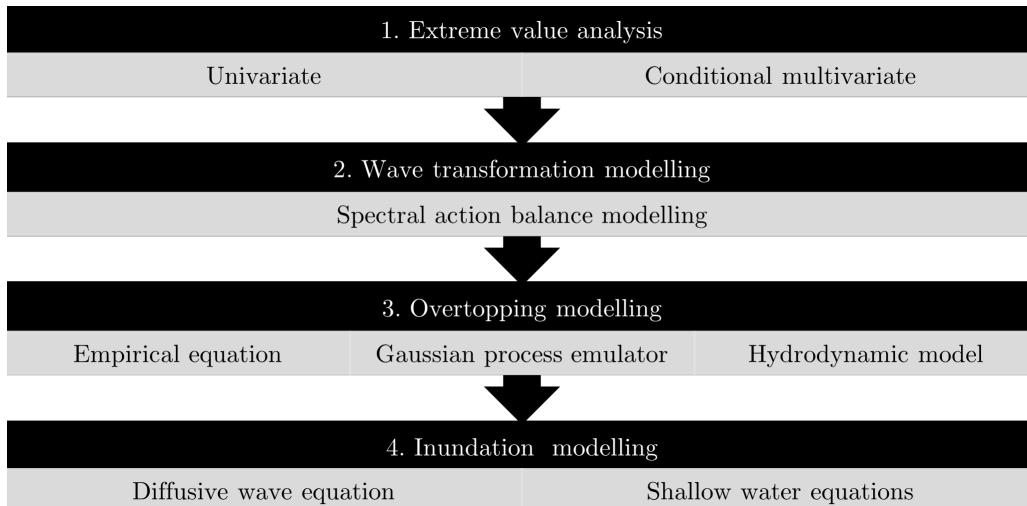


Figure 2: Modelling phases and the techniques which will be applied and compared in their respective phase

1. Extreme value analysis is used to create scenarios (meteorological variable combinations) with a return period of 100 years. There are two methodologies compared in this phase. The univariate methodology considers a singular variable as its basis for scenario creation. This means, one can use traditional extreme value analysis, such as the peak over threshold approach which has been applied in this research. In this research this methodology is applied to create a scenario based on a precipitation event with a return period (RP) of $100y$ and a significant wave height (H_{m0}) with a return period of $100y$. The conditional multivariate methodology refers to the conditional approach developed by Heffernan & Tawn (2004), which allows for explicitly treating the combination of extreme precipitation and an extreme sea state. This approach is however more complex, and much more somewhat more computationally intensive. The application of both approaches is elaborated upon in section 2.3, and appendix B discusses the mathematical procedure of the conditional approach.
2. Wave transformation modelling is the approach used to translate offshore wave input to nearshore sea conditions. The data used in this research is offshore data (as is elaborated upon in section 2.3.1), which makes this a vital step. This research estimates the wave transformation by solving the spectral action balance equations via the open source software SWAN (The SWAN team, 2020b). A more in depth description of this approach can be found in section 2.4.

3. Overtopping modelling translates the nearshore sea state conditions to discharge fluxes into the flood domain over the flood defences. Three different approaches are used and compared in this phase. Firstly, an empirical formula (the new overtopping formula from [van der Meer et al. \(2018\)](#)) is applied at the toe. Secondly, the Gaussian process emulation Bayonet GPE ([Pullen et al., 2018](#)) (similar to a neural network) is applied with the same input. Lastly, a 1DH numerical model (SWASH ([The SWASH team, 2019](#))) is applied over a larger domain in an attempt to capture more accurate wave breaking and overtopping behaviour. Further description of the application of the empirical equation, the GPE and the numerical model can be found in section [2.5.2](#), [2.5.3](#) and [2.5.4](#) respectively.
4. Inundation modelling and interpretation of its results is the last phase of the flood susceptibility analysis. The chosen inundation model (HEC-RAS ([US Army Corps of Engineers, 2021](#))) is a numerical model which solves a greatly simplified version of the Navier-Stokes (similar to SWASH). In this phase two different simplifications of the Navier-Stokes equation are compared. The diffusive wave approximation is a relatively fast and very robust methodology, however this comes at the cost of neglecting inertial terms. The shallow water equations do take these inertial terms into account, which makes this approach more accurate, but less stable and more computationally intensive. The application of the HEC-RAS model and its boundaries is further discussed in section [2.6](#).

2.2 Location

2.2.1 Case study selection

The area of interested of this case study is the coastal town of Eastbourne, which is located at the south coast of England. This town is subjected to a coast with a North Sea wave climate. Typically storms propagate from a south-west direction. However, less common north-easterly storms do occur. Furthermore, the town has a little river delta, which means there is some fluvial flood risk.



Figure 3: Left: Location of Eastbourne in red square; Right: Areal photo of Eastbourne

Many locations around the UK are available for case study due to a generally healthy supply of data. Eastbourne has been chosen for this study since it fulfills certain requirements, which makes it interesting for detailed study. Three hard requirements are listed here and elaborated upon below.

- The location is an urban area
- There is a substantial threat of coastal flooding at the location
- There is a substantial threat of fluvial/pluvial flooding at the location

Firstly, Eastbourne is an urban area. This is a location requirement since this means the location has significant economical and social value. Flood susceptibility estimation at Eastbourne is thus relevant for flood risk reduction strategies to protect these assets. Urban areas are also more prone to pluvial flooding (precipitation flooding), which increases the importance of accurate flood susceptibility estimation.

Secondly, this research compares several methodologies which are used for specifically coastal flood susceptibility estimation. For these methodologies to be relevant, there should thus be some existing coastal flood risk.

According to the long-term flood risk map (shown in figure 4) created by the UK Environmental Agency, Eastbourne has a substantial existing coastal flood risk, making it suitable for this research (Environment Agency, 2019).

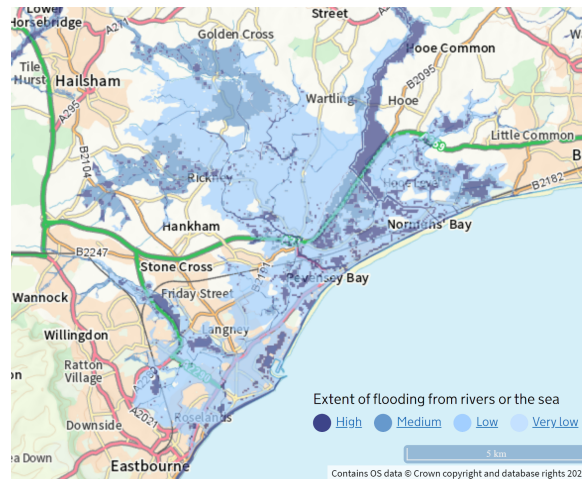


Figure 4: Flood risk of Eastbourne, as estimated by the UK national flood risk map (Environment Agency, 2019). The dark blue shaded area along the coastline is an indication of risk induced by coastal flooding. The blue areas along rivers are an indication of risk induced by fluvial flooding.

Lastly, there needs to be expected pluvial/fluvial flood risk. Having flood susceptibility induced by the coastal boundary, the river boundary and direct precipitation makes for a complex, but frequently occurring problem. It is interesting to quantify the importance of treating more than one type of flooding, which is effectively done by the "smart" scenario selection methodology as explained in section 2.3.2. The long term flood risk map created by the Environmental Agency (figure 4) shows Eastbourne has a significant pluvial/fluvial flood risk and thus fulfills this requirement too.

2.2.2 Case study characteristics

Eastbourne is a town with a population of a little over 100.000 people. The west side of the town has a relatively high elevation (up to $MSL + 200m$). The coastline at the west coast is characterised by large chalk cliffs. Conversely, the center and east side of Eastbourne have very different characteristics. The elevation in the center and east is generally just slightly above mean sea level (MSL), whilst the coastline mainly exists out of shingle beaches. On the east side of Eastbourne the shingle beach coastline is interrupted by the Sovereign Harbour, a marina complex of four small linked harbours. The entrance of this harbour complex consist of twin sea locks which are closed during coastal storms.

Eastbourne has several interesting characteristics with regards to flooding which makes it an interesting choice for a case study. These interesting characteristics are listed here:

1. The center and East coastline of Eastbourne has an interesting coastal climate. The town has mild to moderately sloped beaches, exposed to a moderate to large tidal range, with a moderate to large storm surge during severe sea states. This combination of characteristics will result into a complex, but common situation, in which accurate modelling is required (opposing, e.g., a tide-dominated system). As to relate this to the Ternary shoreline classification diagram, a coast with the preferred characteristics for this study is placed somewhere around the red dot in figure 5.
2. Eastbourne has an easily defined river delta. This means that sufficient historical data on the river system is available. The tidal delta of Eastbourne is also relatively small, which means a large portion can be accurately represented by the inundation domain.

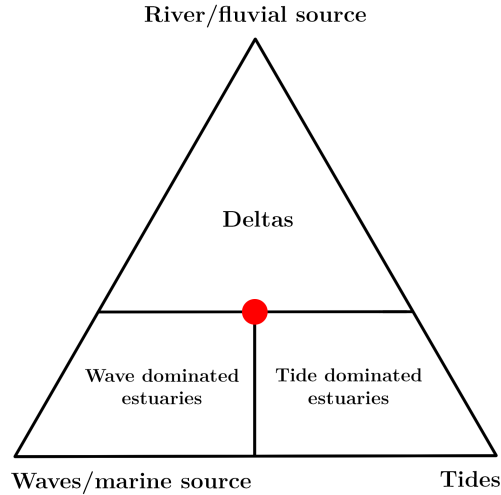


Figure 5: Ternary shoreline classification diagram in which the red dot is pointing out the coastal characteristics of interest. This illustration based on the work of [Dalrymple et al. \(1992\)](#) and [Boyd et al. \(1992\)](#).

3. The center and eastern land soil profiles of Eastbourne are low in chalk content according to the national soil map of England ([Cranfield University, 2013](#)). A high chalk content can increase the probability and severity of groundwater flooding, which is an excluded type of flooding in this study due to time constraints.
4. A preferred characteristic is a region with little to no history of tsunamis or meteotsunamis. Tsunamis/meteotsunamis can cause flooding, but should be accounted for with specialised methodologies. This is why tsunamis/meteotsunamis fall out of the scope of this research. Since Eastbourne has no history of flooding by tsunamis/meteotsunamis, one can safely assume that not accounting for tsunamis/meteotsunamis does not change the overall result of the research.

2.3 Statistical analysis

A statistical analysis of historical data at Eastbourne is required for the first step of the general approach as shown in section 2.1 (extreme value analysis). Firstly, the chosen data sources are given and elaborated upon in section 2.3.1. Secondly, the concept of "smart" scenario selection is explained in section 2.3.2. Lastly, in order to create storm scenarios, a data analysis approach is given in section 2.3.3.

2.3.1 Data sources

This research had to make use of various types of data provided from various sources. This section will elaborate on which sources have been used and why. One can distinguish two different types of data based on their timescale. Firstly, variable data refers to data with a relatively short timescale. For example precipitation data or wave characteristics. Secondly, topographic data refers to spatially varying data describing the elevation of a terrain. The timescale of variations in topographic data is generally much larger than variable data and will be assumed constant in this research.

Variable data

This research has used the following four sources for variable data.

1. The fifth generation ECMWF atmospheric reanalysis of the global climate (ERA5) (coordinates 50.75, 0.25), hourly data (1979 to 2020) ([Copernicus Climate Change Service \(C3S\), 2020](#))
2. Port of New Haven, hourly tidal gauge data (43 years) ([British Oceanographic Data Centre \(BODC\), 2020](#))
3. Herstmonceux West end, hourly precipitation gauge (1992 to 2021) ([Met Office, 2021](#))
4. Langney bridge, 15min river gauge (2016 to 2021) ([Environment Agency, 2021](#))

The variables researched for the simulation of flood events are listed in the following two columns. The numbers behind the variables indicate the used data source.

- H_{m0} : Significant wave height (1)
- I_r : Precipitation intensity (1)
- D_r : Precipitation event duration (3)
- $T_{m-1,0}$: Mean wave period (1)
- $\bar{\theta}$: Mean wave direction (1)
- σ_E : Wave spectral directional width (1)
- u_{10} : Wind speed (1)
- θ_{wind} : Wind direction (1)
- ζ : Water surface elevation (2)
- d_{river} : River water levels (4)

Arguably, the most important data source of this research is the reanalysed ERA5 data. ERA5 data is produced based on many historical observations around the world, advanced modelling and data assimilation systems. This reanalysed data has been used for exploratory data analysis and scenario creation. The reason reanalysed data has been used instead of directly measured data is because it is easily and freely available all over the world, it captures a relatively long period of time (41 years), and the reanalysing procedure may remove some scatter, which leads to a more clear dependence structures between variables.

The reanalysed ERA5 data does however exclude accurate water level elevation measurements, since water level is strongly influenced by local topography. Water level elevation data is however important regarding the analysis of the tidal cycle and storm surge level estimation. This is why it was necessary to use a separate tidal gauge (Port of New Haven). This tidal gauge data has been analysed with the open source Python module UTide* (Bowman, 2021). The modules allows for harmonic analysis on water level time series, in order to find the main tidal constituents. Not only does this give the various tidal amplitudes and frequencies, but by subtracting the tidal signal from the data one finds an estimation of the storm surge. This storm surge estimation has a strong dependence structure on other variables and is included in the scenario creation procedure as discussed in section 2.3.3.

An important weakness of the reanalysed data is representation of short duration events. Especially short but intense local precipitation events are not captured well by reanalysed data as is shown in section 2.6.4. Using only reanalysed precipitation data would lead to misrepresentation of event duration. This is why locally gauged data (at Herstmonceux West end), has been used to find a reasonable estimate for the duration of precipitation events. This is further elaborated upon in section 2.6.4.

Historical observations of a locally measured river gauge have been used to estimate a reasonable upstream boundary condition for the inundation model.

Topographic data

This research makes use of multiple models which have their own domain. Each of these domains has its own topographic data source.

- Coastal domain: Marine DEM (1arcsec) (Department for Environment, Food and Rural Affairs, 2020a)
- Surfzone domain: Surfzone DSM (2m) (Department for Environment, Food and Rural Affairs, 2020b)
- Inundation domain: EA Lidar DSM (1m) (Environment Agency, 2020)
- Land cover data: UKCEH Land Cover Map 2019 (LCM2019) (20m) (UK Centre for Ecology & Hydrology, 2019)

2.3.2 "Smart" scenario methodology

Some flood susceptibility estimation methodologies are very efficient and do not require much computational power. This allows for many simulations, which means one can use statistical analysis on the results. Eastbourne is however a relatively complex case since there are multiple flood types which can cause simultaneous or serial flooding as discussed in section 2.2. In order to resolve complex hydrodynamic interactions between different flood drivers, high resolution 2D flood models are required (Eilander et al., 2020). Hence, one has to apply computationally intensive methodologies. Using a computationally intensive methodology means only a small number of simulations can be made, which in turn means that no valid statistical analysis can be conducted on the results. This is why the statistical analysis is done before the modelling phase by cleverly creating storm scenarios.

*The used Python version of UTide is open source and freely available at <https://pypi.org/project/UTide>

With the "smart" scenario approach is meant, creating various scenarios with the same return period, which represent combinations of different flood types. In the case of Eastbourne (a coastal urban area with a small delta), the flood susceptibility seems mainly governed by coastal and precipitation-driven flooding. One can get an indication of the relation between these types of floods by modelling scenarios with the same return period, in which the boundary conditions are selected based on the type of flooding. For this case study, figure 6 qualitatively shows the boundary combinations of the scenarios. The significant wave height (H_{m0} , a parameter representing the potential energy of a wave climate) and the precipitation intensity (I_r), have been chosen as primary variables for scenario creation due to their respective relation with the flood types. Table 1 quantifies the rareness of one flood type forcing with respect to the other, by giving a return period ratio ($RP_{H_{m0}}/RP_{I_r}$).

It is important to note that the extremity of the individual variables in this table depends on the dependency of these variables. For example, in the case of two variables with a strong positive correlation, a scenario combination leading to a return period ratio of 1, would mean that the return period of the individual variables is close to the return period of the combination. Conversely, if we consider two completely independent variables, a scenario with a return period ratio of 1 would result into relatively common conditions for both individual variables.

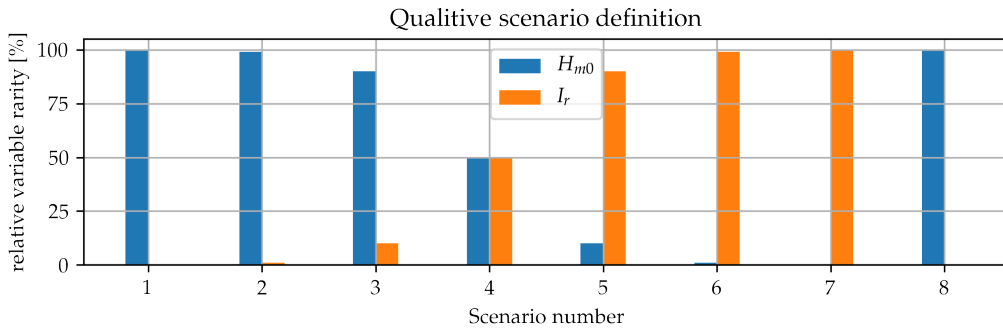


Figure 6: This figure gives a qualitative description of the various scenarios. Two examples are: scenario 1 has a very extreme significant wave height (H_{m0}) in combination with a precipitation intensity (I_r) of zero, and scenario 4 has a H_{m0} with the same return period as the I_r . Note that the I_r severity in scenario 2 and the H_{m0} severity in scenario 6 are very small, but not zero.

Scenario	1	2	3	4	5	6	7	8
$RP_{H_{m0}}/RP_{I_r}$	∞	500	10	1	1/10	1/500	0	∞

Table 1: Qualitative scenario overview. This table quantifies the relative rarity of the primary variables in the various scenarios. The combination of these primary variables will lead to scenarios with the same total return period (100y). The individual variable return periods cannot be given at this point since they depend on the dependence structure of the primary variables.

After conducting the exploratory data analysis, it was found that next to the common south-westerly storm, a rarer and milder north-easterly storms can hit Eastbourne (see the results in section 3.1.1). This type of coastal climate is explored with scenario 8.

The first step in the methodology comparison is effectively already made by implementing this "smart" scenario approach (see figure 2 in section 2.1). One can use a simplified approach by making the assumption of a single flood type dominating over the other. By making this assumption you can treat the flood types as independent, which would reduce table 1 to only scenario 1,7 and 8. This means that one can use an univariate approach (traditional extreme value analysis) for the creation of scenarios, instead of the more complex dependant bi/multivariate extreme value analysis.

2.3.3 Data analysis

The data analysis, as executed in this research, has two parts. First, a general exploratory data analysis is executed to get an understanding of the dependence structure between the variables. After which, the first step of the general approach as shown in section 2.1, the scenario creation, is executed. During the scenario creation

the difference is made between primary variables and secondary variables. Primary variables are the variables on which the scenarios are based, whereas secondary variables are chosen based on the dependence structure.

Exploratory data analysis

The exploratory data analysis starts by plotting the various ERA5 variables against each other in the form of a correlation matrix. Such a correlation matrix plot is helpful in order to observe the general dependence structure because it shows what combinations occur.

The correlation matrix (and correlation coefficients) are less well suited for the description of tail dependence. Tail dependence is however essential when creating extreme storm scenarios. A methodology better suited to describe this, is by plotting the multivariate conditional Spearman's correlation coefficient across a sliding window of values, following Schmid & Schmidt (2007). This methodology has been implemented in the `texmex` package for the programming language R, of which the implementation is discussed in Southworth et al. (2020). The results of this methodology are given and discussed in section 3.1.1.

Lastly, a less formal, but very indicative description of the relation between precipitation and wave height is given by plotting conditional probability density distributions. Such plots show very clearly whether there is a positive dependence between precipitation and the significant wave height. Such a relation could mean that compound storms (storms which result into flooding from both land and sea) are more probable than one might guess.

Primary variables: Univariate

Primary variables are in this research defined as variables directly used for scenario creation. One has to choose one or more variables to base a scenario on, i.e., a significant wave height with a return period of 100 years. If one were to consider every variable as primary, then this would reduce the extremity of the singular variables. This research treats two primary variables for scenario creation. These are the precipitation intensity and the significant wave height. These variables have been selected since they play a primary role in pluvial and coastal flooding according to the flood estimation handbook (Kjeldsen, 2007) and the overtopping manual (van der Meer et al., 2018).

The univariate approach assumes the tails of the primary variables to be independent (or weakly dependent), such that the combination of both variables being extreme during a singular event is very low. This would mean that one can treat coastal flooding and pluvial/fluviial flooding as separate independent processes.

Making this assumption, one can use traditional extreme value analysis methodologies to estimate values with a certain return period for the considered primary variable. There are two traditional extreme value analysis methodologies; the peak-over-threshold (POT) approach and the block maxima approach. The extreme value analysis methodology applied for the univariate case is the POT method (Coles, 2001). The main advantage of this methodology over the block maxima method is that all relevant information (the peaks) are used, whereas using the block maxima method one does not. Another reason for choosing the POT approach is because executing this approach is the first step of the conditional approach (Heffernan & Tawn, 2004).

The execution of the POT approach is a relatively simple task these days, with the help of the statistical programming language R. First one picks a threshold for the considered variable. One can use threshold stability plots and mean residual life plots to find appropriate thresholds. Functions to make these plots are included in the `texmex` package for R, and Southworth et al. (2020) describes how to apply and interpret them.

After an appropriate threshold has been selected, one can fit the generalized Pareto distribution family to the remaining data. One can then use this fit to find variable values with an arbitrary return period. The `texmex` package does also include predefined functions for these operations. Further info regarding the mathematical procedure of the approach and the formulas can be found in appendix B.1.

Primary variables: Conditional multivariate

The univariate approach as outlined in the previous section has as main disadvantage that it does not account for combinations of primary variables. However, the results of the exploratory data analysis (section 3.1.1) do show a positive (tail) dependence. Compound floods (in this case combinations of fluviial/pluvial floods and coastal floods) may thus be more important than one might expect. The conditional multivariate approach by Heffernan & Tawn (2004) allows for extreme value analysis of multiple dependent variables and can thus be used for the creation of compound storm scenarios.

Until recently, the largest downside of the conditional approach was its complexity. Anyone wanting to implement this method was required to thoroughly understand high level mathematics and be very proficient in a programming language to code it up. However, since 2012 all code required to apply the methodology is freely available in the form of an R package called `texmex`.

Appendix B delves into the application and the mathematical background of this approach, but the main steps are summarised here below.

1. Apply the peak over threshold approach to both primary variables separately to gain the marginal distributions.
2. Transform these marginal distributions and the data into Laplace marginals.
3. Fit a regression model of the first variable conditional on the second based on the transformed data.
4. Repeat step 3 now conditioning the second variable on the first (this could be done up to n variables!).
5. Use both marginal distributions and Monte-Carlo sampling to create artificial samples of both variables and use the regression models to find their pairs.
6. Plot the original samples, and the artificial samples with pairs and make Joint exceedance curves with a singular return period (the limits of these curve are the same as the univariate approach).

Secondary variables

Secondary variables are, as mentioned before, the variables which do not directly define the scenarios. These variables are however required as input for the simulations and may have a substantial effect on end result. The main bulk of the considered variables are regarded as secondary, since only precipitation and the significant wave height are used for scenario definition. Variables such as wave period, wind velocity, and storm surge are thus all regarded as secondary variables.

Secondary variables should be chosen based on their dependence structure with the primary variables, which is fixed by the scenario definition. Based on historical data, one can estimate the likeliest value of a secondary variable given a value for one or more primary variables. This is done by finding the maximum of the conditional probability density function (PDF) of the secondary variable (envison taking a slice from a bivariate distribution and finding its maximum). This method becomes less certain when estimating extremes since little extreme data is available by definition. However, one can use the conditional approach (Heffernan & Tawn, 2004) to simulate synthetic extreme data to make this prediction more certain. This approach is applied in this research and is shortly summarised in a visual way here.

First, one should have a primary variable combination to base the secondary variable on. You can then fit a dependence structure of a secondary variable based on one or more primary variables. In this research the secondary variable is estimated based on its relation with the primary variable that has the strongest physical relation to it. So, for example, the wave period is estimated based on its relation to the significant wave height and not on the precipitation. The variable structure can be used to simulate synthetic data (even with a certain threshold if required). One can then take a "slice" of this data (as shown in figure 7 and regard this as a discrete PDF (probability density function) of the secondary variable given a value of the primary variable. Finding the maximum value of this PDF will then give the likeliest value of the secondary variable given the scenario. This approach is described in more detail in appendix B.

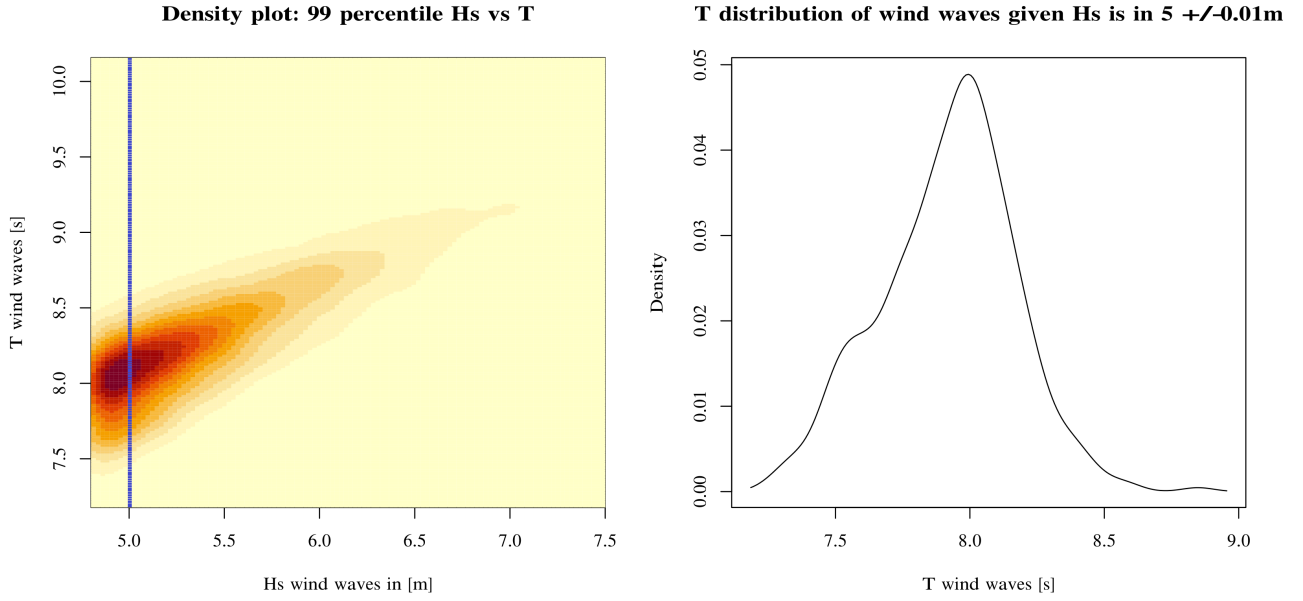


Figure 7: Plotting the joint density function (left) and the conditional PDF (right) based on synthetic data. This approach is applied in order to find the likeliest value of a secondary value based on a fixed primary variable value.

One cannot use the conditional approach to simulate synthetic data for directional variables such as the wind or wave direction (since they do not fit in the GPE family) (Coles, 2001). The likeliest value for directional data will thus be chosen based on historical data alone. A strong directional dependence exists, as can be seen from the correlation matrix in section 3.1.1. This approach is representative for reality due to this strong directional dependency.

2.4 Nearshore wave model (SWAN)

The second phase of the general flood susceptibility estimation approach (as shown in section 2.1 figure 2) is wave transformation modelling via SWAN*. The output of this phase is given in section 3.2 and is used as a boundary condition for phase 3 (overtopping modelling).

SWAN is an open source third generation wave model based on the theoretical concepts presented in Holthuijsen (2007). The basic equation of the model is the spectral action balance equation. This equation can be rewritten to the energy balance equation in the absence of an ambient current which is shown in equation 1 (formulated in Cartesian coordinates). Information regarding the numerical discretization applied by SWAN can be found in the technical documentation (The SWAN team, 2020a).

$$\frac{\partial E(\omega, \theta; x, y, t)}{\partial t} + \frac{\partial c_{g,x} E(\omega, \theta; x, y, t)}{\partial x} + \frac{\partial c_{g,y} E(\omega, \theta; x, y, t)}{\partial y} + \frac{\partial c_{\theta} E(\omega, \theta; x, y, t)}{\partial \theta} = S(\omega, \theta; x, y, t) \quad (1)$$

In which the variables are defined as:

- E : Variance density spectrum [m^2/Hz]
- ω : Angular frequency ($\omega = 2\pi/T$) [rad/s]
- θ : Wave direction [rad]
- S : Spectral energy density (the source term, representing all effects of generation, wave–wave interactions and dissipation per unit time per unit surface area) [$m^2/Hz/^\circ$]
- c_g : Celerity of wave groups [m/s]
- c_{θ} : turning rate of the wave direction due to the change in (nautical) direction [rad/s]

*SWAN is an open source third-generation wave model developed at Delft University of Technology. It is available at <http://swanmodel.sourceforge.net>

Equation 1 describes the spatial and temporal conservation of wave energy (a parameter directly linked to the wave height) on the left hand side, while the right hand gives a sink/source term. The physical mechanisms which can be included in this term are the following:

- Wind input
- Bottom friction induced dissipation
- White capping induced dissipation
- Surfbreaking induced dissipation
- Three-wave interactions (triads)
- Four-wave interaction (quadruplets)

SWAN offers various options regarding the representation of these terms. Table 2 gives an overview of how these terms are represented in this research. Appendix C gives an example of a typical SWAN input file used in this research.

Mechanism	Enabled	Input
Wind	Yes	Constant, scenario dependent
Friction	Yes	Default: cfjon = 0.038
Whitecapping	Yes	Default: Komen
Quadruplets	Yes	Default: DIA method
Depth-induced breaking	Yes	Default: Constant $\gamma_{bi} = 0.73$
Wave induced set-up	No	
Triads	No	
Turbulent viscosity	No	

Table 2: Physics included in the wave modelling (SWAN). More info regarding the chosen methods can be found in SWAN’s technical documentation ([The SWAN team, 2020a](#))

The enabled mechanisms and the chosen methodologies to represent them are relatively straightforward, but the reason as to why three mechanisms have been disabled deserves some further clarification. Calculation of wave induced set-up has been turned off in the SWAN model, because wave induced set-up is already included in the storm surge as calculated in the statistical analysis (based on buoy data). Storm surge has been explicitly included as a scenario creation variable and shows a high dependency on the significant wave height. One should note that this was a non-conservative decision. Triad wave interactions have been turned off since the default values of SWAN are only representative of long-crested waves ([The SWAN team, 2020a](#)). Finding good values to represent the three-wave interactions for this case would be a research of its own and is therefore excluded from the scope of this research. Lastly, the turbulent viscosity has been turned off because this term is expected to be relatively small and difficult to accurately represent.

Domain & discretisation (SWAN)

The 2D nearshore model domain reaches from the coordinates 50.70° (latitude), 0.06° (longitude) to 50.92° , 0.42° , which corresponds to about 25.3km by 25km. The domain and its bathymetry is shown in figure 8.

As mentioned in section 2.3.1, the SWAN domain (figure 8) makes use of the DEFRA Marine DEM, which has a resolution of one arcsecond ($\approx 30m$). A disadvantage of using this DEM is that it stops at mean sea level. During a coastal storm we find that the water level can rise to around 3 meters above mean sea level (surge and tide). Making this difference even larger is a bathymetry mismatch between the DEFRA DEM marine (SWAN domain) and the more accurate DEFRA sufzone DSM (Overtopping bathymetry). The mismatch between this data is at some places up to 3 meters. This means that the SWAN domain ends before reaching a water depth of 0 meters.

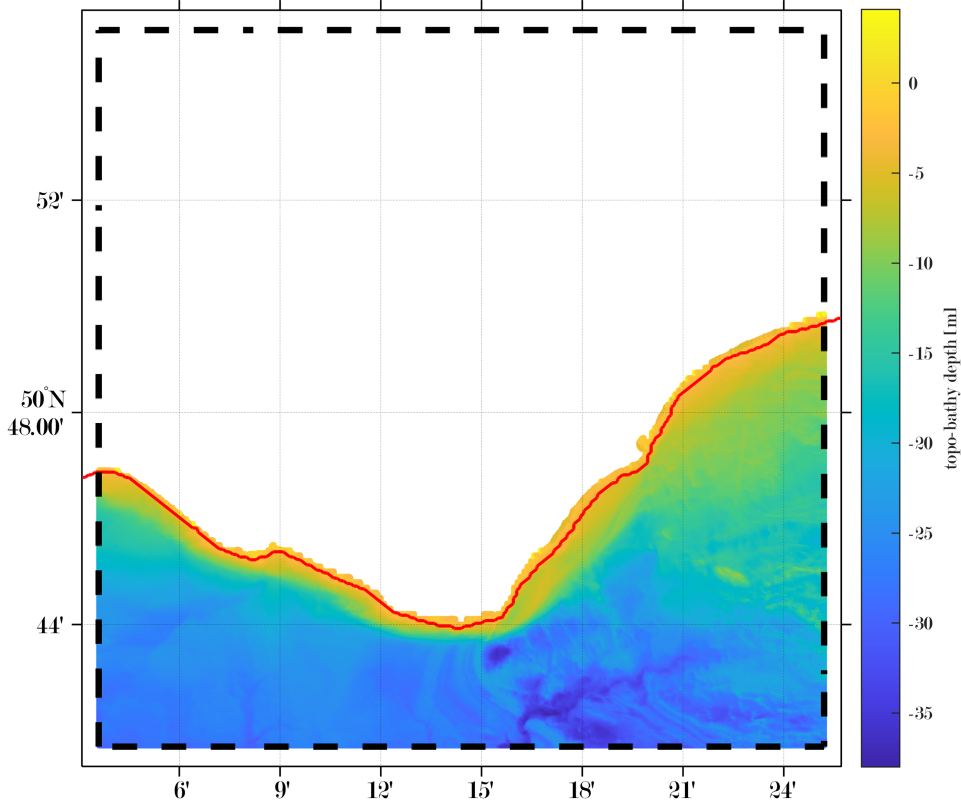


Figure 8: SWAN domain with coastline and bathymetry

For the spatial discretisation, a flexible triangular mesh has been generated using the `OceanMesh2D*` MATLAB toolbox Pringle et al. (2020) (see figure 9). A flexible mesh was used since preliminary results using a rectangular mesh showed a high resolution was required in the surf zone region. The generated mesh has a resolution (triangle edge length) of approximately 20 meters in relatively shallow zones, whilst cells go up to 100 meters in deeper water. The grade of the mesh (α_g) ensures the size transition smoothness and is set to 0.35 in accordance with the user guide (Roberts & Pringle, 2020). The used feature width (R), ensuring adequate inclusion of the shallow zone has been set to 100 triangles.

*OceanMesh2D is open source and freely available at <https://github.com/CHLNDDDEV/OceanMesh2D>

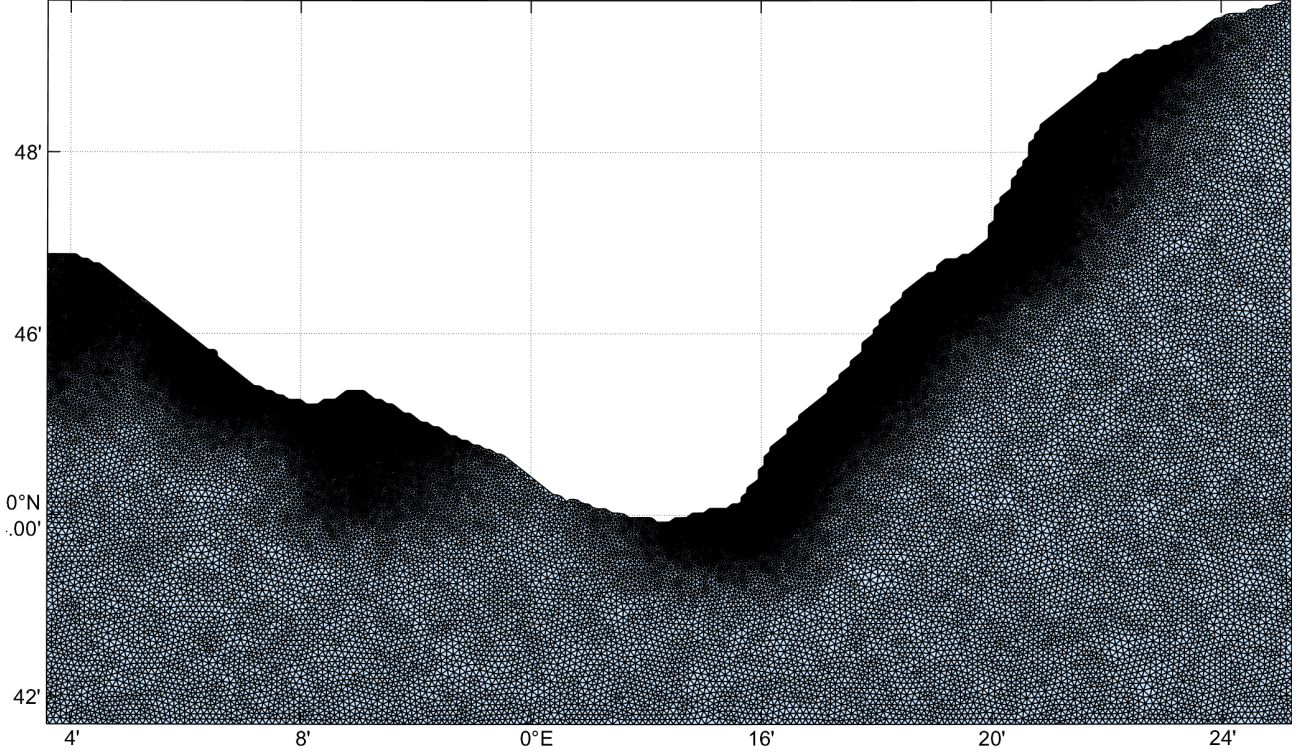


Figure 9: Flexible mesh used for wave modelling (SWAN)

To adequately capture the directionality of storms, use is made of 72 directional bins representing all angles ($\Delta\theta = 5^\circ$). And in order to capture the various relevant wave periods, 31 frequency bins, reaching from 0.03 to 0.6 Hz (logarithmically distributed), have been used. This number of frequency bins is based on the recommended frequency resolution of $\Delta f/f = 0.1$ (The SWASH team, 2019).

Scenario input (SWAN)

The SWAN simulations use the storm scenarios, as defined via the data analysis (section 2.3.3), as input (boundary) conditions. These input conditions are given in table 5 of results-section 3.1.2, where they are further discussed.

The input conditions of table 5 on its self are not enough to define the offshore SWAN boundaries. One should also define a spectrum and a coefficient regarding directional spreading. Research on historical data has shown that bimodal sea states are relatively rare at the coast of Eastbourne (Dhoop, 2018). This is why a traditional JONSWAP spectrum, with an average peak enhancement factor ($\gamma_{jonswap}$) of 3.3 has been implemented. A constant factor of directional spreading (standard deviation) of 30° has been chosen based on the reanalysed ERA5 data. Furthermore, the typical $\cos^m(\theta - \theta_{peak})$ distribution for directional spreading is assumed.

2.5 Overtopping estimation techniques

The third phase of the flood susceptibility estimation approach (as shown in section 2.1) is wave overtopping modelling using three different methodologies. These three methodologies do share a general overtopping estimation approach, which will be discussed first in section 2.5.1. After which, the three methodologies are discussed in ascending order of complexity. Firstly, the application of the empirical overtopping equation is discussed in section 2.5.2. Secondly, the application of a Gaussian process emulator approach is discussed in section 2.5.3. And lastly, the application of a numerical approach using SWASH, is discussed in section 2.5.4.

2.5.1 General overtopping estimation approach

The offshore wave model SWAN of the previous phase is ran in 2DH mode (see section 2.4). This means one can define overtopping domain boundaries at arbitrary points in or along this domain. The empirical method and the GPE (Gaussian process emulator) method are both strictly one-dimensional approaches, whilst the numerical method is very computationally intensive in 2DH. This is why the overtopping estimation is conducted using multiple representative 1DH domains.

Three main cross sections have been defined to be representative of coastline segments as shown in figure 10. Only three main cross sections are used for simplicity's sake, to keep the computational time feasible and to make the result interpretation more manageable. Cross sections of these locations reaching up to 2km offshore, are visible in appendix E.3.

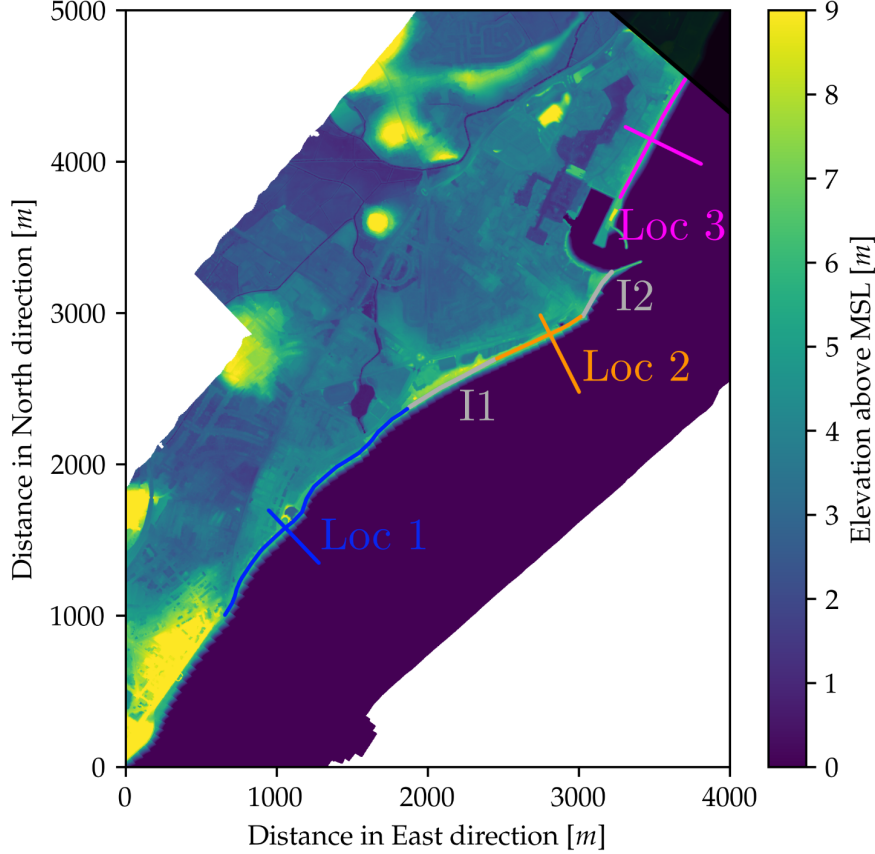


Figure 10: Representative locations; coloured: main locations, grey: intermediate locations

Next to the three main coastline sections, two intermediate sections have been defined as well (see figure 10). These intermediate sections have a singular characteristic which prevents them from being part of the main cross sections. At intermediate section one (I1) the ground level is 1 to 2 meters higher than at locations 1 and 2, where as at intermediate section 2 (I2) the shore normal angle is significantly different from location 2. Overtopping estimations at these intermediate sections are approximated via a neighbouring main location and then empirically corrected for their respective deflecting characteristic. Estimations made for intermediate sections using the empirical method are corrected with this method as well, and estimations made with the GPE are corrected using the GPE approach. Using the numerical approach it self to correct its intermediate sections would be relatively computationally intensive, which is why a combination of the empirical approach and the GPE approach is used instead.

2.5.2 Empirical overtopping equation (EurOtop)

The traditional methodology of estimating overtopping rates is via an empirical formula. The current (European) standard for this approach, given by the EurOtop Manual (equation 4.3) (van der Meer et al., 2018), is the "new" overtopping formula shown in equation 2. According to the manual, the overtopping rates found by empirically derived equations as this one, should be regarded as, "at best" within a factor of 1 to 3 of the actual overtopping rate.

$$\frac{q}{\sqrt{g \cdot H_{m0}^3}} = \frac{0.023}{\sqrt{\tan \alpha}} \gamma_b \cdot \xi_{m-1,0} \cdot \exp \left[- \left(2.7 \frac{R_c}{\xi_{m-1,0} \cdot H_{m0} \cdot \gamma_b \cdot \gamma_f \cdot \gamma_\beta \cdot \gamma_v} \right)^{1.3} \right] \quad (2)$$

Of which the variables are defined as:

- q : Overtopping rate [$l/s/m$]
- g : Gravitational acceleration (9.81) [m/s^2]
- H_{m0} : Significant wave height defined using the spectral moment $m0$ [m]
- α : Beach slope angle [$^\circ$]
- γ : Influence factors, see table 3 [-]
- $\xi_{m-1,0}$: Iribarren parameter (surf similarity parameter) defined using the $m - 1, 0$ spectral moment (see equation 3) [-]
- R_c : Crest height (defined as the height difference between the SWL and the crest top) [m]

The Iribarren number should be defined as shown in equation 3 for this approach (van der Meer et al., 2018).

$$\xi_{m-1,0} = \frac{\tan \alpha}{\sqrt{H_{m0}/L_{m-1,0}}} = \frac{\tan \alpha}{\sqrt{H_{m0}/(1,56 \cdot T_{m-1,0}^2)}} \quad (3)$$

The approach makes use of four different influence factors which are defined as shown in table 3 and described below.

Variable	Symbol	Value
Influence factor for a berm	γ_b	1
Influence factor for roughness elements on the slope	γ_f	0.9
Influence factor for a wall at the end of the slope	γ_v	1
Influence factor for oblique wave attack	γ_β	$1 - 0.0033 \beta $

Table 3: Influence factors of the empirical approach and the GPE approach

- The coast of Eastbourne does not have any berms and the description of the bathymetry would not benefit from including one, hence there is no berm reduction ($\gamma_b = 1$).
- Accurately describing the roughness of the beach profile is relatively challenging. The shoreline of Eastbourne consists mainly of pebble beaches. The overtopping formula (equation 2) is mainly used for a hard structures and no recommended roughness factor (γ_f) could be found in literature. Therefore, a most likely conservative value of 0.9 is assumed.
- The coastline of Eastbourne is in reality protected by an additional wall on most dike crests. This wall does, however, not show up properly in the bathymetry files (resolution of 1m) due to its slenderness. This makes it difficult to accurately include, especially in the numerical approach. Therefore, the additional wall is neglected in all approaches ($\gamma_v = 1$).
- According to the EurOtop Manual (equation 5.29) (van der Meer et al., 2018) one should include an oblique wave attack reduction factor of $\gamma_\beta = 1 - 0.0033|\beta|$ when using equation 2 for short crested waves. In this formula β is defined as the angle of wave attack with a maximum/minimum value of $\pm 80^\circ$.

Input of overtopping formula

The overtopping formula (equation 2) requires both geometric input and wave conditions. The beach slopes of the respective locations remain constant for each scenario and have been estimated based on the beach profiles (see appendix E.3). Locations 1 to 3 have average slopes of 1:9.24, 1:8.56 and 1:7.54 respectively.

The remaining input variables are calculated by the SWAN model via the method as explained in section 2.4. These values differ per location and per scenario.

2.5.3 Gaussian Process Emulator (Bayonet GPE)

Bayonet GPE is a generic metamodelling overtopping model, based on the application of Gaussian process emulation (GPE) techniques (Pullen et al., 2018). The concept is somewhat similar to traditional artificial neural networks (ANN), but it improves upon them by including the uncertainty within the physical model data. The main reason for including specifically this overtopping estimation method is because it is the approach currently used in the UK National Risk Assessment (Aldridge et al., 2017). The approach is very computationally efficient similarly to the overtopping formula method (section 2.5.2) and uses the same input boundary.

Application of Bayonet GPE

Bayonet GPE uses geometric input similarly to the overtopping formula. The approach improves upon the overtopping formula in this regards because it gives the user the option to specify additional features, such as including multiple slopes and the width of the toe. Attempts to represent the bathymetry profiles more accurately by including two different slopes, or a berm led to very large Mahalanobis distances. The Mahalanobis distance represents the distance from the center of training data, and a large distance does thus indicate that the GPE is most likely incapable of reproducing an accurate estimate. Hence, the various cross sections were best described as simple sloped structures (see figure 11), which does not include the additional features Bayonet GPE offers.

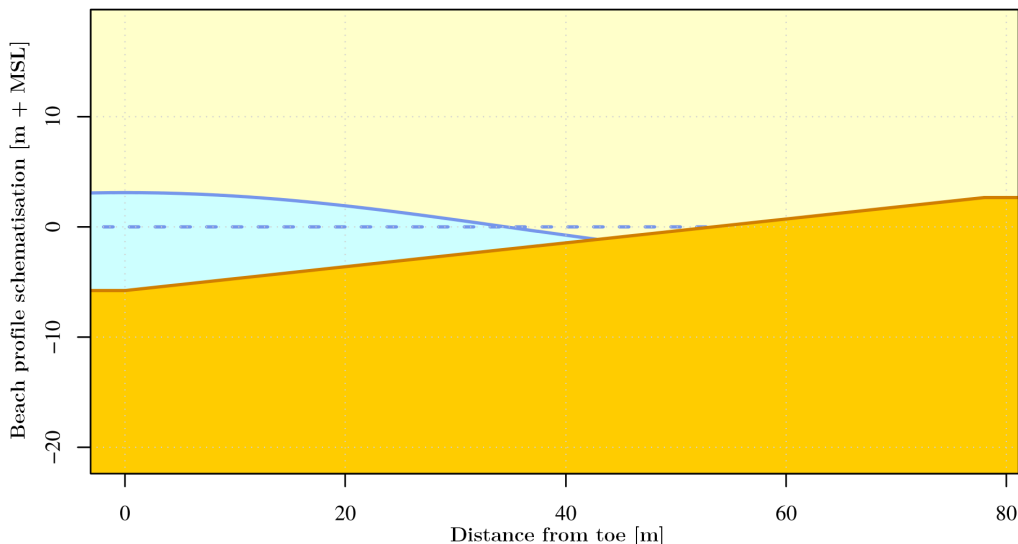


Figure 11: Bayonet structure input example (location 1). Orange line: represents the beach profile; dashed blue line: the average water level (with respect to still water); solid blue line: Sine wave giving a representation of the wave conditions.

Bayonet GPE can be used in two ways. One can use the user interface to calculate one scenario and location at a time, or one can use batch processing to calculate all of them in one go. Since this research compares 5 locations and 8 scenarios, use was made of batch processing.

Input of Bayonet GPE

The wave condition input of Bayonet is the same as the input of the overtopping formula since both methods use input estimated at the toe of the structure. The only difference is that bayonet uses the wave period ($T_{m-1,0}$) and wave direction (β) directly as input variables, whereas the overtopping equation used dimensionless variants (the Iribarren number ξ , and the oblique wave attack reduction factor γ_β). The input of of the GPE is further discussed as output of the SWAN model in section 3.2.

2.5.4 Numerical modelling of the surfzone and beach (SWASH)

Hydrodynamic numerical modelling is an approach that fundamentally differs from the empirical formula and the GPE. Instead of fitting empirical relations, the method approximates the behaviour of water derived from the laws of physics. The open source model SWASH* (developed by the SWASH team) is a numerical tool capable of simulating unsteady, non-hydrostatic, free-surface, rotational flow. The governing two-dimensional

*SWASH is freely available at <http://swash.sourceforge.net>

equations of this model describe the depth-averaged, non-hydrostatic, free surface flow of an incompressible fluid over a varying bed topography shown by equation 4 and 5 (Zijlema, 2020). Further information regarding the numerical discretisation used by SWASH can be found its technical documentation (Zijlema et al., 2011).

$$\text{Conservation of volume : } \frac{\partial \zeta}{\partial t} + \nabla \cdot \mathbf{q} = 0 \quad (4)$$

$$\text{Conservation of momentum : } \frac{\partial h\mathbf{u}}{\partial t} + \nabla \cdot (\mathbf{q} \otimes \mathbf{u}) + gh\nabla\zeta = - \int_{-d}^{\zeta} \nabla p dz - c_f \mathbf{u} \|\mathbf{u}\| \quad (5)$$

In which the symbols are defined as:

- ζ : water level elevation with respect to mean water level [m]
- d : depth from bottom to mean water level [m]
- h : total height of the water coulomb ($h + \zeta + d$) [m]
- \mathbf{u} : flow velocity vector [m/s]
- \mathbf{q} : mass flux vector ($\mathbf{q} = \mathbf{u}h$) [m^2/s]
- p : non-hydrostatic pressure (normalised by the density) [$Pa \ m^3/kg$]
- c_f : dimensionless friction coefficient [-]

SWASH makes use of a computational grid in order to approximate equation 4 and 5. The horizontal discretisation approach of this grid differs from the vertical approach. For the horizontal direction a structured or unstructured mesh needs to be supplied. The cells of this mesh stay constant in geometry over time. In the vertical direction, a number of layers needs to be defined. The vertical time-varying water coulomb will then be divided over these layers, which means that the vertical geometry does change over time.

Usage of a hydrodynamic model for the estimation of overtopping is the most complex and advanced approach. However, this does not automatically mean that this hydrodynamic modelling is also the most accurate mode. It is important to realise that the empirical equation and the GPE are the more established solutions for overtopping estimation, whilst the hydrodynamic model is more experimental. A limitation of SWASH is that even though it uses vertical layers, it is a depth integrated model. This means that it is unable to represent the overturning (plunging) waves or overhanging structures. SWASH does however account for the lack of plunging wave dissipation via the application of a hydraulic jump analogy (Smit et al., 2013).

Numerical models are often better at describing wave breaking behaviour than spectral action balance solving models (such as SWAN) since they incorporate breaking behaviour implicitly. Most notable is the implicit inclusion of infra gravity wave generation in numerical models, a physical mechanism spectral action balance solving models struggle with. It is thus wise to select a coupling point between the wave model (SWAN) and the numerical model (SWASH) far enough offshore to incorporate wave breaking. The best location of this coupling point can be estimated based SWAN output. Appendix E.3 shows the evolution of various parameters along the shore normal profiles of location 1 to 3. Based on these plots, the decision has been made to fix the coupling point to a fixed distance of 2km off shore (defined at $MSL + 0m$). Increasing the size of the domain to such an extent does however mean that directionality may play a significant role within it.

Representing directionality in the numerical model

SWASH can be used in 2 dimensional mode with optional vertical layers (2DH) or in 1 dimensional mode with optional vertical layers (1DH). Representing the directionality of the problem is especially important when dealing with westerly coastal storms at Eastbourne, because Eastbourne is partially sheltered from these storms (as has been discussed in section 2.2). Because of this, attempts have been made to model waves from the breaking point until overtopping in 2DH with the TU Delft HPC08 cluster (using up to 80 CPU's). Sadly, various issues regarding instability arose. After these failed attempts the decision was made to focus on 1DH modelling due to time restrictions. 1DH modelling does also have the benefit of being much more computationally efficient, hence usage of the HPC08 cluster was no longer required. Due to the sheltered nature of Eastbourne, wave energy dissipation by refraction cannot be neglected however. Refraction has therefore been incorporated explicitly with the help of a frequency-dependent refraction coefficient.

Implementation of refraction in 1D

If we assume the energy of waves to stay constant between wave rays as a wave approaches the shore, then one can express the change in wave height as a multiplication of a shoaling and a reflection coefficient (see equation 6)(Judith Bosboom, 2021)*.

$$\frac{H_2}{H_1} = K_{sh}^* K_{ref}^* = \sqrt{\frac{c_1 n_1}{c_2 n_2}} \sqrt{\frac{b_1}{b_2}} \quad (6)$$

In which the variables are defined as:

- H_m : Wave height at position m [m]
- K_{sh} : Dimensionless shoaling coefficient [-]
- K_{ref} : Dimensionless refraction coefficient [-]
- c_m : Wave celerity at position m [m/s]
- n_m : Ratio between group celerity and higher phase celerity ($n = c_{group}/c$) at position m [-]
- b_m : Conceptual width of a wave ray at position m [m]

A 1D numerical model will be able to capture the effect of shoaling, however refraction is a 2 dimensional problem. If one assumes the shore to be approximately uniform, then one can approximate the refraction coefficient in the following manner according to the well-known Snell's law.

$$k_{ref} = \sqrt{\frac{b_1}{b_2}} = \sqrt{\frac{\cos(\theta_1)}{\cos(\theta_2)}} \quad (7)$$

In which θ is the wave angle at the respective location. One can explicitly account for refraction by multiplying each wave height with this factor at the coupling point. This will not lead to a perfect representation of the problem, since the reduction of the wave height due to refraction is a gradual process and the shore is not uniform. However, to incorporate refraction accurately, one should turn to 2DH hydrodynamic modelling.

The refraction we try to represent is from the coupling point till the shoreline (the 1D domain). It is reasonable to assume the waves to be approximately shore normal at the shoreline, which will simplify the $\cos(\theta_2)$ term of equation 7 to 1. However, SWAN does not output individual waves, but a wave spectrum. One can apply this method to a spectrum by multiplying each frequency bin of the spectral energy density ($S(f)$) with the square of the respective refraction factor, since $E = \frac{1}{2}\rho g a^2$. In which θ_1 is a vector with the mean directions of the various bins. This leads to equation 8. The result of applying this correction methodology is discussed in section 3.3.1.

$$S_2(\vec{f}) = \cos(\theta_1(\vec{f})) S_1(\vec{f}) \quad (8)$$

Model discretisation

The approach uses 1D shore normal cross section bathymetry files derived from the surfzone DSM ($2m$) (Department for Environment, Food and Rural Affairs, 2020b) using a third order spline. In order to represent the bathymetry accurately, the computations are also discretised using $2m$ cells. The timesteps of the runs are adaptive selected to match the default Courant number requirement of $0.2 \leq C \leq 0.5$. The duration of the simulations is 2 hours and 15 minutes, of which 15 minutes is spin-up time (The SWASH team (2019) recommends 10 to 15% of the total run time).

Frequency dispersion should be represented reasonable if $Kh \leq 7$ (The SWASH team, 2019)(in which K is the wave number and d is the depth). The highest Kh value estimated by SWAN value was 6.24 in scenario 8 and this was outside the area of interest, which means that frequency dispersion should be adequately represented.

In order to get stable runs for all scenarios, two different input files were used. Relatively stable runs could be solved using a relatively small water depth threshold (DEPMIN) of $1mm$, and the relatively mild Superbee flux-limiter, whilst the less stable runs required a higher water depth threshold of $5mm$, and the Koren flux-limiter. An example of an input file describing the latter simulation can be seen in appendix D. Flux limiters are numerical techniques that force monotonicity of the solution in order to increase stability (more info regarding this approach can be found in Zijlema et al. (2020)).

*Most commonly these coefficients refer to the shoaling and refraction ratios with respect to the deep water condition. However, in this report they refer to the ratio with respect the the SWAN-SWASH coupling point.

In order to keep the approach computationally efficient only three vertical equidistant layers have been used. Initial comparisons between SWAN and SWASH output did however seem to suggest that using only 3 vertical layers does not represent dissipation by surf breaking well enough. The applied solution to incorporate accurate surf-breaking whilst keeping the computational demand low is by making 3 computationally expensive 20 layer runs (one for each location), and adjusting the wave breaking behaviour to match the results close to the shoreline. This approach has been applied and its results are discussed in section 3.3.

Input of the numerical approach

The numerical approach uses input calculated by the near shore wave model (SWAN) similar to the empirical approach and the GPE. The coupling point between the SWAN model and the numerical approach is however defined further of shore and the numerical approach allows for spectral input. Spectral wave input gives a better description of the wave climate than the significant wave height (H_{m0}) and the wave period (T). This can be especially relevant with regards to overtopping since a wide spectrum may have long waves which are unlikely to break, whilst a narrow spectrum with the same H_{m0} and T may not include these long waves. The input values of the numerical approach are further discussed as result of the SWAN simulation in section 3.2.

2.6 Inundation modelling

2.6.1 Numerical approach

Inundation modelling can be executed in different ways with various tools (Teng et al., 2017). The method executed in this research makes use of a numerical hydrodynamic model (similar to SWASH) called HEC-RAS*. Numerical modelling was chosen since it is able to describe complex flow dynamics and does not require extensive historical inundation data in contrast to many conceptual or empirical approaches. The HEC-RAS model was chosen since it is an established engineering tool for which much documentation is available.

Generally, numerical inundation models solve equations based on the conservation of mass and the conservation of momentum. Using these conservation laws to describe the motion of viscous fluid substances, results into the well-known Navier-Stokes equations. Depth-integrating these equations, while assuming the horizontal length scale is much larger than the vertical length scale, and assuming a constant density results into the much more manageable shallow water equations (SWE) also known as the Saint-Venant equations. The one dimensional version of these equations is given in equation 9 and 10 for the sake of simplicity (Zijlema et al., 2020). HEC-RAS solves the two dimensional variant of these equations.

$$\text{Conservation of volume : } \frac{\partial \zeta}{\partial t} + \frac{\partial uh}{\partial x} = 0 \quad (9)$$

$$\text{Conservation of momentum : } \frac{\partial u}{\partial t} + u \frac{\partial u}{\partial x} + g \frac{\partial \zeta}{\partial x} + c_f \frac{u|u|}{h} = 0 \quad (10)$$

In which the variables are defined as:

- ζ : Elevation of water level with respect to the mean water level [m]
- t : Time [s]
- u : Flow velocity in x direction [m/s]
- h : Height of the water column, from bottom to elevation ($h = \zeta + d$) [m]
- x : Location in x direction of a Cartesian coordinate system [m]
- g : Gravitational acceleration (9.81) [m/s^2]
- c_f : Dimensionless friction coefficient [-]

The long wave assumption results into an inability to represent the progression of short waves (in contrast to the approach SWASH used), but these are often seen as less relevant when estimating the extent and severity of a flood. The full SWE set is therefore often used when simulating inundation.

Another popular approach is using the diffusive wave approximation to the shallow water equations (DSW). The diffusive wave approximation is derived by assuming the exchange of horizontal momentum is dominated by gravity, friction, and pressure. This assumption effectively allows one to neglect the local acceleration term

*HEC-RAS is freely available at <https://www.hec.usace.army.mil/software/hec-ras>

$\frac{\partial u}{\partial t}$ and the adjective acceleration term $u \frac{\partial u}{\partial x}$ of the momentum equation (equation 10). Due to this additional assumption, the DSW approach is less accurate than the full SWE approach. The DSW equations do, however, allow for more efficient solving and a larger time step.

The "no inertia" approximation is often justified by claiming the flooding plain area has a slowly evolving topography. However, whether this approximation still holds in urban areas is questionable. Costabile et al. (2017) compared the results of a measured experiment, the full SWE and the DSW approximation. The research concluded that the DSW approximation led to a poor description of inundation around buildings. This poor description is caused by the DSW approximations inability to capture shock waves around buildings. Detailed description may however not always be required for the flood susceptibility estimation, which is what is researched by this paper. The HEC-RAS manual (US Army Corps of Engineers, 2021) recommends to always apply both sets of equations and to only use the DSW approximation, if it proves to be valid for the task at hand. Using the full SWE with the same discretisation may however not always be computationally feasible.

In order to compare the practical usability of both the SWE and the DSW equations, runs of similar computational cost will be made with both approaches. This means that the computational efficiency of the DSW will be compensated by using a spatial resolution to represent the domain. Given the restrictions in computational resources, it was decided to use runs with a computational demand of around six hours on typical 4 core work laptop (it is worth mentioning that HEC-RAS allows for parallel processing). To achieve this computational cost the full SWE runs were made using a spatial grid with a resolution of $8m \times 8m$, while the DSW runs used a spatial resolution of $4m \times 4m$. These resolutions may seem relatively large, but HEC-RAS makes use of an elevation volume/area relationship to represent the underlying terrain of each cell more accurately (see US Army Corps of Engineers (2021) for more information). The traditional Eulerian-Lagrangian Method solver option (SWE-ELM) of HEC-RAS has been chosen over the Eulerian Method solver (SWE-EM), since it is more computationally efficient*. In both cases a time step was chosen based on stability.

2.6.2 The inundation domain

Ideally, one would model the entire rain catchment area in order to properly capture the catchment response to a precipitation event. Modelling the whole catchment surrounding Eastbourne would however require more computational power than is available. Since the flood susceptibility of the whole of Eastbourne is estimated, it makes sense to model all areas within Eastbourne with a relatively high flood risk (defining risk as susceptibility · consequence).

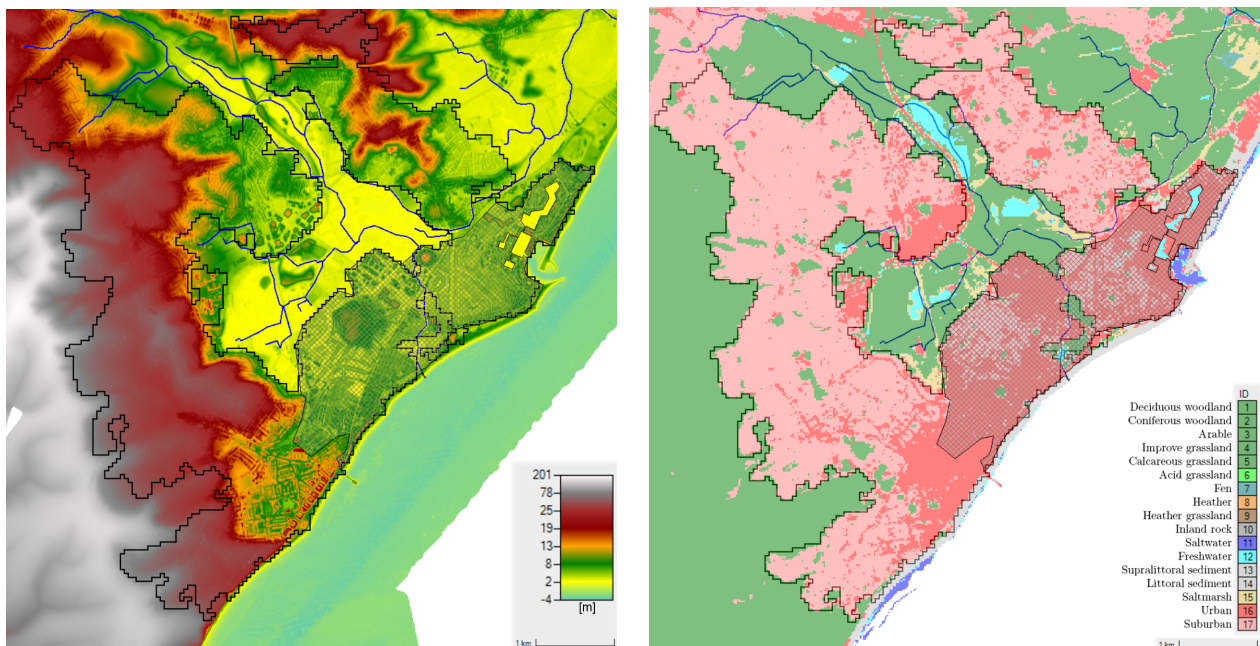


Figure 12: Left: Elevation of Eastbourne; Right: Land cover of Eastbourne

*The exact discretisation methodology of these solvers could not be cited, since they have not been publicly published by the US Army Corps of Engineers.

The flood susceptible area (and thus the inundation domain) of Eastbourne is estimated based on elevation data (figure 12, left) and land cover data (figure 12, right). Larger versions of these maps are visible in appendix E.6. The north and east sides of Eastbourne have large topographic gradients. Severe inundation is unlikely to occur in these areas, since water can flow downstream easily. In the middle of Eastbourne (technically outside of the town borders) we find large flat fields. These fields are likely susceptible to fluvial flooding, but the economic and non-monetary consequences are relatively low. This case study will thus focus on the urban and sub-urban south-eastern part of Eastbourne (the hashed region in figure 12). This susceptible area with high monetary and non-monetary value (thus high risk) will be used as the inundation domain.

A numerical inundation model requires land cover data to estimate the imperiousness and roughness of the cells. This research makes use of the UKCEH LCM2019 data (UK Centre for Ecology & Hydrology (UKCEH), 2020) which does not have standard and published imperiousness and roughness values. Because of this, the UKCEH LCM2019 land cover types have been matched to their equivalent parts used by the US Army Corps of Engineers (2021). The used roughness and impervious values are presented in table 4.

ID	Name	N_{Manning}	%Impervious
1	Deciduous woodland	0.16	0
2	Coniferous woodland	0.16	0
3	Arable	0.05	0
4	Improve grassland	0.04	0
5	Calcareous grassland	0.04	0
6	Acid grassland	0.04	0
7	Fen	0.04	50
8	Heather	0.05	0
9	Heather grassland	0.05	0
10	Inland rock	0.03	0
11	Saltwater	0.035	100
12	Freshwater	0.035	100
13	Supralittoral sediment	0.03	0
14	Littoral sediment	0.03	0
15	Saltmarsh	0.07	75
16	Urban	0.2	90
17	Suburban	0.12	65

Table 4: Land cover classes from UK Centre for Ecology & Hydrology (UKCEH) (2020) with Manning coefficient and impervious percentages estimated based on the HEC-RAS 2D user manual (US Army Corps of Engineers, 2021)

After the Crumbles Sewer river enters the inundation domain it flows southwards until it eventually fills the Crumbles Pond at Princes Park. From the Crumbles Pond, water can flow via a 100 meter unnamed stream to a culvert, from which then flows into the sea. The culvert is a 2.3m square box culvert with tidal flap with a length of 243m Eastbourne borough council (1987). The invert of the culvert is fixed at $MSL - 0.03m$, although the EA Lidar DSM (1m) data (Environment Agency, 2020) suggests that a 17cm layer of sediment has formed over the years. The culvert is included in the inundation modelling via normal 2D flow between cells.

2.6.3 Overtopping boundaries

At the coastal boundaries of the inundation domain overtopping can occur. The three overtopping estimation methodologies discussed in section 2.5 give constant average overtopping rates given a constant coastal forcing (the peak of the storm). In order to be conservative, the largest overtopping rates of the 3 overtopping methods have been selected per scenario. For estimation of overtopping discharge over the course of a coastal storm, use is made of the DNV recommended typical significant wave height design storm profile (figure 13)(Nestegård et al., 2006). The profile is based on a single tidal cycle with a peak lasting six hours.

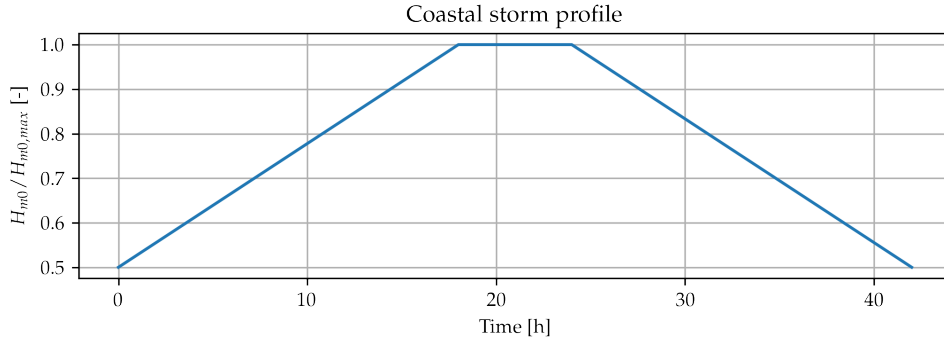


Figure 13: Coastal storm profile expressed relative to the maximum significant wave height from [Nestegård et al. \(2006\)](#)

Using this storm profile, one could estimate the overtopping rates using all three overtopping methodologies as they vary over time. This would be a relatively easy task using the empirical formula (discussed in section 2.5.2), a somewhat more complex task using the GPE (discussed in section 2.5.3) and a very difficult task using the numerical model (discussed in section 2.5.4) due to the required computational demand. Hence, it was decided to calculate a dimensionless overtopping profile by calculating the time varying overtopping rate via the overtopping formula (equation 2) and dividing it over its maximum value. The end result of this approach are storm profiles very similar to figure 13, but expressed in overtopping discharge instead of significant wave height (see figure 14). These profiles can simply be multiplied with their respective constant overtopping rates (discussed in section 3.3).

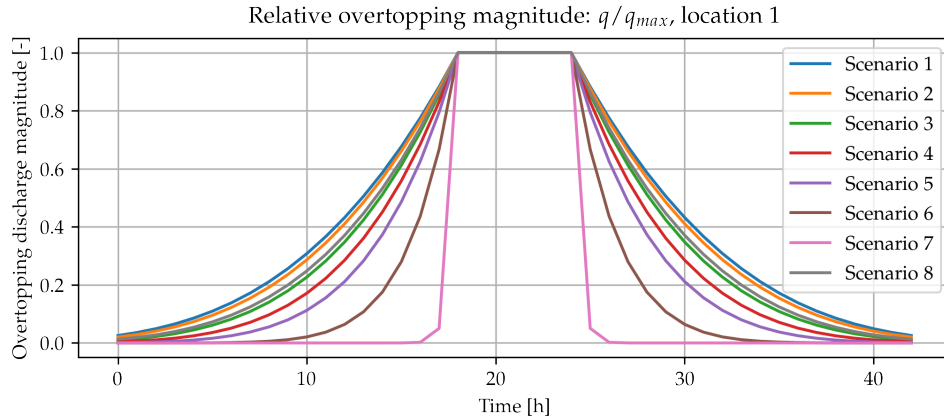


Figure 14: Coastal storm profiles expressed relative to the maximum overtopping rates calculated with the overtopping formula (equation 2).

One can calculate the total input discharge of the overtopping boundaries by multiplying the specific discharges per meter with the lengths of the shoreline segments, and summing them. Such plots give a general description of the overtopping boundary and are included in the boundary summary plots shown in appendix E.7.

2.6.4 Precipitation boundary

The data analysis (described in section 2.3.3) yields scenarios with a constant peak precipitation rate (similar to the peak overtopping rate as described in section 2.6.3). One may expect, since decoupled hourly data is used, that the found storm scenarios should also have a duration of around 1 hour. The reanalysed ERA5 data does however not represent short but intense precipitation events properly. One can investigate this property further by creating intensity-duration-frequency (IDF) curves with both the reanalysed ERA5 data and locally measured data (see figure 15). These curves have been created with python code based on scripts written for the Imperial College module "CI9-EE-21 Rainfall-Runoff Modelling and Flood Hydrology" by Dr Athanasios Paschalis.

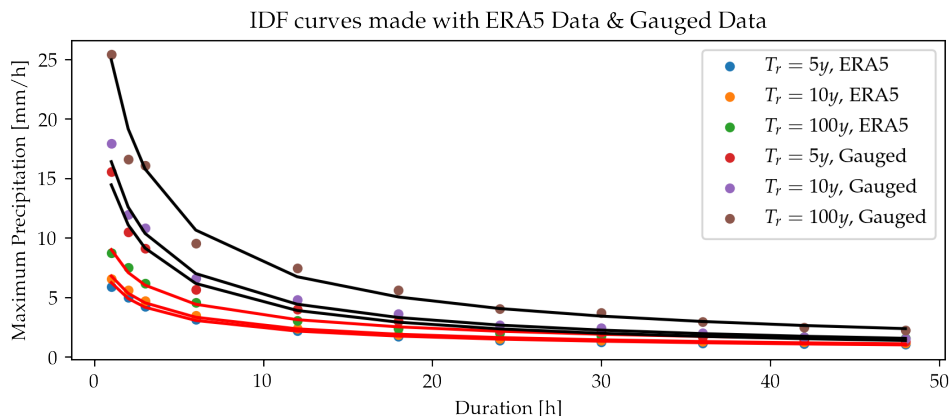


Figure 15: Intensity-Duration-Frequency (IDF) curves made with ERA5 data (red) and gauged data (black).

One can see from figure 15 that the reanalysed ERA5 data does indeed severely underestimate, especially the shorter duration events. Estimating the precipitation event duration based on the reanalysed ERA5 data, would thus misrepresent the severity of the storms. This is why the decision was made to use locally measured data instead of reanalysed ERA5 data.

IDF curves like the ones of figure 15 have been used to find realistic rainfall event durations that fit with given rainfall intensities and return periods. Precipitation intensity values are taken from the extreme value analysis results (see section 3.1.2) and fitting return periods are found from the original marginal (Pareto) distributions. Now with the return periods and precipitation intensities determined, one can use IDF curves based on measured data to find realistic precipitation event durations. The found durations using this method range between 5 and 13 hours and seem reasonable.

Following the current design practice, a specific design precipitation storm profile type is used. The UK's flood estimation handbook recommends using a hyetograph profile of the form as shown in figure 16, which is implemented in this research (Kjeldsen, 2007). Looking at the worst coastal storms and rainfall events, no clear evidence suggesting a certain amount of time-lag was found. Because of this is chosen to synchronise the peaks of the precipitation event and the overtopping.

By multiplying the precipitation intensity with the total area, one can calculate the total influx of water as a discharge. This discharge has been plotted over time and is visible per scenario in the boundary condition summary (appendix E.7).

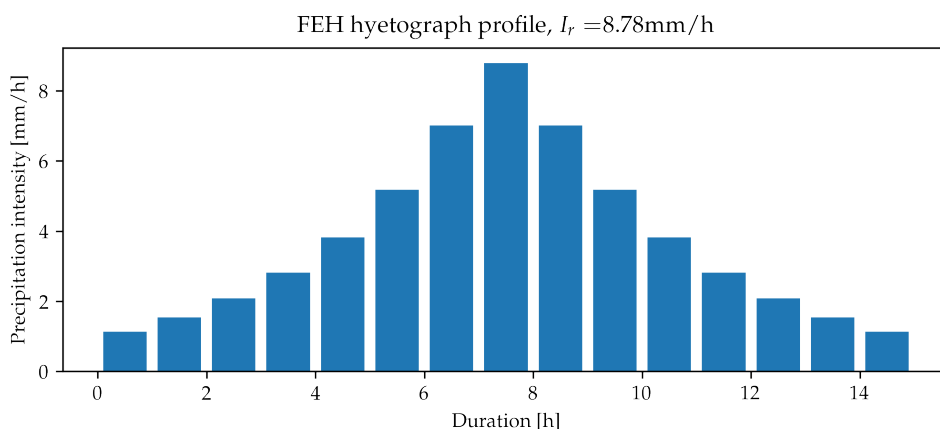


Figure 16: Precipitation hyetograph block profile of scenario 7 based on Kjeldsen (2007)

2.6.5 River boundaries

There are two types of river boundaries within the inundation domain; namely, an upstream boundary and a downstream boundary. Firstly, there is a single upstream river boundary within the domain where the Crumbles Sewers meets the northern domain edge. Making a worst case scenario assumption, the water level

at this boundary is fixed around 10cm below ground level (at $MSL + 2m$) for each scenario. Representing the catchment response to precipitation via empirical relations has been considered, but was turned down due to time constraints.

Secondly, there is one downstream boundary where the culvert of the Crumbles Pond meets the sea. The sea level during the computation is simulated as a simple M2 tidal cycle + an additional storm surge level outputted by the SWAN model. The tidal cycle is synchronised with the coastal forcing since the storm profile (figure 13) is based on a single tidal cycle. This water level boundary is shown per scenario in the boundary condition summary (appendix E.7).

Additional tidal amplitudes are as likely to increase the water level as they are likely to decrease it, which is why they have been omitted. The susceptibility of Eastbourne to tidal flooding is not further investigated within this research.

2.6.6 Flood severity comparison

Expressing the severity in a simple comparable manner is less straightforward than one may think. Inundation maps are very insightful and convey especially much spatial information, but they are difficult to compare. Hence, the decision is made to create inundation curves showing the percentage of area versus the minimal inundation height as well. Inundation of non-urban area is filtered out in these curves since the consequences of flooding non-urban area are generally much lower than urban/sub-urban area. Figure 17 shows an example of such curves as flood scenario 1 progresses over time. It shows, for example, that about 8% of the domain had an inundation of at least 0.5m (whilst being classed as urban/sub-urban), at 1 day and 5 hours into the simulation (the red line). The red line shows the moment in time at which the volume of water within the inundation domain was at its maximum. This snapshot of the flood event is chosen to represent the worst moment and will be used in the comparison.

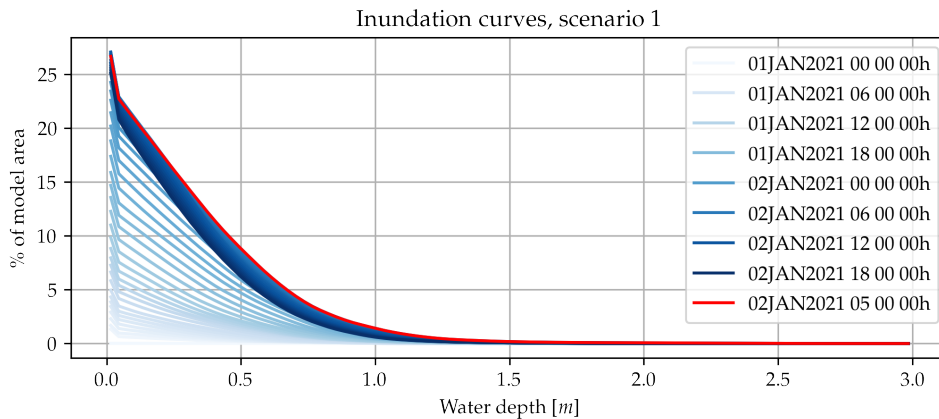


Figure 17: Inundation curve showing the percentage of the area against the minimal inundation depth as scenario 1 progresses over time. Start of scenario at 01-01-2021 00:00:00. Red line: Maximum water volume inside the domain

3 Results

The results of this research have been divided in four sections. Firstly, section 3.1 discusses the results of the statistical analysis and the created storm scenarios. Secondly, section 3.2 discusses the output of the wave model SWAN, which is used as the boundary condition for the overtopping estimation methodologies. Thirdly, section 3.3 discussed the output of the three overtopping estimation methodologies. Lastly, section 3.4 discusses the inundation maps, the inundation curves, and compares these based on the two governing equations.

3.1 Statistical analysis and model scenario selection

The first sub-question as defined in section 1.2, is: "How to generate representative storm scenarios?" In order to answer this question one should first research local historical data, followed by the creation of various scenarios. The results of an exploratory data analysis are presented in section 3.1.1, whilst the scenario creation results are presented in section 3.1.2. This first sub-question is further addressed in section 3.4, which discusses the inundation severity of the various scenarios.

3.1.1 Exploratory data analysis

An exploratory data analysis for the creation of model scenarios has been conducted in two stages. In the first stage the general dependence structure is analysed by interpreting the correlation matrix containing various input variables (figure 18). In the second stage the extremal dependence is further analysed by calculating the Spearman correlation over a rolling window. A closer look is then taken at the relationship of precipitation and wave height by conditioning the significant wave height distribution on precipitation (figure 19).

General dependence structure

The first step of the exploratory data analysis is analysing the general dependence structure of the variables via a correlation matrix. The entire correlation matrix is visible in appendix E.1 and a smaller matrix is shown in figure 18. First of all, we can clearly see a very strong dependence between the significant wave height and the mean wave period. This is what one would expect because higher waves are longer as well and will therefore have larger periods (Holthuijsen, 2007).

Secondly, we find another very clear dependency between the significant wave height and the wind speed. This makes much sense as well since the wind generates wind waves (which dominates over swell).

Thirdly, we find a very clear dependence structures between high waves and winds towards a direction around $-1.23rad$ from north. This means that very high waves ($> 5m$) have only been generated in case of a south-westerly wind. This make much sense when looking at geometry of the English channel (figure 3). A wind from the south-east has more fetch length than from any other direction. Waves can also be generated from the north-east, but these waves cannot grow as big since they have to pass the narrow part of the channel at Dover. Including a north-easterly storm scenario is however interesting, since Eastbourne does not have any natural protection (cliffs) against these storms.

Lastly, no very clear dependence structure can be observed related to precipitation from these plots. It looks like there may be some positive dependence between precipitation and wind speed, but no conclusions can be derived from this. The next section investigates this relation further.

Correlation matrix

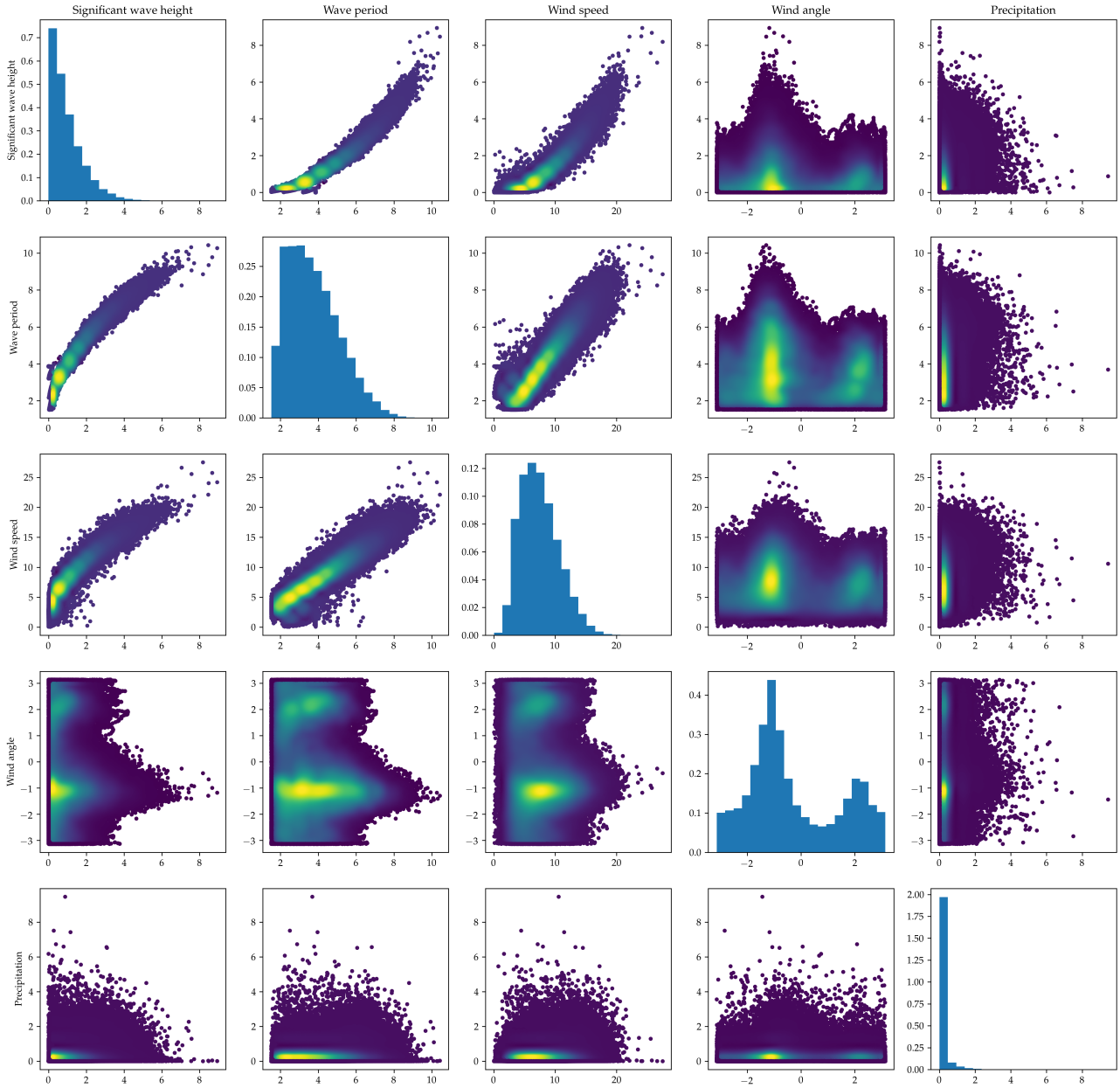


Figure 18: Correlation matrix showing dependence structures of various input variables

Tail dependence

A very intuitive manner of describing tail dependence is by plotting the discrete conditional probability density distributions of two variables. Figure 19 shows the probability density distribution of the significant wave height conditioned on the precipitation. One can clearly see that a higher precipitation condition does also lead to a higher chance of large waves.

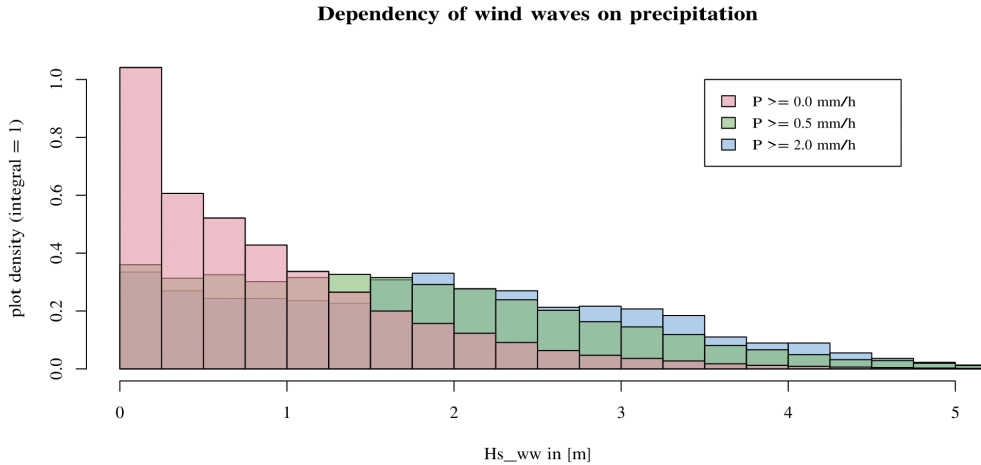
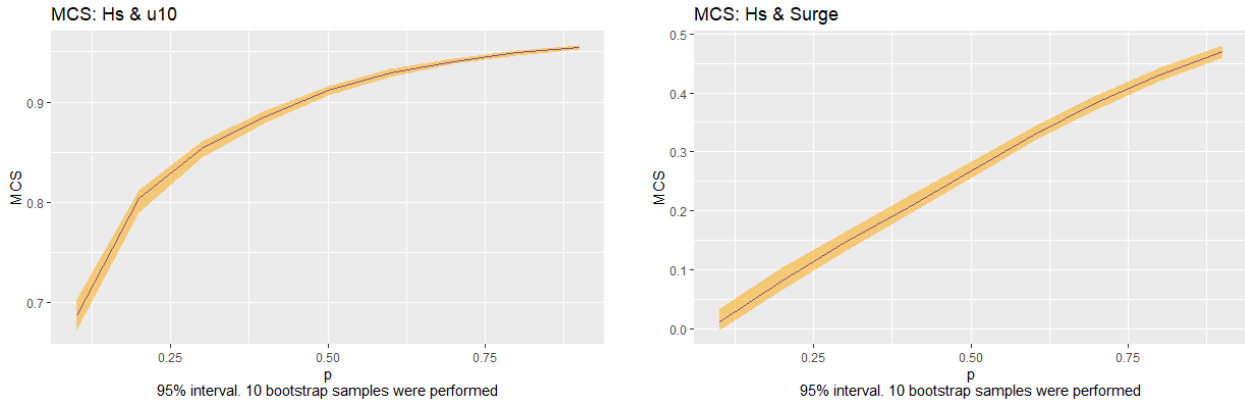


Figure 19: Distribution of the significant wave height of wind waves conditioned on precipitation

A more formal way to illustrate a tail dependence structure is via χ & $\bar{\chi}$ plots following Coles et al. (1999) or by plotting the multivariate conditional Spearman's correlation coefficient (MSC) over a sliding window following Schmid & Schmidt (2007). Both methodologies have been implemented in the `texmex` package of the programming language R. Plots of the latter approach are shown in figure 20 and 21. The χ & $\bar{\chi}$ plots have also been made and gave similar results, which is why they have been omitted.



(a) MSC on a rolling window illustrating very strong positive tail dependence between H_{m0} and u_{10} .

(b) MSC on a rolling window illustrating moderate positive tail dependence between H_{m0} and storm surge.

Figure 20: The bivariate case of the multivariate conditional Spearman's correlation coefficient (MSC) over a rolling window showing the extremal dependency of u_{10} on H_{m0} (20a) and storm surge on H_{m0} (20b).

In the bivariate case, the MSC as defined by Schmid & Schmidt (2007) is an alternative to the traditional Spearman's ρ coefficient and can be interpreted as such. The Spearman correlation coefficient is bounded by $[-1, 1]$, which indicates a perfect Spearman correlation (the variables are perfect monotone functions of each other). Using a sliding window of data is a way of showing tail dependence. One calculates the MSC value multiple times whilst conditioning on both variables as we require them to be larger, similar to what is done in figure 19.

Figure 20 shows 2 clear examples made from the ERA5 data close to Eastbourne. Figure 20a shows the relation between the significant wave height and the wind speed at 10m. We see an already relatively strong

Spearman correlation coefficient of around 0.7 when using all data (0th percentile). However, as we move further up the tail, and require both variables to be large, we see this coefficient increase even further. This shows that during mild conditions there is some correlation but also some randomness. However, when high waves or fast winds occur, then there is an even stronger dependency.

We find a similar relation when looking at the MSC's between the significant wave height and storm surge in figure 20b. When including all data, we find almost no correlation at all. But, as we move further up the tail of the distributions, we see a clear increase of the correlation. This makes perfect sense as well, since (wind) waves and surge are both driven by the wind. Including all data means that many calm sea states are included, which again means much randomness. And this random part is once again removed as we require our variables to be larger.

Now, having illustrated the concept of the MSC on a sliding window with two relatively trivial relationships, we once again look at the relationship between the significant wave height and precipitation. Including all data we find a very mild MSC of around 0.1. However, similar to the previous two cases, we find that the correlation coefficient goes up as we require the variables to be larger. This can also be explained from a physical standpoint; the amount of precipitation which can fall is dependent on the amount of moisture content carried by the wind. More wind will thus both increase the (wind) wave height and the influx of moisture content, which in turn leads to precipitation.

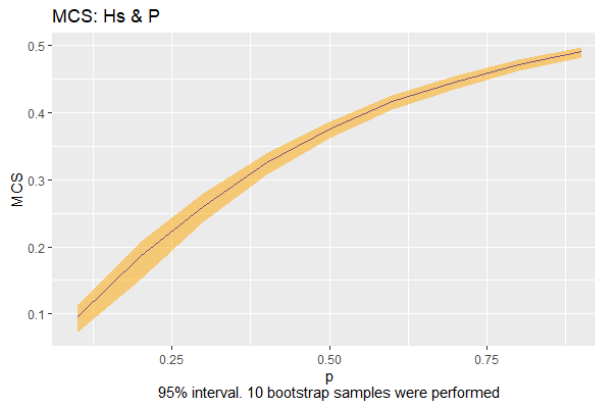


Figure 21: MSC on a rolling window illustrating a moderate positive tail dependence between H_{m0} and precipitation.

A positive tail dependence indicates that one should not assume the significant wave height and the precipitation intensity to be independent when considering large values. Making this assumption regardless would lead to an underestimation of especially compound flood events. The susceptibility of Eastbourne to such events is further investigated in section 3.4.1.

3.1.2 Scenario creation

The primary variables, as defined in section 2.3.3, of this research are the significant wave height (H_{m0}) and rainfall intensity (I_r). By applying the conditional approach (Heffernan & Tawn, 2004), one can represent the dependence structure of variables and use it to simulate more (synthetic) samples as is explained in section 2.3.3 and appendix B. Using both the synthetic samples and the measured samples one can create joint exceedance curves with fixed return periods. The mathematical description of such plot is $P(H_{m0} \geq x, I_r \geq y) = T^{-1}$.

Joint exceedance curves conditional on both H_s and P

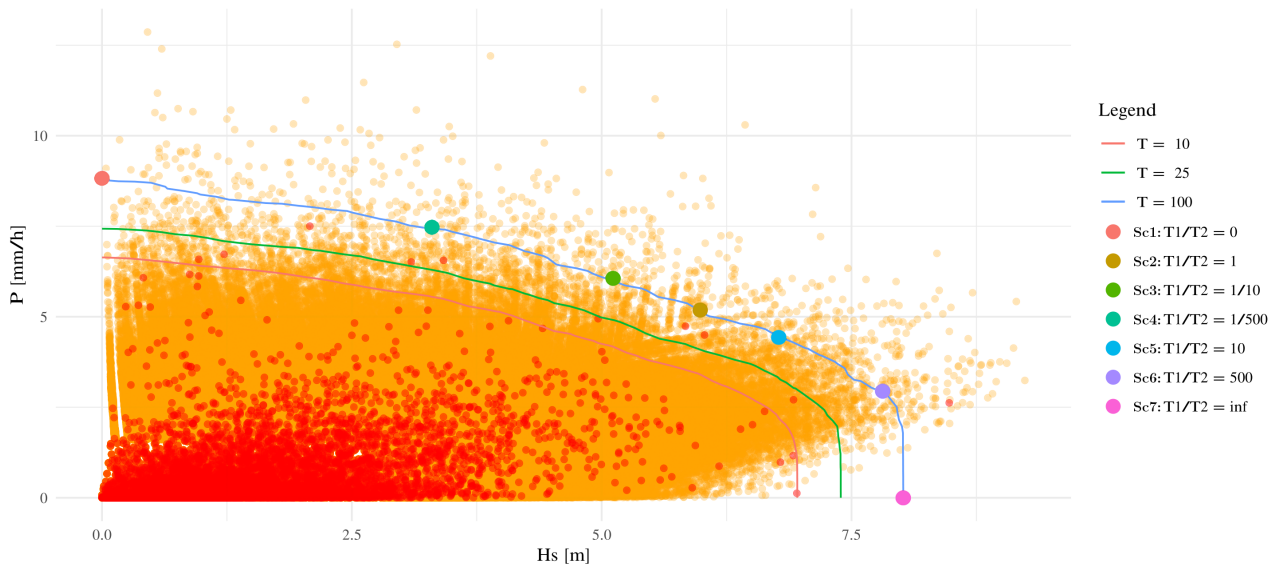


Figure 22: Scenarios with a return period of 100y created via the Heffernan & Tawn (2004) approach. Red dots: Era5 samples; amber dots: simulated samples

Figure 22 shows the 7 south-westerly storm H_{m0} and precipitation scenarios as defined by their return period ratio in table 1 of section 2.3.2. The added benefit of using the joint exceedance curves is that the limits (the red marker and pink marker in figure 22) describe the singular marginal (Pareto) distributions. This means that the conditional approach effectively includes the univariate approach (as explained in section 2.3.3). The downside of this is that the limits may not be very realistic scenarios.

Figure 22 also clearly illustrates the positive dependence between significant wave height and precipitation at Eastbourne, as was predicted by the results of the exploratory data analysis (section 3.1.1). We see especially clearly that extreme high waves ($H_{m0} > 7$) are almost certainly accompanied by some precipitation. Only treating a singular coastal scenario without any precipitation would thus be unwise.

Secondary variables are defined as variables chosen based on their dependence structure with a primary variable. The likeliest value of a secondary variable is chosen, given a determined value for the primary variable that has the strongest physical relationship. Primary variable values are the scenarios given in section 22. The method used to estimate the likeliest secondary variable values is summarised in section 2.3.3 and further explained in section B. By applying this methodology, the full scenario input conditions are found. These scenarios are shown in table 5.

Scenario	$RP_{H_{m0}}/RP_{I_r}$	H_{m0}	I_r	$T_{m-1,0}$	surge	$\theta_{peak} [^\circ N]$	$\ u_{10}\ $
1	∞	8.02	0.	9.50	0.97	-70.32	24.73
2	500	7.81	2.93	9.48	0.88	-70.32	24.26
3	10	6.77	4.41	9.03	0.76	-70.32	22.23
4	1	5.99	5.16	8.62	0.64	-70.32	20.41
5	1/10	5.12	6.03	8.05	0.57	-70.32	18.71
6	1/500	3.30	7.43	6.84	0.43	-70.32	14.76
7	0	0.	8.78	6.55	0.26	-70.32	12.69
8	∞	5.87	0.	7.88	0.69	117.46	19.58

Table 5: Scenario input conditions*

The scenarios in table 5 match the findings of the exploratory data analysis. We find that scenarios with a high significant wave height (H_{m0}) have a longer wave period ($T_{m-1,0}$), a higher storm surge (*surge*) and a stronger wind speed ($\|u_{10}\|$). Notable is the wave period of scenario 8 (north-easterly storm). The north-easterly storm appears to have a shorter wave period with regard to its wave significant height, indicating a higher wave steepness (Wave height over wave length) than the south-westerly storm variant.

*The wind direction and the wave direction showed an almost 1 to 1 dependency, which is why only one directional variable has been included in the scenario definitions.

3.2 Nearshore wave model (SWAN)

The nearshore wave model SWAN is applied in 2D to estimate wave conditions for overtopping at the three different shoreline segments (location 1 to 3). Figure 23 shows an example of the 2D output SWAN gives. The output locations for the empirical formula and the GPE is at the toe of the beach*, whilst the numerical approach uses the conditions at 2km from the shoreline.

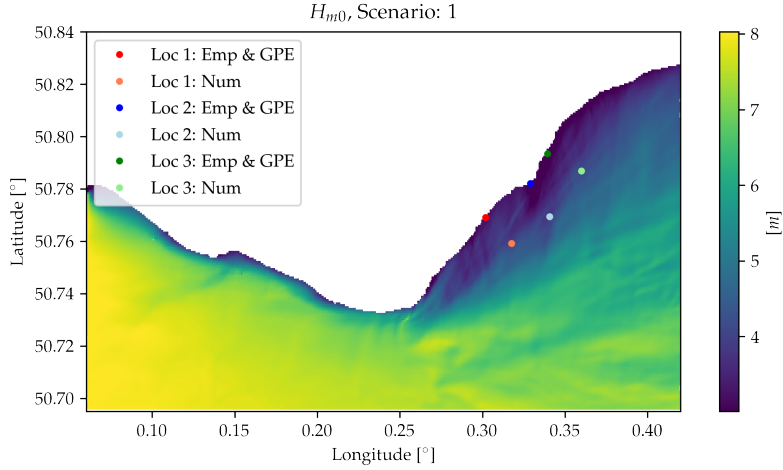


Figure 23: 2 dimensional SWAN output showing the evolution of the significant wave height (H_{m0}) in scenario 1. The various colored markers indicate the coupling points for the overtopping methodologies.

Sea state at the toe used by the empirical formula and the GPE

It would be difficult to interpret the sea state from tables since it is described by several variables for 3 locations and 8 scenarios. This is why these values are given in the form of a plot. Figure 24 shows the variables as used by the empirical formula of equation 2 and figure 25 gives two alternative variables used by the GPE.

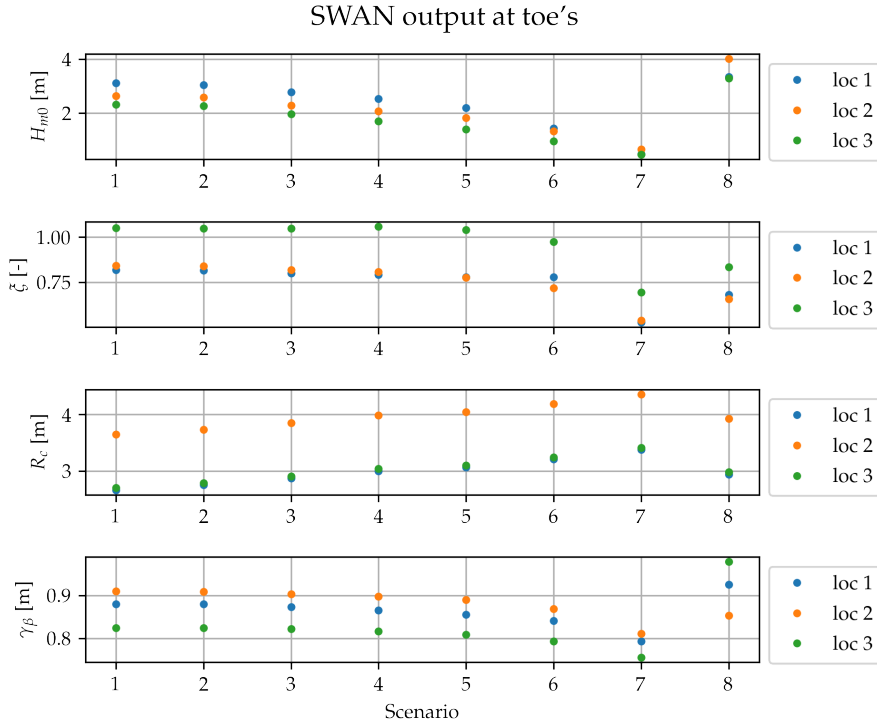


Figure 24: SWAN output at toe's used for overtopping estimation via the empirical formula and the GPE

*The overtopping formula (equation 2) and Bayonet GPE are both supposed to make use of wave input at the toe of the structure. However, in the case of a beach the exact location of the toe is somewhat dubious. The eventually used location was the edge of the SWAN domain ($MSL - 2m$ to $MSL - 3m$).

Significant wave height (H_{m0}): Notably, scenario 8 has a higher significant wave height than scenario 1 at the coupling point, even though scenario 1 has a higher significant wave height at the sea boundary. This is due to a large amount of refraction since the coastline of Eastbourne is sheltered by cliffs in case of south-westerly storms.

Iribarren number (ξ): The Iribarren numbers decrease as the scenarios get milder from 1 to 7, this is due to a decrease in wave period as we see in figure 25. Notable is the lower Iribarren number of scenario 8. Easterly storms have a somewhat larger wave steepness than westerly storms as was shown in the data analysis (section 3.1.2). One can also see that location 3 has a systematically higher Iribarren value, which is caused by a steeper beach profile.

Crest level relative to SWL (R_c): The crest levels increase as expected when storms get milder. Notable is location 2, which has a crest level almost a meter higher than locations 1 and 3.

Oblique wave reduction factor (γ_β): We find an increasing overtopping reduction caused by the wave angle as the scenarios get milder. This is caused by waves turning more towards the in the case of longer and higher waves than in the case of shorter and smaller waves. Scenario 8 has very different values since this is an easterly storm (opposing the westerly storms modelled in scenarios 1 to 7). We find lower reduction values for Easterly storms since there are no cliffs sheltering the Eastbourne from the east side.

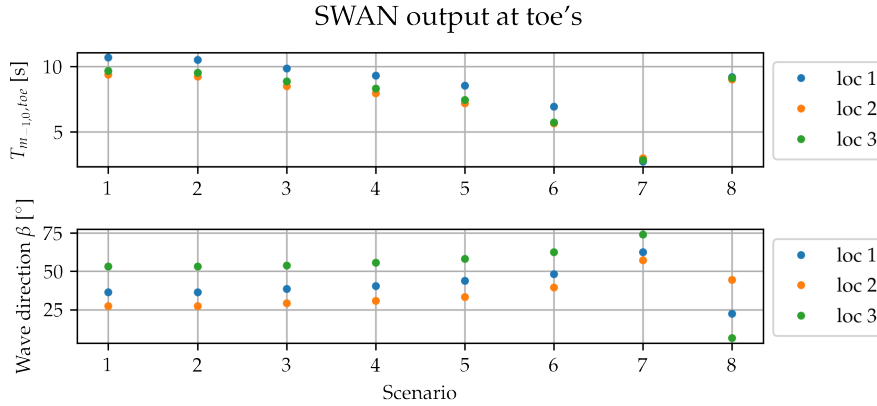


Figure 25: Additional SWAN toe output for Bayonet GPE

Input of the numerical approach

Instead of using parametric input, as is used by the empirical formula and the GPE, the SWASH model allows for spectral input. Spectral input allows for a more accurate description of the sea state. The spectral input method does not use a single wave height (such as the significant wave height (H_{m0})) and a single wave period (such as the mean wave period ($T_{m-1,0}$)) to represent the distribution of energy of a sea state. Instead SWASH uses the distribution of wave energy expressed using the variance density over the wave frequency.

Figure 26 shows the wave spectrum input of scenario 1 to 8 at location 1. Appendix E.5 shows the wave spectra of all scenarios for all 3 locations. Notable is scenario 8, which has more energy and a higher peak frequency. This indicates scenario 8 has high waves, which could cause more overtopping. However, it also shows scenario 8 has shorter wave periods, which is known to reduce overtopping.

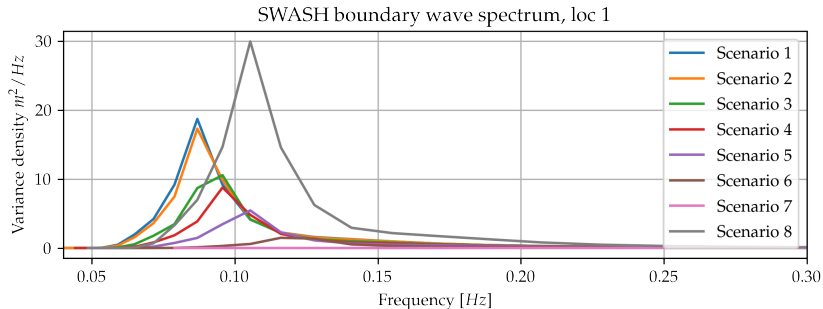


Figure 26: Example of SWASH wave spectrum input, location 1

3.3 Overtopping results and comparison

This section addresses the results regarding the second sub-question as defined in section 1.2: "How do different overtopping estimation methodologies compare to each other?" First, the necessity of correcting the numerical approach with regards to refracting and breaking is discussed, after which the overtopping results are given. These results consist of a comparison of the outcomes of the three different overtopping estimation methodologies as defined in section 2.5, and an analysis of this outcome.

3.3.1 Correcting the numerical approach for refraction and breaking

Explicit correction for refraction

Eastbourne lies relatively sheltered by cliffs from the typical south-westerly storm. Initial results showed that this caused a substantial amount of refraction. Since a one dimensional approach is incapable of implicitly including this phenomenon, it was decided to use an explicit correction methodology as explained in section 2.5.4. Applying this method gives frequency dependent refraction coefficients. Figure 27 shows the found refraction coefficients at location 1 as an example. Note that the wave spectra, used as input for *SWASH*, are multiplied with k_{ref}^2 since the wave energy is proportional to H_{m0}^2 . The refraction curves of all three locations are visible in appendix E.2. Especially shorter waves seem to be susceptible to dispersion by refraction.

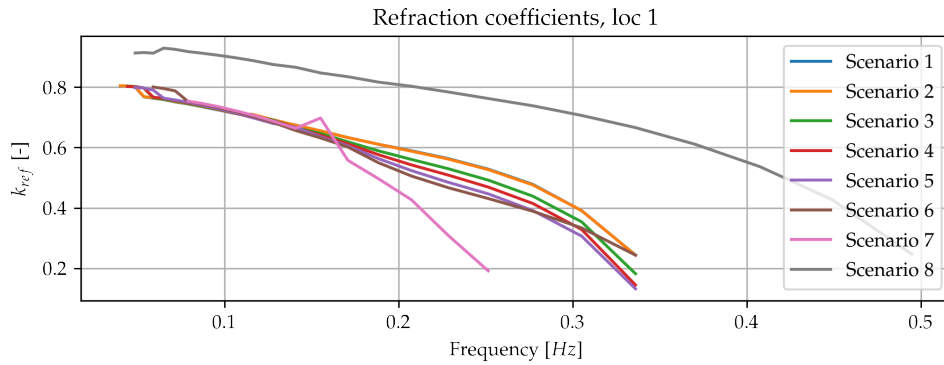


Figure 27: Example of frequency varying refraction coefficients, location 1. Scenario 1 and 2 overlap almost exactly.

Figure 28 shows an example of how this approach affects the significant wave height evolution. The blue line shows the significant wave height over a shore normal cross section as calculated by a 2D wave model (*SWAN*). The orange line shows the overestimation one finds if the entire 1D wave spectrum is forced in a 1D wave model run. The green line shows this same 1D wave model run, but now including the explicit refraction induced wave spectrum reduction as formulated in equation 8. This 1D wave model run seems much more representative and finds a very similar significant wave height value at the end of the *SWAN* domain. This confirms that \tilde{m} significant wave height reduction was caused by refraction. It also shows that the approach results into a seemingly very reasonable estimate. The red line shows the significant wave height evolution as estimated by a 1D numerical model run that includes the explicit refraction. This run finds a somewhat higher value. This actually expected since wave models (spectral action balance solving models) do not include infra gravity waves, whilst *SWASH* does capture this energy.

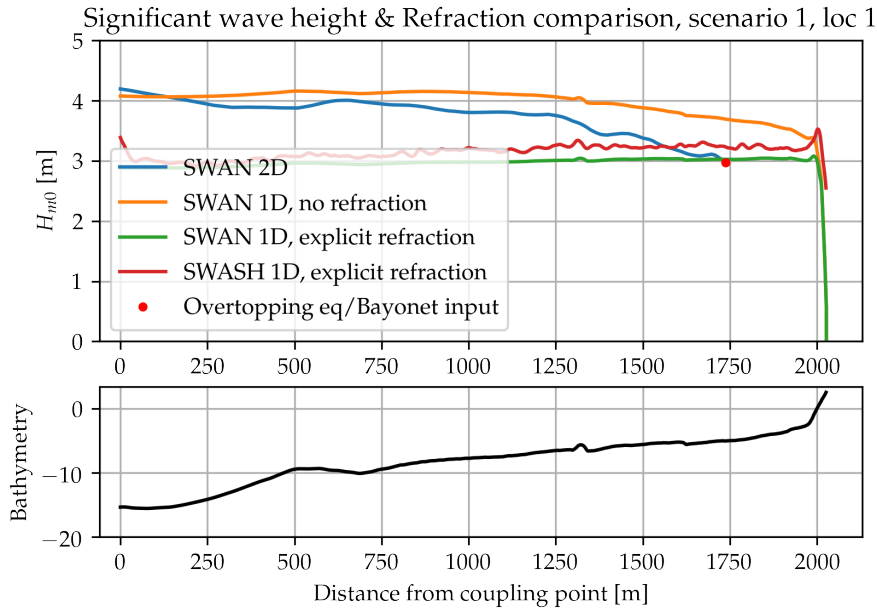


Figure 28: Significant wave height (H_{m0}) comparison showing the effect of refraction

Correction for accurate depth induced breaking

Initial results showed that using only three vertical layers did not lead to an adequate representation of depth-induced wave breaking. *SWASH* offers to option to use additional breaking parameters to force breaking using a hydraulic jump analogy (Smit et al., 2013). The α_{break} parameter gives a range of maximum steepness requirement, whilst the β_{break} parameter gives a reduced maximum steepness requirement for active cells.

This approach is illustrated in figure 29 by comparing the significant wave height evolution of normal simulations made 3 layers, 20 layers, and a simulation made with 3 layers while using fitted breaking parameters. It is important to note that the break parameters are chosen in such a way to represent the wave climate at the coastline and not further off shore. The breaking parameters giving the best results were $\alpha_{break} = 0.28$ & $\beta_{break} = 0.14$.

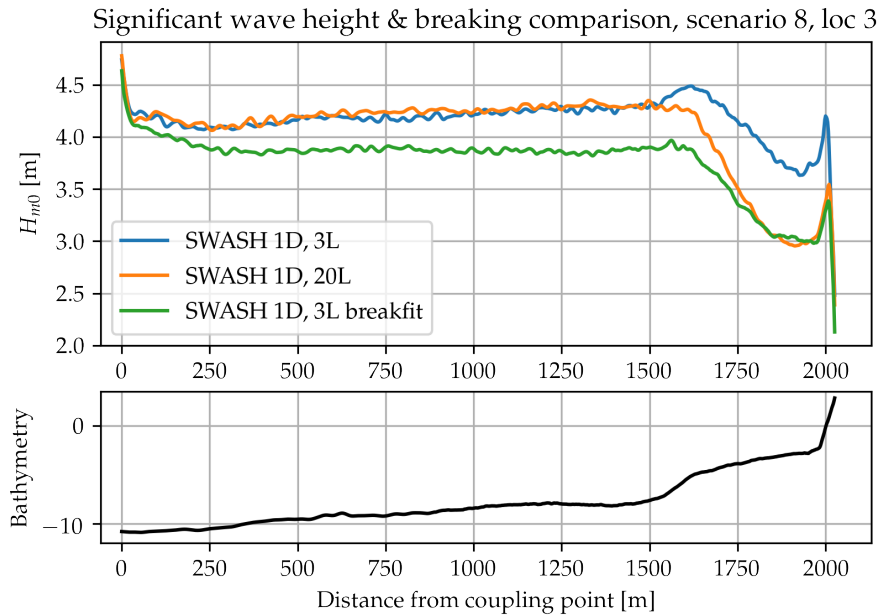


Figure 29: Significant wave height (H_{m0}) comparison for breaking behaviour

3.3.2 Overtopping estimations

The average overtopping rates for the 8 different scenarios, the three different methodologies and the three main locations are presented in plot form in figure 30. This plot form has been chosen over a traditional table, since a table would be relatively large and difficult to interpret.

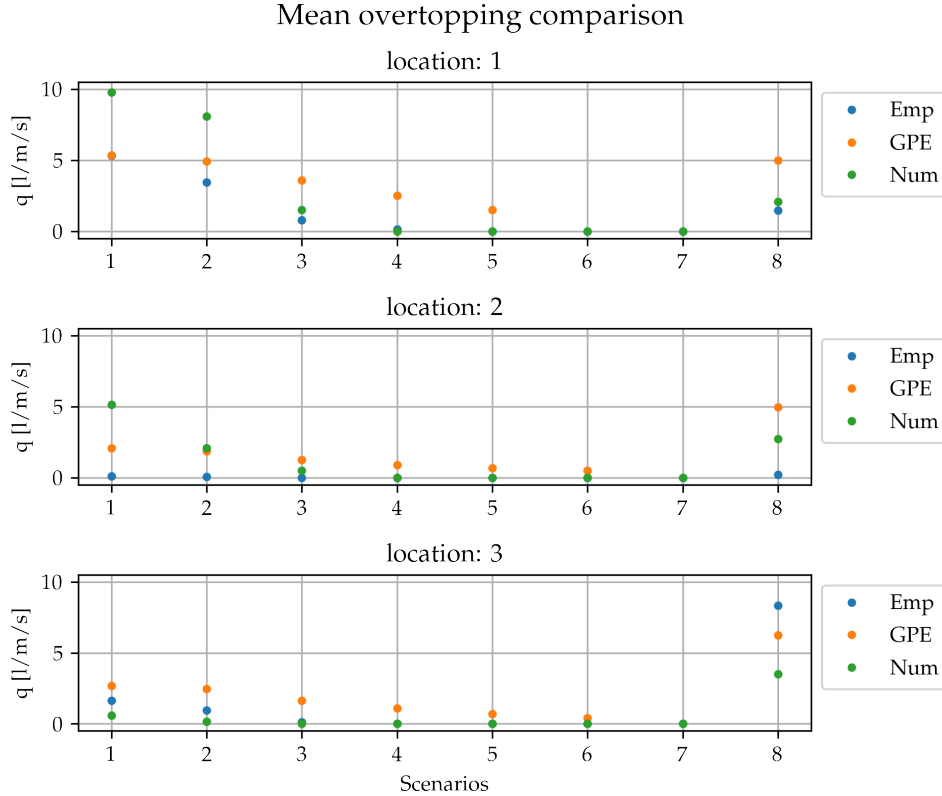


Figure 30: Comparison of the average overtopping discharge*

One can make various observations from these findings. The most notable remarks have been listed here.

1. The numerical models seems to agree relatively well with the empirical formula and the GPE.
2. The overtopping discharges for a $T=100y$ event seem to match with Eastbourne's coastal flood history. No coastal flood events, with a higher consequences severity classification than "Minor", have occurred at Eastbourne in recorded flood history (from 1915) (Haigh et al., 2017).
3. None of the methods exhibit a clear bias based on these results.
4. The numerical model finds slightly more overtopping at location 1 + scenario 1 and location 2 + scenario 2, which may be caused by the inclusion of the infra gravity waves.
5. The empirical equation finds almost no overtopping in location 2 (higher crest level), whereas the other methodologies do find some.
6. The three overtopping methodologies do not show the same behaviour for scenario 8.
7. GPE finds a higher mean overtopping discharge for scenario 8 than the other methods. The GPE does however state that this scenario is well within its training data (classified as green). Whereas all other scenarios were said to be acceptably close to the training data (classified as amber).

One can investigate the overtopping behaviour further by comparing the wave spectra of the SWAN and the SWASH model. The SWAN model can output the 1D (and 2D) directional spectra directly, whilst for the SWASH

***Note:** All three overtopping estimation methods are said to estimate the discharge accurately within a factor of 3 of the actual overtopping discharge (van der Meer et al., 2018)(Pullen et al., 2018)(Suzuki et al., 2017). This accuracy does however decrease for all methods when estimating low overtopping rates ($q < 1l/s$).

output Python code based on the scripts written for the TU Delft module "CIE4325 Ocean waves" by Dr. Marion Tissier and Prof.dr. Ad Reniers has been used. Figure 31 shows the wave spectra of the two models at the "toe" of the beach (the red dot in figure 28) during scenario 1 at location 1.

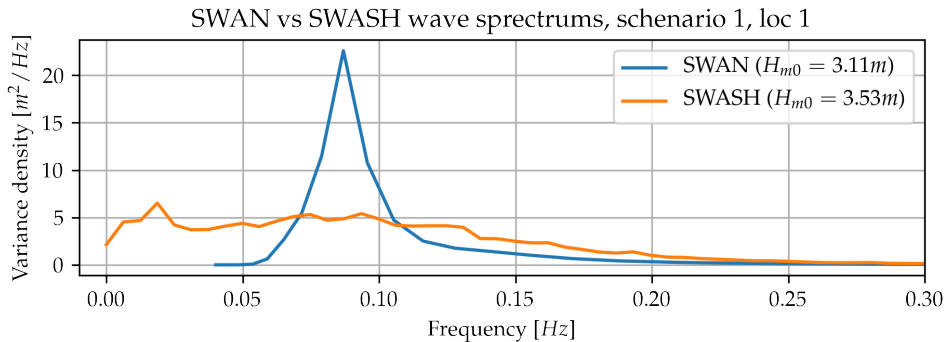


Figure 31: SWAN - SWASH wave spectrum comparison, scenario 1, location 1

Note that the empirical approach and the GPE both disregard the full (SWAN) wave spectrum and only use the significant wave height H_{m0} (given in the legend of figure 31) to represent wave energy. We find as expected no energy in the infra gravity domain (low frequencies) of the SWAN spectrum. Also, since triads are turned off, we find less energy in the shorter waves compared to SWASH. These two processes cause the SWASH spectra to be much wider than the SWAN spectra. However, both the empirical approach and the GPE (the approaches using SWAN input at the toe) do not include the width of the spectrum as input. The significant wave height calculated by the SWAN model is slightly lower than the SWASH estimation. This could very well be a consequence of the SWAN model not including infra gravity waves. This could also be the reason for the slightly lower overtopping predictions by the empirical approach and the GPE found at location 1 in scenario 1 (see figure 30).

Figure 32 makes the same comparison as figure 31, but for the north-easterly storm scenario at location 3. Location 3 is of special interest for this scenario since the wind and wave direction are almost exactly shore normal. Refraction reduces especially the wave energy of waves with a short period as has been shown by section 2.5.4 figure 27 (and appendix E.2). However, the lack of this reduction is not clearly visible from figure 32. The SWASH spectrum of figure 32 seems to remain somewhat more peaked than in figure 31. However, we do clearly see the same behaviour of the spectrum being flatter than the SWAN estimation due to the previously mentioned reasons. Notable for this scenario is that the numerical approach does not estimate the highest overtopping volume even though the significant wave height of the SWASH model is 0.54m higher at the "toe" of the beach. This is most likely caused by the high degree of uncertainty in all three approaches.

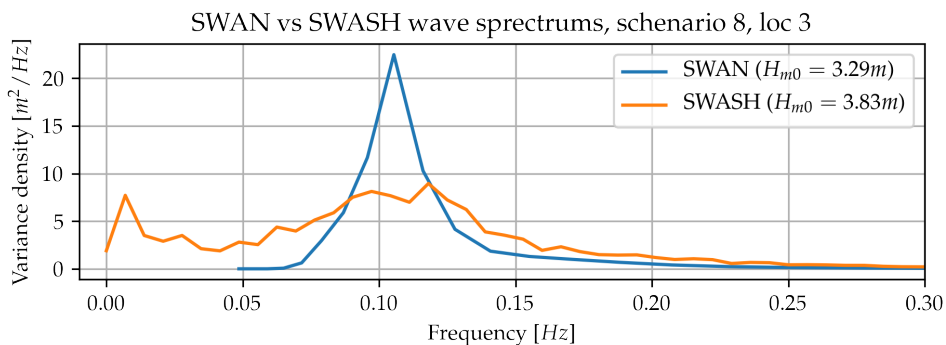


Figure 32: SWAN - SWASH wave spectrum comparison, scenario 8, location 3

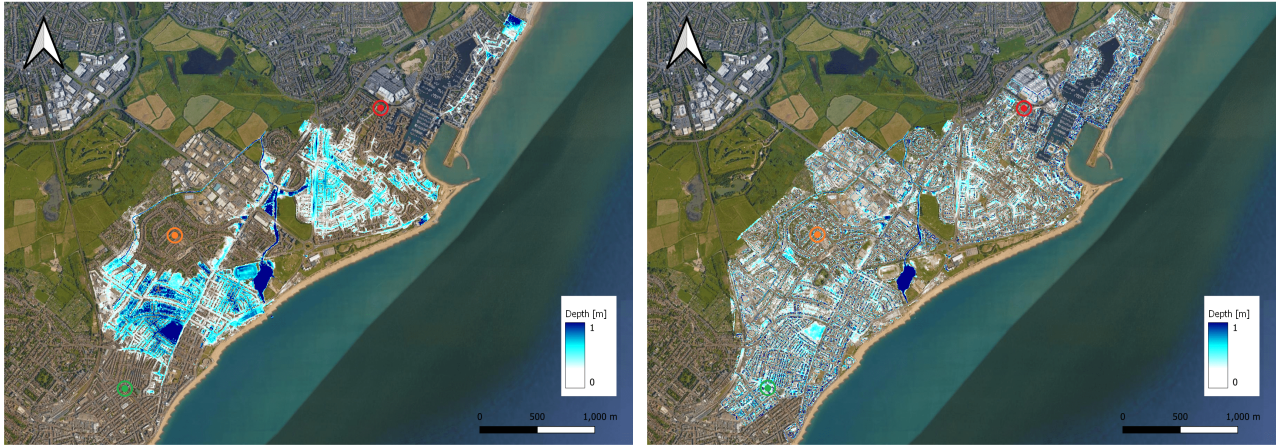
3.4 Inundation modelling

The inundation modelling results help with answering two sub-questions. Firstly, the first sub-question "How to generate representative storm scenarios?" will be addressed by estimating the inundation severity of the various scenarios in section 3.4.1. Secondly, the third sub-question "What set of governing equations should be solved when using numerical inundation modelling for the estimation of flood susceptibility?" will be addressed

in section 3.4.2. In section 3.4.2 inundation simulations made using two different governing equations (the full SWE and DSW) are compared and discussed.

3.4.1 Inundation severity estimation

Inundation resulting from the 8 different scenarios, as defined in section 3.1.2 by table 5, has been estimated using the methodology as described in section 2.6. The resulting inundation maps of all scenarios are visible in appendix E.8. Figure 33 shows the inundation maps of the two limit scenarios (scenarios 1 and 7) created via the univariate approach (as explained in section 2.3.3). These two maps illustrate the two different flood patterns caused by the two flood types (coastal and pluvial).



(a) Inundation extend of a once in 100 year coastal storm (Scenario 1) using DSW equations (b) Inundation extend of a once in 100 year precipitation event (Scenario 7) using DSW equations

Figure 33: Comparison of inundation caused by a coastal flood event (left) and pluvial flood event (right)

One can clearly see that the pluvial flood scenario (figure 33b) results into a more spread out inundation pattern. The reason for this is that coastal flooding is a much more local process than pluvial flooding. There are various clear regions which remain completely dry during the coastal scenario, but do flood due to ponding during the precipitation event. Clear examples are the area behind the harbour in the East (red marker), the hilly area in the south-west (green marker), and the elevated district (Roselands) in the west (orange marker). The two western areas remain dry during the coastal event due to their topography, whilst the area in the East is protected by the harbour (water can freely flow away into the harbour).

Inundation curves have been generated following the method as described in section 2.6.6. These curves (shown in figure 34) illustrate not only the extent of the flooding but also the severity. The y-axis of this plot gives the percentage of the flood domain, whereas the x-axis gives the minimal inundation depth found on that percentage of the flood domain. For example, scenario 1 resulted into around 8% of the inundation domain having an inundation depth of 0.5m whilst being classed as urban/suburban.

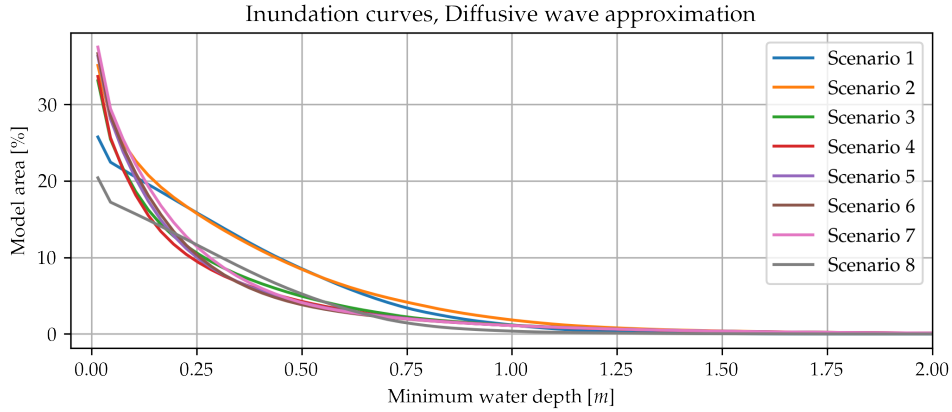


Figure 34: Inundation comparison of the 8 scenarios calculated via the DSW approximation on a $4m \times 4m$ grid. Scenario definition is shown in table 1 and the input conditions are given in table 5.

Based on the inundation curves of figure 34 one can make the following observations:

- The scenarios with intense coastal forcing lead to the most severe inundation. Scenario 2, a compound storm with intense coastal forcing and mild precipitation (defined via a return period ratio of $RP_{H_{m0}}/RP_{I_r} = 500$), leads to the most severe inundation.
- All scenarios with precipitation lead to more inundated area than scenarios without precipitation.
- A once in a hundred year south-westerly coastal flood (scenario 1) leads to more inundation than a once in a hundred year north-easterly coastal flood (scenario 8). This is most likely caused by the higher storm surge which is affiliated with the south-westerly storm and the lower wave period which is affiliated with the north-easterly storm.

3.4.2 Comparison of governing equations

Inundation curve comparison

The inundation curves show in section 3.4.1 (figure 34), were created by solving the diffusive wave approximation of the shallow water equations (DSW) with a $4m \times 4m$ (referred to as "high") spatial resolution. Figure 35 shows these same curves, but this time the full set of shallow water equations (SWE) have been solved with an $8m \times 8m$ (referred to as "low") spatial resolution. Both methods seem to yield similar results, but we can find some notable differences by subtracting the two results as is shown in figure 36.

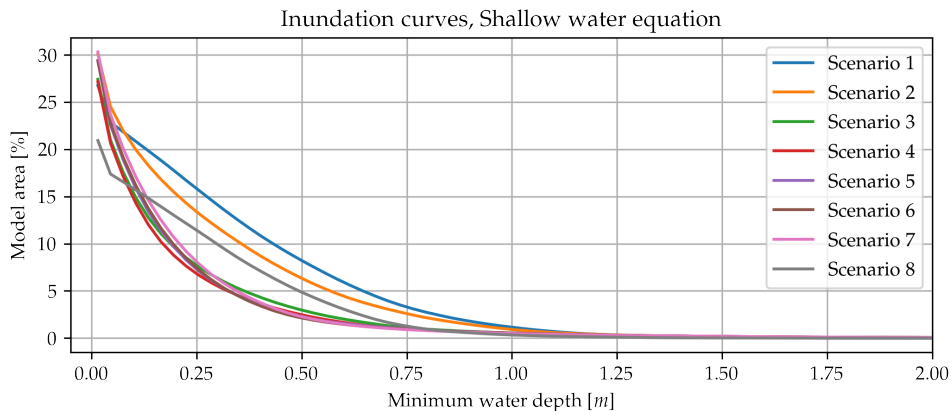


Figure 35: Inundation comparison of the 8 scenarios calculated via the SWE approximation on an $8m \times 8m$ grid

Figure 36 is the result of subtracting the low spatial resolution SWE curves (figure 34) from the high spatial resolution DSW curves (figure 35). Positive values do thus indicate that the DSW simulations find more inundation. The DSW simulation finds significantly more inundation for all scenarios with precipitation, whilst scenarios without precipitation seem to be less effected. This effect could be caused by the different governing

equations, but it is more likely to be caused by the different spatial resolution. Coarsening the spatial resolution causes the topography to flatten. This means that smaller local depressions become less deep and thus less water will accumulate. This also explains why we only see this phenomenon at scenarios with precipitation. Namely, the precipitation causes inundation in the form of local ponding, which are precisely the depressions which get flattened.

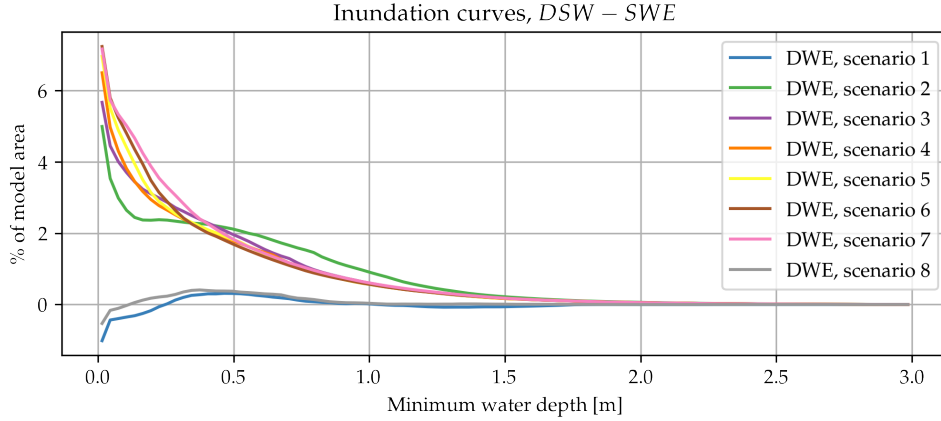


Figure 36: Difference between the inundation curves obtained via the high resolution DSW simulation and the low resolution SWE simulation (DSW-SWE)

This theory is further investigated by making a third type of simulation in which the DSW scheme is used in combination with a low resolution $4m \times 4m$ spatial grid. Figure 37 compares the results of such a simulation in the case of scenario 7 (precipitation event with a 100y return period). The figure shows that the DWE simulation and the SWE simulation have remarkably similar inundation curves given the same spatial discretisation. Since the other runs with precipitation show similar trends, one can conclude that the difference between the DSW and the SWE simulations shown in figure 36 are probably mainly caused by the different spatial discretisation.

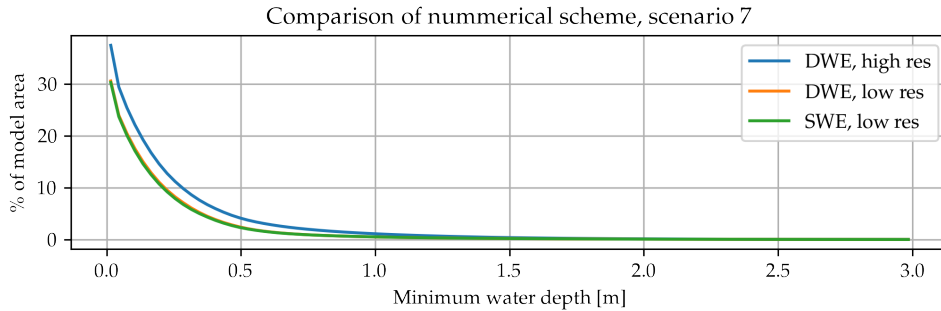


Figure 37: Comparison of governing equation and spatial resolution for scenario 7

Inundation peak time lag

When looking at the time between the peak of the flood event and the peak of the inundation (the inundation peak time lag), one can find some notable behaviour as well. Table 6 shows this time lag for all scenarios calculated with both the SWE and the DSW equations.

Scenario	1	2	3	4	5	6	7	8
DSW [h]	8	3	4	3	4	6	7	8
SWE [h]	7	8	3	3	4	5	6	7

Table 6: Comparison of inundation peak time lag between the high resolution DSW run and the low resolution SWE run

First of all, we can clearly relate these values to the forced boundary conditions as summarised in appendix E.7. The overtopping boundary has a relatively long time scale, which is why scenarios 1 and 8 find a relatively

large inundation peak time lag as well. Ignoring scenario 2 for now, we find that if present, the inundation peak time lag is mainly dominated by precipitation. Simulations with shorter precipitation events such as scenarios 3 and 4 find smaller inundation peak time lags, whilst scenarios with longer precipitation events such as scenario 7 find larger inundation peak time lags.

Secondly, when comparing the time lags of the high spatial resolution DSW simulations with the low spatial resolution SWE simulations, we find a clear relation with the notable exception of scenario 2. The SWE simulations have a systematically lower time lag, which indicates a narrower outflow discharge curve. This concept is illustrated with help of a simple box model in figure 38. By narrowing the outflow curve one effectively decreased the amount of time in which $Q_{in} > Q_{out}$ holds. In this simple box model, maximum volume is found at the tipping point of $Q_{in} = Q_{out}$. One can once again relate this change in behaviour to the change in spatial resolution. Reducing the spatial resolution does also reduce the representation of obstacles, which thus reduces the implicit roughness. With this smoother version of the domain, water is able to flow out of the domain more easily, which thus narrows the outflow curve.

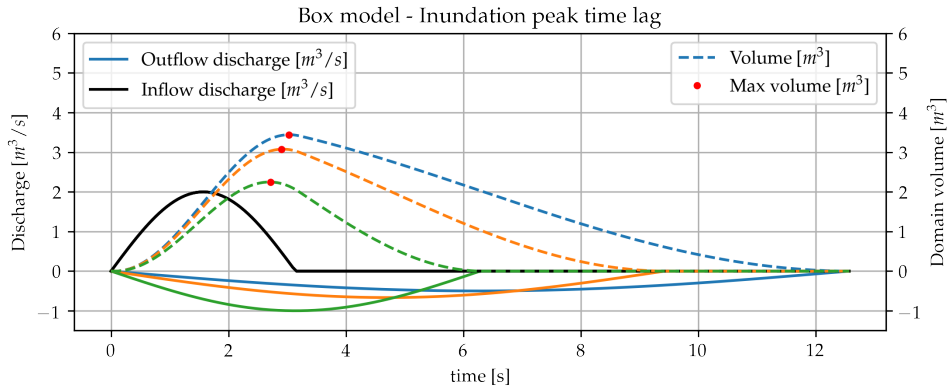


Figure 38: Illustration of the inundation peak time lag phenomenon using a simplistic box model

Scenario 2 displays somewhat different behaviour, which can be explained in a similar fashion. The high spatial resolution DSW simulation reaches peak inundation directly after the precipitation event, whilst the low spatial resolution SWE simulation reaches it at a later point when the overtopping influx reduces. Precipitation generally has a longer flow path towards the river or the sea than overtopping due to its large spatial cover. Reducing the implicit roughness by decreasing the spatial resolution would thus effect the outflow curve of precipitation more than the outflow curve of overtopping. This effectively reduces the respective inundation contribution of the precipitation. As noted on before, the reduction in local ponding by using a coarser grid does also reduce the amount of precipitation induced inundation. This reduction of contribution is likely the cause of why the overtopping boundary dominates the inundation peak time lag over the precipitation boundary for the SWE simulation and not for the DSW simulation. This change in behaviour does explain the peculiar DSW-SWE curve shown in figure 36 too.

4 Discussion

This chapter serves to reflect on the methodologies proposed by section 2 and the subsequent results as shown in section 3. Firstly, the applied methodology is critically evaluated in section 4.1. Secondly, the results are clarified by comparing them to the findings of previous studies in section 4.2. Both sections cover the research chronologically following the phases as outlined in figure 2 of section 2.1. Lastly, potential implications of the results are discussed based on personal interpretation in section 4.3.

4.1 Evaluation of applied method

This section lists various remarks on the applied methodologies of this research.

Scenario creation procedure

- There may be a bias in the representation of marginal distributions due to the applied decoupling method, which may include some double counting. Due to the multivariate nature of the approach decoupling of data is relatively difficult. The applied decoupling approach consisted of using the daily maxima instead of defining various separate storm events. Using the daily maxima instead ensures the structure of the data remains and it is easy to implement, but can lead to double counting of longer storms.
- The selection of the duration of both the coastal forcing and the precipitation event are not derived via a statistical approach. The duration of the precipitation was chosen based on the inundation duration frequency (IDF) curves, in order to correct for the negative bias of intense precipitation events with a short duration of the ERA5 data (Jiang et al., 2021) (Kawohl, 2020). Whereas the duration of the coastal storm has been based on current design practice. An alternative method of including duration in the statistical scenario creation is suggested in section 5.4.

Coastal boundary representation

- It should be noted that an attempt was made to numerically model the entire surfzone till overtopping in 2DH using the hydrodynamic model SWASH on the TU Delft HPC08 cluster computer. Regrettably, many issues regarding instability were encountered. Stability was only achieved by adding much numerical diffusion, which altered the solution to such extent that it was decided to forgo this approach and focus on 1DH.
- The applied methodology to represent storm surge is somewhat simplified. Storm surge levels have been estimated based on tidal gauge data and have been applied as constant in both space and time. SWAN has the ability to compute local wave set-up, but this has been turned off in order to prevent double counting. Assuming storm set-up as constant in space is reasonable due to the size of the domain, and assuming a constant storm surge over time is conservative. However, using a time varying storm surge profile based on the significant wave height profile, would have been more representative.
- The numerical overtopping approach includes the surf zone in an attempt to capture depth-induced wave breaking more accurately than the heavily parameterised approach applied by SWAN. It was however difficult to pick a well defined coupling point based on breaking characteristics, even if use had been made of scenario and location varying points. Because of this, the SWASH model will not fully capture all depth-induced breaking for all location and scenario combinations.
- A large remark on the numerical approach is the overtopping discharge found during the 20 layer computations. The 20 layer computations found up to 6 times more overtopping as was found using only 3 layers. Suzuki et al. (2014) performed a sensitivity analysis and concluded that numerical overtopping estimation is much more sensitive to changes in the numerical discretisation than the representation of wave transformation. Using more than 3 layers for overtopping estimations seems unconventional, and no further information could be found regarding this phenomenon. The 20 layer computation seemed to grossly overestimate, however, judging from the estimations made using the empirical formula and the Gaussian process emulator (GPE). The overtopping estimations made with three layers whilst fitting wave breaking behaviour on the 20 layer simulations, did however agree very well with the overtopping formula and the GPE.
- A shortcoming of all three overtopping methodologies, as applied in this research, is the exclusion of morphodynamics. The coast of Eastbourne is protected by a shingle beach. The morphology of shingle beaches can drastically change over the course of a coastal storm, which can even lead to a breach. Such a breach would lead to a much more intense and localised flood event than considered in this research.

Inundation severity estimation procedure

- The representation of the incoming river boundary, as fixed at a high water level, may lead to some overestimation of the fluvial flood susceptibility. The modelled river (the Crumbles Sewer) has a relatively strong tidal character, which is not well captured because of this assumption. This misrepresentation means the outflow culvert has to discharge a relatively high baseflow, which reduces its efficiency in reducing the inundation severity.
- This research used the worst case scenario assumption: "the urban drainage system is filled completely". This assumption is conservative, but can lead to misrepresentation of the flood susceptibility. The flood susceptibility will overestimated because of this assumption. This overestimation will most likely be larger for pluvial flood events due to the global nature of precipitation, whereas the more local overtopping is more likely to overload the local urban drainage capacity.
- The inundation domain definition has a large direct influence on the inundation curves. By defining the inundation boundaries further land inwards, one effectively raises area susceptible to pluvial flooding, whilst the area susceptible to coastal flooding will remain mostly unchanged due to its local nature. The inundation modeller can thus directly effect the respective importance of pluvial and coastal flooding by defining the inundation boundaries.

4.2 Clarification of results and comparison with previous studies

In the statistical analysis, presented in section 3.1, various relations between variables were found and used for scenario creation. Most notable was the positive relation between the significant wave height and the precipitation intensity. A positive relation between (wind) waves and precipitation would be relatively trivial given a positive partial dependence structure between wind speed and precipitation intensity. Such dependence structure matches the findings of [Zscheischler et al. \(2021\)](#). They researched the spatial structure of this relation in central Europe and found Spearman ρ correlation coefficients up to 0.7. Making the found result even more plausible is the yet to be published results of an ongoing research by [Halliday et al. \(2020\)](#). They found a nation-wide correlation between wind speed and pluvial flooding, which was especially strong in the south-west of England. An explanation for this relation is that the amount of precipitation which can fall, is dependent on the influx of moisture content carried by the wind. In other words, higher winds means more rain can be supplied. Another study, [Paprotny et al. \(2018\)](#), confirms these findings by finding an especially large correlation between storm surge and precipitation in the West of the UK as well.

Another reason for this result could be based on directionality. south-westerly winds are more likely to carry large amounts of moisture since there is no landmass on this side. The results showed that large storms in the English Channel mainly propagate from the south-west to the north-east. Winds from this direction do have a longer effective fetch length, which allows for more energy transfer and thus larger waves. However, according to the results rarer and milder storms can also propagate from the north-east to the south-west. This result was also found by [Dhoop & Mason \(2018\)](#), which stated that only 2 mild storms from the north-east have occurred in the last 16 years.

The inundation duration frequency (IDF) curves based on ERA5 precipitation data showed a negative bias regarding intense short-term events. This phenomenon is a known flaw of the ERA5 precipitation data and has been shown by many previous studies such as [Jiang et al. \(2021\)](#) and [Kawohl \(2020\)](#).

The three overtopping models gave relatively similar results, which gives strength to their validity. When considering the known uncertainty of the techniques, these predictions seem even more reasonable. All three methods are said to predict overtopping discharge accurately within a factor of 3 of the actual discharge ([van der Meer et al., 2018](#))([Pullen et al., 2018](#))([Suzuki et al., 2017](#)). All estimations larger than $1l/s$ seem to be within this factor of 3 of each other. Lower estimations do diverge more, but difficulty with the estimation of low overtopping discharge is a known flaw of all three methods.

Another indication of the overtopping estimations being valid is the coastal flood history of Eastbourne. No very large overtopping discharges ($q > 100l/s$) have been recorded by in UK's coastal flooding database (going back to 1915) ([Haigh et al., 2017](#)). Hence, it makes sense that the found overtopping discharge predictions are maximally $10l/s$. Regrettably, there is no data available to compare the overtopping predictions against. This would have given much insight regarding the accuracy of the three approaches.

Furthermore, the observed spectral behaviour of the SWAN and SWASH model seem to agree well with the findings of [Ryu et al. \(2020\)](#). The research showed that SWASH was able to represent wave transformation accurately whereas SWAN estimated and overly peaked spectrum. This result is however somewhat trivial given

SWAN's incapability of representing the infra gravity domain (Filipot & Cheung, 2012) and the fact that three-wave interactions have been excluded. However, the estimated loss of wave energy caused by the exclusion of the infra gravity domain is moderate, which explains why the SWASH method does not give substantially larger overtopping discharges.

The areas with systematically low inundation seem to agree fairly well with the low flood risk zones of the UK's national "Flood Map for Planning" service*. This is however most likely mainly a function of the local bathymetry. Inspecting the current Eastbourne Strategic Flood Risk Assessment report (Scott Wilson, 2008), one finds extensive research on overtopping induced flooding. The overtopping inundation maps of Scott Wilson (2008) agree very well with the inundation maps of scenario 1 (a once in a 100y overtopping event). The inundation found by Scott Wilson (2008) is more severe than estimated in this report, but they also used a larger return period (500y).

Conversely, the Eastbourne Strategic Flood Risk Assessment has not treated pluvial flooding in much detail, even though they do identify it as a threat. However, in 2013 nation wide assessment regarding pluvial flooding has been executed via the "Risk of Flooding from Surface Water" map (Environment Agency (EA), 2019). They found milder inundation, but this is can be explained by their inclusion of the urban drainage system (using a steady outflow across the catchment of 12mm/hr) and their shorter event durations (1, 3 and 6h). The areas of severe inundation do seem to match the results of scenario 7 relatively well. Regrettably, no nation-wide or local compound flood simulation result could be found for validation purposes of scenarios 2 to 6.

The differences in the inundation results of simulations made with the full shallow water equations (SWE) and the simulations made with the diffusive wave approximation seemed overshadowed by the change in spatial resolution. The observed differences between the simulations (change in inundation severity and a change in the inundation peak time lag) match the findings of Ozdemir et al. (2013). In theory the full SWE should lead to a better representation of the inundation caused by a flood event. Costabile et al. (2017) even showed that the local difference can be substantial. However, the gain in computational efficiency by choosing the DSW equations did allow for a better representation of the topography, which seems more important in the grand scheme. Especially when estimating the total flood susceptibility via inundation curves, we found very similar results if the spatial resolution matched. Regrettably, there is no flood inundation data available to compare the estimations against. Such data would have been valuable to this research since it would allow for prediction quality assessment.

Lastly, assuming the DSW runs are the most representative, we found that scenario 2 leads to the most severe inundation. Scenario 2 is a compound storm scenario with extreme coastal forcing and a mild precipitation event. This results match the findings of Hendry et al. (2019). They stated that especially locations with a south-western coast climate have a relatively high chance of compound flooding. They also state that this relation has most likely been underestimated in risk assessment due to a lack of consideration.

4.3 Potential implications

The results showed that if one did not account for compound effects, then they would have made a slight underestimation regarding the flood susceptibility of Eastbourne. This underestimation would, however, have no significant effect on decision making regarding flood mitigation strategies most likely. The positive dependency between precipitation and wind waves is, however, a relation which varies over space. Areas on the south-west coast of the UK have, for example, have shown a stronger positive correlation (Halliday et al., 2020). One should thus include compound storms in flood susceptibility assessments, unless historical data shows no significant positive dependency between flood driving mechanisms. This can be shown by for example plotting the Spearman rank correlation coefficient over a sliding window, as was done in this research.

The three overtopping estimation methodologies showed similar results. The numerical approach takes advantage of using the entire wave spectrum and includes better representation of wave transformation, but the numerical discretisation leads to much added uncertainty. The empirical formula and the GPE are well established engineering methodologies, but simplify the problem and are known to be imprecise. The results of the three overtopping methodologies as applied in this research agreed well, and no conclusive best approach could be defined. The numerical approach does however look relatively promising. See 5.4 for recommendations regarding further research on this topic.

*The "Flood Map for Planning" service provided by the UK Environment Agency (EA) and freely available at <https://flood-map-for-planning.service.gov.uk>

The inundation modelling results showed that increasing the accuracy of the topography can have a more significant impact on the results than using a more physically accurate set of governing equations. This is especially vital if the computational demand is large and the modeller has to decide between a high spatial accuracy or a more accurate representation of physics. This result was found by comparing spatial discretisations of a $4m \times 4m$ and an $8m \times 8m$ grid. One can however hypothesise, that by increasing the spatial accuracy, at some point, a tipping point is reached at which using a more accurate set of governing equations does become more influential. This concept is discussed as a recommendation for further research in section [5.4](#).

5 Conclusion

The goal of this research is to analyse the differences between various flood susceptibility estimation techniques, in order to clarify the strengths and weaknesses of these respective techniques. The coastal town of Eastbourne, located at the south coast of England, serves as a case study. Both pluvial, coastal, and compound storm scenarios have been modelled with multiple techniques and the results have been analysed. The objective of this project has been converted to the following main research question:

How do different modelling techniques influence the overall flood susceptibility estimation?

This question has been subdivided into three manageable sub-questions as shown in section 1.2. First, the main findings regarding these three respective questions are discussed in section 5.1 to 5.3. Subsequently, a recommendation regarding future research on this topic is given in section 5.4.

5.1 Representative storm scenario generation

The coastal town of Eastbourne has been chosen for case study based on its interesting flood characteristics. An exploratory data analysis was executed to find notable dependence structures between the flood related variables. The analysis showed a moderate positive dependence structure between the significant wave height and the precipitation intensity. Such a dependency could signal a high compound flood susceptibility, an area of research which has recently been gaining attention. Subsequently, two extreme value analysis methodologies were executed for storm scenario creation. A traditional methodology (the peak of threshold (POT) approach), which does not allow for compound events, and a more complex methodology (the conditional approach (Heffernan & Tawn, 2004)) which does.

The different storm scenarios displayed vastly different inundation behaviour based on the magnitude of forcing at the various boundaries. Coastal storms induced a more intense localised inundation pattern, whereas precipitation storms led to more inundated area in the form of less severe, more globally distributed ponding. The severity of the various scenarios were objectively compared via inundated area curves. The most severe flooding was induced by storm scenario 2, a compound storm with extreme coastal forcing and mild precipitation. Even though, a compound storm scenario led to the most severe flood event, the fully coastal storm (scenario 1) did lead to a flood event of the same magnitude. This would suggest that flood mitigation strategies, based on the traditional POT approach, do only slightly underestimate the overall flood susceptibility in the case of Eastbourne. Additionally, a milder north-easterly coastal storm scenario with the same return period was simulated as well, since Eastbourne has less natural protection against such storms. However, this scenario led to less severe flooding than the more common south-westerly storm.

5.2 Overtopping estimation comparison

Three different overtopping estimation methodologies have been implemented for the 8 storm scenarios at 3 representative locations of the coastline of Eastbourne. All three methods used input conditions calculated by the 2D spectral action balance resolving wave model SWAN. The three methods consist of an empirical formula (the "new" overtopping formula of van der Meer et al. (2018)), a Gaussian process emulator (Bayonet GPE described by Pullen et al. (2018)) and a 1DH hydrodynamic numerical model (SWASH described by The SWASH team (2019)). The application of a numerical model is especially interesting, since they allow for accurate representation of wave transformation without relying on parametrization. A hydrodynamic model such as SWASH implicitly includes infragravity waves, a mechanism SWAN is unable to represent, which can be of great significance for overtopping.

The results showed that all three methodologies agree fairly well. The results did not indicate a significant bias in one of the methods. The estimations are of the order of magnitude one would expect based on the coastal flood history of Eastbourne. Discharge estimations above $1l/s$ did not vary more than a factor of three, which is the typical confidence interval of all three methods. Estimations below $1l/s$ did vary more. However, the high uncertainty regarding the estimation of low overtopping discharge is a known weakness of all three methods. For the case study of Eastbourne, all three methods seem evenly applicable. The hydrodynamic SWASH model does include more physical mechanisms, but its sensitivity to the numerical discretisation adds additional uncertainty. Additionally, the hydrodynamic model methodology required explicit refraction correction, and the fitting of breaking parameters on computationally intensive runs to perform reasonable. The numerical methodology does, however, have the potential to outperform the empirical formula and the GPE due to its ability to include more physical processes.

5.3 Governing equations of inundation modelling

The hydrodynamic model HEC-RAS (described by [US Army Corps of Engineers \(2021\)](#)) has been used to model the inundation of the 8 different storm scenarios, in order to estimate the flood severity and the inundation pattern. These 8 simulations have been performed twice in order to compare two sets of governing equations. Namely, diffusive wave approximation of the shallow water equations (DSW) and the full shallow water equations (SWE). The DSW approach is more computationally efficient, which allows for a higher spatial resolution ($4m \times 4m$). The SWE scheme required an $8m \times 8m$ spatial resolution in order to reach a similar computational cost, but represents the physics of flowing water more accurately.

The results showed a significant difference between the two types of simulations. Simulations made with the SWE scheme predicted systematically less severe inundation than their DSW counter parts. And the time between the peak of the storm and the peak of the inundation was systematically shorter for the SWE simulations compared to the DSW simulations. Both of these phenomena can be explained as consequences of varying the spatial resolution of the inundation estimations. Additional DSW $8m \times 8m$ simulations showed mainly small localised differences to their SWE counter parts and the resulting inundation curves were remarkably similar. In the case of Eastbourne it is thus most likely more accurate to use a fine spatial discretisation in combination with the computationally efficient DSW equations, than using the physically more accurate SWE approach on a coarser grid.

5.4 Recommendations

The execution of this project led to various recommendations for future research. These recommendations consist of both advice on how to improve upon the applied methodology and new topics for future research.

Future research could improve the applied scenario creation methodology in the following ways:

- A more sophisticated decoupling methodology such as the method outlined by [Ferro & Segers \(2003\)](#) could be performed to detach storms. Such an approach would lead to a more accurate representation of the marginal distributions in the extreme value analysis. This does mean that separate decoupling is required for precipitation and coastal storms, but the conditional approach of [Heffernan & Tawn \(2004\)](#) can handle this by using a family of conditional models.
- Instead of using reanalysed ERA5 precipitation data and correcting its bias with a duration based on gauged data, one can use only gauged precipitation data from the start. One may even consider using precipitation and coastal storm duration as a third and fourth primary variable. By including these variables as primary variables, you would be able to estimate short intense storms and longer storms with the same return period.

The following topics for future research arose regarding the estimation of overtopping :

- Numerical estimation of overtopping could potentially estimate overtopping more accurately than the other reviewed approaches due its inclusion of infra gravity waves and since it takes advantage of the full wave spectrum. The results of this research and the results of [Suzuki et al. \(2014\)](#) showed that overtopping estimation via hydrodynamic numerical modelling is very susceptible to changes in (vertical) discretisation. It would be interesting to research this relation and to establish what discretisation leads to the most accurate representation of overtopping. Such a study would benefit greatly from experimental data such as overtopping measurement from flume experiments.
- The validity of the methodologies and their respective errors were difficult to judge in this research since there were no measurements to compare with. A research comparing estimations to measurements is required to define and compare the accuracy of the three approaches in a valid manner.

Recently, advances were made regarding the in situ measurement of overtopping over flood defences ([Pinnell et al., 2019](#)). A new overtopping monitoring system called “WireWall” is being developed by HR Wallingford. Overtopping data acquired from such a system would allow for the validation of overtopping simulations by modelling historical events.

- The numerical model methodology was used to both improve the representation of wave transformation and to predict overtopping. It would be interesting to see how the empirical formula and the GPE perform if wave transformation from breaking point till the toe was estimated via numerical modelling.

The following topics for future research arose regarding the estimation of flood severity via inundation modelling:

- The results showed that spending computational resources on a finer spatial discretisation was more beneficial than spending it on a more physically accurate set of governing equations. One can, however, hypothesise there to be a tipping point, at which, it is more beneficial to use more accurate governing equations over an even finer spatial discretisation. Would the found results for instance still hold if spatial resolutions of $2m \times 2m$ and $4m \times 4m$ had been used? And subsequently, how fine should the resolution actually be for accurate flood susceptibility estimation based on inundation curves in an urban area?

Such a study would benefit greatly from flood inundation data. Promising advancements regarding flood mapping are currently made within the field of remote sensing. Traditional optical satellite imaging has difficulty with regards to cloud coverage. Microwave based flood mapping does, however, allow for inundation estimation during cloudy storms (Anusha & Bharathi, 2020). Such a technique could be used to validate inundation estimations by comparing the measured inundation data to simulations of the historical event.

- The applied approach could be extended for risk analysis and subsequently economically optimised risk mitigation strategies. First of all, one can use inundation curves for the objective assessment of flood susceptibility by comparing inundation curves of various areas. Secondly, one can use the output of the inundation model (inundation depth and flow velocity) together with cadastral maps and population data to estimate areas with high risk. Objectively identification of these areas is important for the development of effective flood risk mitigation strategies.

Lastly, in this research we found that a compound flood scenario led to the most severe flood. Regardless, it was found that the exclusion of compound flooding in risk assessment, would most likely lead to a decent representation of the actual risk in the case of Eastbourne. It would be a very valuable tool to be able to estimate when computationally intensive compound flood simulations are required. In this research a moderately strong positive tail dependence structure was found between the significant wave height (H_{m0}) and the rainfall intensity (I_r). One can speculate that the strength of this tail dependence may be a valuable parameter to estimate whether compound flood assessment is required or not. This concept could be further investigated by estimating the flood susceptibility as executed in this report at various locations.

References

1. Aldridge, T., Gunawan, O., Forder, K., Rastall, P., Gouldby, B., Hames, D., ... Haigh, I. (2017, 01). *National risk assessment: Coastal flooding impact analysis. methodology report*.
2. Anusha, N., & Bharathi, B. (2020). Flood detection and flood mapping using multi-temporal synthetic aperture radar and optical data. *The Egyptian Journal of Remote Sensing and Space Science*, 23(2), 207-219. Retrieved from <https://www.sciencedirect.com/science/article/pii/S1110982318303041> doi: 10.1016/j.ejrs.2019.01.001
3. Asselman, N. (2009). *Flood inundation modelling - model choice and proper application*. Deltares. Retrieved from <http://resolver.tudelft.nl/uuid:0ad78bbf-8a82-4da7-9c01-15b6b61ea8d7>
4. Battjes, J., & Stive, M. (1985, 11). Calibration and verification of a dissipation model for random breaking waves. *Journal of Geophysical Research* 90(C5), 9159-9167. (1985), 90. doi: 10.1029/JC090iC05p09159
5. Bowman, W. (2021). *Utide 0.2.6*. Retrieved from <https://pypi.org/project/UTide/>
6. Boyd, R., Dalrymple, R., & Zaitlin, B. (1992). Classification of clastic coastal depositional environments. *Sedimentary Geology*, 80(3), 139 - 150. Retrieved from <http://www.sciencedirect.com/science/article/pii/003707389290037R> (Research Conference on Quaternary Coastal Evolution) doi: 10.1016/0037-0738(92)90037-R
7. British Oceanographic Data Centre (BODC). (2020). *Uk tide gauge network, gauge number: 194050*. Retrieved from https://www.bodc.ac.uk/data/hosted_data_systems/sea_level/uk_tide_gauge_network/
8. Coles, S. (2001). *An introduction to statistical modeling of extreme values*. London: Springer-Verlag.
9. Coles, S., Heffernan, J., & Tawn, J. (1999, Dec 01). Dependence measures for extreme value analyses. *Extremes*, 2(4), 339-365. doi: 10.1023/A:1009963131610
10. Copernicus Climate Change Service (C3S). (2020). *The era5 global reanalysis*. Retrieved from <https://cds.climate.copernicus.eu/cdsapp#!/home> doi: 10.1002/qj.3803
11. Costabile, P., Costanzo, C., & Macchione, F. (2017). Performances and limitations of the diffusive approximation of the 2-d shallow water equations for flood simulation in urban and rural areas. *Applied Numerical Mathematics*, 116, 141-156. Retrieved from <https://www.sciencedirect.com/science/article/pii/S0168927416301106> (New Trends in Numerical Analysis: Theory, Methods, Algorithms and Applications (NETNA 2015)) doi: 10.1016/j.apnum.2016.07.003
12. Couasnon, A., Eilander, D., Muis, S., Veldkamp, T. I. E., Haigh, I. D., Wahl, T., ... Ward, P. J. (2020). Measuring compound flood potential from river discharge and storm surge extremes at the global scale. *Natural Hazards and Earth System Sciences*, 20(2), 489-504. Retrieved from <https://nhess.copernicus.org/articles/20/489/2020/> doi: 10.5194/nhess-20-489-2020
13. Cranfield University. (2013). *Natmap - national soil map*. Retrieved from <https://data.gov.uk/dataset/ea1442bf-ba77-42cc-80e7-2ea339ccb28a/natmap-national-soil-map>
14. Dalrymple, R. W., Zaitlin, B. A., & Boyd, R. (1992, 11). Estuarine facies models; conceptual basis and stratigraphic implications. *Journal of Sedimentary Research*, 62(6), 1130-1146. doi: 10.1306/D4267A69-2B26-11D7-8648000102C1865D
15. Davison, A. C., & Smith, R. L. (1990). Models for exceedances over high thresholds. *Journal of the Royal Statistical Society. Series B (Methodological)*, 52(3), 393-442. Retrieved from <http://www.jstor.org/stable/2345667>
16. Department for Environment, Food and Rural Affairs. (2020a). *Defra's marine digital elevation model (dem) - 1 arc second (south)*. Retrieved from <https://data.gov.uk/dataset/e05d3f72-8e67-4cc0-aa2e-abb79e14243c/defra-s-marine-digital-elevation-model-dem-1-arc-second-south>
17. Department for Environment, Food and Rural Affairs. (2020b). *Surfzone digital elevation model 2014*. Retrieved from <https://data.gov.uk/dataset/46bc8e73-68d4-4574-9096-695b782b7cc1/surfzone-digital-elevation-model-2014>

18. Dhoop, T. (2018, 01). *Occurrence of bimodal seas around the english coastline.*
19. Dhoop, T., & Mason, T. (2018). Spatial characteristics and duration of extreme wave events around the english coastline. *Journal of Marine Science and Engineering*, 6(1). Retrieved from <https://www.mdpi.com/2077-1312/6/1/14> doi: 10.3390/jmse6010014
20. Eastbourne borough council. (1987). *Eastbourne park district plan - review of hydrology and hydraulics.* Binnie & Partners. Retrieved from <http://nora.nerc.ac.uk/14426/1/N014426CR.pdf> (oai:nora.nerc.ac.uk:14426)
21. Eilander, D., Couasnon, A., Ikeuchi, H., Muis, S., Yamazaki, D., Winsemius, H. C., & Ward, P. J. (2020, sep). The effect of surge on riverine flood hazard and impact in deltas globally. *Environmental Research Letters*, 15(10), 104007. doi: 10.1088/1748-9326/ab8ca6
22. Environment Agency. (2019). *Long term flood risk map.* Retrieved from <https://flood-warning-information.service.gov.uk/long-term-flood-risk>
23. Environment Agency. (2020). *Lidar composite dsm 2017 - 1m.* Retrieved from <https://data.gov.uk/dataset/80c522cc-e0bf-4466-8409-57a04c456197/lidar-composite-dsm-2017-1m>
24. Environment Agency. (2021). *Langney bridge rl monitoring station.* Retrieved from <https://riverlevels.uk/east-sussex-langney-bridge-rl#.YIFaxh3iubg>
25. Environment Agency (EA). (2019). *What is the risk of flooding from surface water map?* Retrieved from https://assets.publishing.service.gov.uk/government/uploads/system/uploads/attachment_data/file/842485/What-is-the-Risk-of-Flooding-from-Surface-Water-Map.pdf
26. Ferro, C. A. T., & Segers, J. (2003). Inference for clusters of extreme values. *Journal of the Royal Statistical Society: Series B (Statistical Methodology)*, 65(2), 545-556. doi: 10.1111/1467-9868.00401
27. Filipot, J.-F., & Cheung, K. F. (2012). Spectral wave modeling in fringing reef environments. *Coastal Engineering*, 67, 67-79. Retrieved from <https://www.sciencedirect.com/science/article/pii/S0378383912000750> doi: 10.1016/j.coastaleng.2012.04.005
28. Forzieri, G., Feyen, L., Russo, S., Vousdoukas, M., Alfieri, L., Outten, S., ... Cid, A. (2016). Multi-hazard assessment in europe under climate change. *Climatic Change*, 137(1), 105-119. doi: 10.1007/s10584-016-1661-x
29. Gallien, T., Sanders, B., & Flick, R. (2014). Urban coastal flood prediction: Integrating wave overtopping, flood defenses and drainage. *Coastal Engineering*, 91, 18-28. Retrieved from <https://www.sciencedirect.com/science/article/pii/S0378383914000775> doi: <https://doi.org/10.1016/j.coastaleng.2014.04.007>
30. Gouldby, B., Sayers, P., Mulet-Marti, J., Hassan, M. A. A. M., & Benwell, D. (2008). A methodology for regional-scale flood risk assessment. *Proceedings of the Institution of Civil Engineers - Water Management*, 161(3), 169-182. doi: 10.1680/wama.2008.161.3.169
31. Haigh, I. D., Ozsoy, O., Wadey, M. P., Nicholls, R. J., Gallop, S. L., Wahl, T., & Brown, J. M. (2017, Aug 01). An improved database of coastal flooding in the united kingdom from 1915 to 2016. *Scientific Data*, 4(1). Retrieved from <https://www.surgewatch.org> doi: 10.1038/sdata.2017.100
32. Hall, J. W., Dawson, R. J., Sayers, P. B., Rosu, C., Chatterton, J. B., & Deakin, R. (2003). A methodology for national-scale flood risk assessment. *Proceedings of the Institution of Civil Engineers - Water and Maritime Engineering*, 156(3), 235-247. doi: 10.1680/wame.2003.156.3.235
33. Halliday, O., Shaffrey, L., Tsaknias, D., Cloke, H., & Siddaway, A. (2020, May). Understanding the relationship between extremes of wind and inland flooding in the UK. In *Egu general assembly conference abstracts* (p. 20230).
34. Heffernan, J. E., & Tawn, J. A. (2004). A conditional approach for multivariate extreme values (with discussion). *Journal of the Royal Statistical Society: Series B (Statistical Methodology)*, 66(3), 497-546. doi: 10.1111/j.1467-9868.2004.02050.x

35. Hendry, A., Haigh, I. D., Nicholls, R. J., Winter, H., Neal, R., Wahl, T., ... Darby, S. E. (2019). Assessing the characteristics and drivers of compound flooding events around the uk coast. *Hydrology and Earth System Sciences*, 23(7), 3117–3139. Retrieved from <https://hess.copernicus.org/articles/23/3117/2019/> doi: 10.5194/hess-23-3117-2019
36. Holthuijsen, L. H. (2007). *Waves in oceanic and coastal waters*. Cambridge University Press. doi: 10.1017/CBO9780511618536
37. Jiang, Q., Li, W., Fan, Z., He, X., Sun, W., Chen, S., ... Wang, J. (2021). Evaluation of the era5 reanalysis precipitation dataset over chinese mainland. *Journal of Hydrology*, 595, 125660. Retrieved from <https://www.sciencedirect.com/science/article/pii/S0022169420311215> doi: 10.1016/j.jhydrol.2020.125660
38. Judith Bosboom, M. J. S. (2021). *Coastal dynamics*. Delft: TU Delft Open. doi: 10.5074/T.2021.001
39. Kawohl, T. O. (2020). *Evaluation of era5, era5-land, and imerg-f precipitation with a particular focus on elevation-dependent variations*. Retrieved from <https://ediss.sub.uni-hamburg.de/handle/ediss/6194>
40. Keef, C., Papastathopoulos, I., & Tawn, J. A. (2013). Estimation of the conditional distribution of a multivariate variable given that one of its components is large: Additional constraints for the heffernan and tawn model. *Journal of Multivariate Analysis*, 115, 396 - 404. Retrieved from <http://www.sciencedirect.com/science/article/pii/S0047259X12002436> doi: 10.1016/j.jmva.2012.10.012
41. Kjeldsen, T. R. (2007). *Flood Estimation Handbook, Supplementary Report No. 1*. Centre for Ecology & Hydrology (UK). Retrieved from <http://nora.nerc.ac.uk/id/eprint/2637/1/KjeldsenFEHSR1finalreport.pdf>
42. Met Office. (2021). *Hourly rain obs, herstmonceux west end*. Retrieved from <https://catalogue.ceda.ac.uk/uuid/dbd451271eb04662beade68da43546e1>
43. Nestegård, A., Ronæss, M., Hagen, ø., Ronold, K., & Bitner-Gregersen, E. M. (2006, 05). New dnv recommended practice dnv-rp-c205 on environmental conditions and environmental loads..
44. Ozdemir, H., Sampson, C. C., de Almeida, G. A. M., & Bates, P. D. (2013). Evaluating scale and roughness effects in urban flood modelling using terrestrial lidar data. *Hydrology and Earth System Sciences*, 17(10), 4015–4030. Retrieved from <https://hess.copernicus.org/articles/17/4015/2013/> doi: 10.5194/hess-17-4015-2013
45. Paprotny, D., Vousdoukas, M. I., Morales-Nápoles, O., Jonkman, S. N., & Feyen, L. (2018). Compound flood potential in europe. *Hydrology and Earth System Sciences Discussions*, 2018, 1–34. Retrieved from <https://hess.copernicus.org/preprints/hess-2018-132/> doi: 10.5194/hess-2018-132
46. Pinnell, R., Pullen, T., Silva, E., Brown, J., Yelland, M., Pascal, R., ... Jones, D. (2019, 12). Wirewall laboratory and field measurements of wave overtopping.. doi: 10.18451/978-3-939230-64-9_117
47. Pringle, W. J., Wirasaet, D., Roberts, K. J., & Westerink, J. (2020). Global Storm Tide Modeling with ADCIRC v55: Unstructured Mesh Design and Performance. *Geoscientific Model Development Discussions*, in review. doi: 10.5194/gmd-2020-123
48. Pullen, T., Liu, Y., Morillas, P., Wyncoll, D., Malde, S., & Gouldby, B. (2018, 06). Bayonet gpe: A generic and practical overtopping model that includes uncertainty. *Maritime Engineering*, 171. Retrieved from <https://eprints.hrwallingford.com/1318/1/HRPP777.pdf> doi: 10.1680/jmaen.2017.31
49. Roberts, K., & Pringle, W. (2020, 09). Oceanmesh2d: User guide - precise distance-based two-dimensional automated mesh generation toolbox intended for coastal ocean/shallow water [Computer software manual]. doi: 10.13140/RG.2.2.21840.61446/2
50. Russell, A. (2018). *Managing the coast in a changing climate*. Retrieved from <https://www.theccc.org.uk/publication/managing-the-coast-in-a-changing-climate>
51. Ryu, K. H., Shin, C. H., Jeong, W.-M., & Baek, W.-D. (2020). Applicability of swash model for wave field data reproduction in namhangjin coastal area. In N. Trung Viet, D. Xiping, & T. Thanh Tung (Eds.), *Apac 2019* (pp. 945–951). Singapore: Springer Singapore. doi: 10.1007/978-981-15-0291-0_129

52. Schmid, F., & Schmidt, R. (2007). Multivariate conditional versions of spearman's rho and related measures of tail dependence. *Journal of Multivariate Analysis*, 98(6), 1123-1140. Retrieved from <https://www.sciencedirect.com/science/article/pii/S0047259X06000662> doi: 10.1016/j.jmva.2006.05.005
53. Scott Wilson. (2008). *Eastbourne strategic flood risk assessment 2008*. Eastbourne Borough Council and Wealden District Council. Retrieved from <https://www.lewes-eastbourne.gov.uk/planning-policy/strategic-flood-risk-assessment-sfra>
54. Smit, P., Zijlema, M., & Stelling, G. (2013). Depth-induced wave breaking in a non-hydrostatic, near-shore wave model. *Coastal Engineering*, 76, 1-16. Retrieved from <https://www.sciencedirect.com/science/article/pii/S0378383913000215> doi: 10.1016/j.coastaleng.2013.01.008
55. Southworth, H., Heffernan, J. E., & Metcalfe, P. D. (2020). texmex: Statistical modelling of extreme values [Computer software manual]. (R package version 2.4.4)
56. Suzuki, T., Altomare, C., Veale, W., Verwaest, T., Trouw, K., Troch, P., & Zijlema, M. (2017). Efficient and robust wave overtopping estimation for impermeable coastal structures in shallow foreshores using swash. *Coastal Engineering*, 122, 108-123. Retrieved from <https://www.sciencedirect.com/science/article/pii/S0378383916302435> doi: 10.1016/j.coastaleng.2017.01.009
57. Suzuki, T., Altomare, C., Verwaest, T., Trouw, K., & Zijlema, M. (2014, 06). Two-dimensional wave overtopping calculation over a dike in shallow foreshore by swash. In (Vol. 1). doi: 10.9753/icce.v34.structures.3
58. Teng, J., Jakeman, A., Vaze, J., Croke, B., Dutta, D., & Kim, S. (2017). Flood inundation modelling: A review of methods, recent advances and uncertainty analysis. *Environmental Modelling & Software*, 90, 201-216. Retrieved from <https://www.sciencedirect.com/science/article/pii/S1364815216310040> doi: 10.1016/j.envsoft.2017.01.006
59. The SWAN team. (2020a). Swan scientific and technical documentation [Computer software manual]. Retrieved from <http://swanmodel.sourceforge.net/download/zip/swantech.pdf>
60. The SWAN team. (2020b). User manual swan cycle iii version 41.31a [Computer software manual]. Retrieved from <http://www.swan.tudelft.nl>
61. The SWASH team. (2019). User manual swash version 6.01 [Computer software manual]. Retrieved from <http://www.tudelft.nl/swash>
62. UK Centre for Ecology & Hydrology. (2019). *Land cover map 2019 (lcm2019)*. Retrieved from <https://catalogue.ceh.ac.uk/documents/31f4887a-1691-4848-b07c-61cdc468ace7>
63. UK Centre for Ecology & Hydrology (UKCEH). (2020). *user guide for ukceh land cover maps*. Retrieved from <https://www.ceh.ac.uk/services/lcm2019-lcm2018-and-lcm2017>
64. US Army Corps of Engineers. (2021). *Hec-ras 2d user's manual - creating land cover*. Retrieved from <https://www.hec.usace.army.mil/confluence/rasdocs/r2dum/latest>
65. van der Meer, J., Allsop, W., Bruce, T., Rouck, J., Kortenhaus, A., Pullen, T., ... Zanuttigh, B. (2018). *Eurotop: Manual on wave overtopping of sea defences and related structures - an overtopping manual largely based on european research, but for worldwide application (second edition 2018)*. Retrieved from <http://www.overtopping-manual.com>
66. Zijlema, M. (2020). Computation of free surface waves in coastal waters with swash on unstructured grids. *Computers & Fluids*, 213, 104751. Retrieved from <https://www.sciencedirect.com/science/article/pii/S0045793020303212> doi: 10.1016/j.compfluid.2020.104751
67. Zijlema, M., Delft University of Technology, F. o. C. E., & Geosciences. (2020). *Computational modelling flow and transport: Course cie4340*. TU Delft. Retrieved from <https://repository.tudelft.nl/islandora/object/uuid%3A5e7dac47-0159-4af3-b1d8-32d37d2a8406>
68. Zijlema, M., Stelling, G., & Smit, P. (2011). Swash: An operational public domain code for simulating wave fields and rapidly varied flows in coastal waters. *Coastal Engineering*, 58(10), 992-1012. Retrieved from <https://www.sciencedirect.com/science/article/pii/S0378383911000974> doi: 10.1016/j.coastaleng.2011.05.015

69. Zscheischler, J., Naveau, P., Martius, O., Engelke, S., & Raible, C. C. (2021). Evaluating the dependence structure of compound precipitation and wind speed extremes. *Earth System Dynamics*, *12*(1), 1–16. Retrieved from <https://esd.copernicus.org/articles/12/1/2021/> doi: 10.5194/esd-12-1-2021

Appendices

A Summarising current flood susceptibility assessment practice

This appendix gives a summary of the original literature research report written for this thesis. The full original report was not written with the intention of making it publicly available, but the report has been rewritten for the technical writing module (WM0201TU-ENG) taught at TU Delft. This rewritten version of the report is available [here*](#).

A.1 General

Much research has been done on flood risk analysis, and many methodologies have been established. Giving a complete overview all methodologies is beyond the scope of this research, but having a thorough understanding of the commonly applied methodologies is required. This section will thus attempt to give a concise overview of the currently commonly used methodologies based on the physical processes represented by the flood risk assessment. The heading of table 7 gives 4 main flood driving mechanisms. The body of this table lists often treated processes per flood driving mechanisms.

Coastal flooding	Fluvial (river) flooding	Pluvial flooding	Ground water flooding
Flood defence failure	Baseflow	Areal runoff	Local water bodies
Infra gravity waves	Flood defence failure	Overland flow	Precipitation
Overtopping/Overflow	Flood wave propagation	Precipitation	Soil conductivity
Sea level rise	Precipitation	Urban drainage	Storage capacity
Storm surge	Overland flow		
Tides			
Tsunamis/Meteo tsunamis			
Wind waves			

Table 7: Flood driving mechanisms and processes being treated in conventional in risk analysis.

A.2 Spatial scale

Risk assessment methodologies are often differentiated based on the size of the area of interested. The UK methodology for national-scale flood risk assessment for example is quite general and simplistic, but therefore widely applicable and rigid. This methodology defines flood planes as areas protected by a group of flood defences. The probability of failure of a flood defence is estimated based on the design failure probability of the defences and failure is assumed independent. Multiple scenarios are created and the flood intensity is based on empirical relations. Next a inundation shape is assumed based on the type of flood event and flood depth is again estimated via empirical relations. Many scenarios are then ran through this procedure and a flood probability map is created (Hall et al., 2003). This procedure does not represent many physical processes. But again this is the trade off made in order to get singular widely applicable procedure.

The UK methodology for regional-scale flood risk assessment does treat the physical processes in more detail. This methodology starts by defining a hydraulic forcing per treated flood defence. Hydraulic forcing dependent probability of failure curves are generated per flood defence based on data while considering 2 failure modes (piping and rear phase erosion). At failure, a breach is assumed and severity curves (bound by probabilities of occurrence) are used to find the most likely breach dimensions. Next and overtopping or a weir equation is used to estimate the flood volume which is then spread out via a simplified bathtub type model. This procedure is once again run for many failure scenarios in order to obtain an flood probability map of the considered flood plane (Gouldby et al., 2008). These are just two examples of typical flood risk assessment methodologies. They share the common trade of being widely applicable.

A.3 Accurate representation of the physical mechanisms

Methodologies start to represent the physics more accurately when they are developed to represent certain specific flood driving mechanisms, or when the area of interested is smaller. This is now possible since the methodology is less constricted by being widely applicable, and the smaller areal scale of these type of in depth

*<https://www.overleaf.com/read/qvvhzqncmvyx>

studies requires less computational effort. Research on the specific coastal flooding mechanisms can for example be represented by more accurate methodologies.

An example of a widely applied methodology (due to its computational efficiency) regarding coastal flooding is the following. Extreme scenarios of wind, surge and offshore wave spectrum's are estimated based on historical data. The near shore wave climate is then represented by a spectral action balance model (such as SWAN). And an overtopping equation/neural network (such as the EurOtop NN) is then used and forced by the model output to estimate a discharge. This methodology is even fast enough to do real time flood risk predictions with, but it subjected to some simplification (Aldridge et al., 2017).

The coastal flooding can however be represented even more accurately. A combination of spectral action balance and oceanic circulation models can be solved simultaneously with extreme meteorological forcing to obtain extreme estimates for the wave climate, the shoaling and the tide. Spectral action balance models are less accurate in the near shore region (mostly due to the negligence of infragravity waves). This is why many in depth studies represent this region via numerical hydrodynamic models. Frequency dispersion effects in this region is of relative importance as well, which is why Boussinesq models or fast layered models (not depth averaged) are often used in this specific region. Boussinesq type models eliminate the vertical direction from flow equation similar to the shallow water equations. Boussinesq type models do however retain part of the vertical structure by representing its effects as a function of time and space.

The fluvial (river) flood mechanism is often approached via a more simplistic methodology in risk assessment. For example a direct extreme value analysis can be performed on the river discharge or water level. Other studies try to estimate the river runoff based on precipitation and base flow. One can try to estimate the processes more accurately via hydrological modelling. These are conceptual models that try to present relatively large scale processes within a catchment via empirical equations which are fitted to data. Once a discharge input is obtained via one of these methods 2D numerical models can be used to calculate inundation in the catchment. However, some methodologies such as the UK's methodologies for flood risk assessment do not use such models, but estimate the discharge per individual flood defence given an extreme forcing scenario. The inundation assessment is then done after the derivation of the flood volume.

The pluvial flood mechanism is often researched within an urban context. Heavy precipitation needs to be artificially drained via sewer systems due to the generally bad natural drainage in urban areas. Governmental organisations asses the sewer system via modelling techniques including the elevation of the area and the sewer system. Representing the contribution of the sewer system is a difficult task for non governmental research agencies since the sewer system layout and dimensions are not publicly available usually. This is why research often assumes the contribution of the urban drainage to be negligible for the estimation of the initial inundation. This is justified by making the worse case assumption of the urban drainage system being filled during an extreme storm. Precipitation intensity distributions are usually represented by so called "design storms", since probabilistic representation by using many events is very computationally demanding. Countries will usually have their own standards regarding these distributions.

A relatively low amount of research has been conducted on groundwater flood risk assessment. This is most likely caused by the much smaller spatial scale of groundwater flooding (incidence are most commonly local). Representing subsurface flows is a difficult challenge since they are difficult to measure and validate. Groundwater flow models do exist and are often used in other types of research, such as when ground water extraction is conducted or when salt intrusion is an issue. However, the implementation of groundwater flow models for flood risk assessment is a relatively new concept.

A.4 Compound effects

The interaction between flood driving mechanisms is often referred to as the compound effects. Research which includes such effects does often focus on the specific contribution and the interaction of specific flood driving mechanisms. A typical example is including the effect of coastal storm surge on a delta flood risk analysis (storm surge can heighten the lower river boundary). Pluvial and fluvial flooding methodologies are also often intertwined due to their co-occurrence in many urban areas.

A typical methodology which addresses compound effects to a certain extend is to asses all flood defence protecting a flood plain individually. The failure of these defences are often assumed independent, but the forcing is not. Research on dependent coastal, pluvial and river forcing has been conducted on specific projects, but it is rarely incorporated in general flood assessments practice.

A new progression of compound flood research is the modelling the ocean, near shore, overtopping/overflow and land inundation using a single numerical model. Such a model needs to be relatively fast while still

incorporating the contributing physical mechanisms (conflicting requirements). The newly developed SFINCS model by Deltares attempts to do exactly that. The model makes some arguable simplifications (negligence of advection in the momentum equation), but can be ran in combination with a Monte Carlo type research, due to its high computational efficiency.

A.5 Discussion on current common practice methodologies

No singular best methodology for flood risk assessment exist. The methodology to be used should be based on two main aspects of the study. The spatial scale of the assessment and the dominant flood driving mechanisms of the location. Representing too much detail in projects with a large spatial scale would make the assessment infeasible, whereas representing negligible flood mechanisms would result into an inefficient methodology. Detailed research of interacting flood mechanisms is rarely conducted in flood risk assessment, because the time scale of such projects is often constricted. Neglecting details and interactions can however lead to miss representation of the overall flood risk, therefore this should always be done with care.

B The conditional approach for multivariate extreme values

The conditional approach for multivariate extreme values, first formulated by [Heffernan & Tawn \(2004\)](#), overcomes some of the problems most traditional approaches have to cope with. This section tries to summarise this approach as implemented in this research, using the `texmex` package written for the programming language R. The approach can broadly speaking be summarised in 2 main steps ([Southworth et al., 2020](#)). The first step comprises of marginal distribution fitting via the peak over threshold approach, while the second step covers the conditional modelling.

B.1 The peak over threshold approach (POT)

Extreme value theory explains, when using appropriate normalisation of the threshold excesses, while the threshold u tends to the upper end point of the distribution, the tail distribution shall be part of the generalised Pareto distribution (GPD) family (given the distribution of the original data is smooth enough and certain non-degeneracy conditions of the limit distribution are satisfied) ([Coles, 2001](#)). This means that whatever the distribution of the original data might be (with notable exceptions such as directional data), if a sufficiently high threshold has been selected the tail distribution can be well approximated by the GPD, which has the distribution function as shown in equation 11 and 12 ([Davison & Smith, 1990](#)).

$$P(X \leq x) = 1 - \left\{ 1 + \xi \left(\frac{x - u}{\sigma} \right) \right\}^{-1/\xi} \quad \text{for } x > u \cap \xi \neq 0 \quad (11)$$

$$P(X \leq x) = 1 - \exp \left(-\frac{x - u}{\sigma} \right) \quad \text{for } x > u \cap \xi = 0 \quad (12)$$

In which:

- u : Threshold for fitting;
- σ : Scale parameter > 0 ;
- ξ : Shape parameter $\in \mathbb{R}$.

Although it is common to parameterise the GPD as shown in equation 11, the `texmex` package reparameterises the scale parameter σ as $\phi = \log(\sigma)$. It uses this approach due to three main reasons [Southworth et al. \(2020\)](#). First of all, numerical algorithms used for optimising the log-likelihood are said to converge more reliably when using this approach. Secondly, it automatically fulfills the $\sigma > 0$ constrain (a constrain which arises when modelling with covariates). And lastly, ϕ is more likely to have a Gaussian-like distribution.

Two standard threshold selection aids (further explained by [Coles \(2001\)](#)) are threshold stability plots and the mean residual life (MRL) plot. These 2 aids have been implemented in the `texmex` package and have been used for threshold selection. The threshold stability and mean residual life (MRL) plots of the considered variables and the resulting chosen thresholds are visible [here*](#).

B.2 Conditional POT

The conditional multivariate approach as developed by [Heffernan & Tawn \(2004\)](#) starts by fitting the marginal distributions of the individual variables as summarised in paragraph B.1. The method then continues by transforming these marginals and estimates the dependence structure of secondary variables based on the threshold excess of a chosen primary variable via a regression type model ([Southworth et al., 2020](#)).

The dependence structure of the marginal distributions is not described on the original scale of the margins. Instead, the margins are transformed to a standard margin. The original paper of [Heffernan & Tawn \(2004\)](#) transformed the marginal distributions of the data to Gumbel marginals. However, more recent research ([Keef et al., 2013](#)) has shown that additional constrains in the model formulation, can be added by using the Laplace distribution instead. Using this newer method helps overcome problems regarding negative dependence, parameter identifiability and drawing conditional inferences, which is why this method has been applied in this research. Transformation of the marginals has been done via the general probability integraltransform formula as cited in equation 13 ([Southworth et al., 2020](#)).

*<https://1drv.ms/w/s!Auz0LY1jddqQgqYsAf6DmYC9s3pa2Q?e=2L1g43>

$$Y_i = (G^{-1}(F_i(X_i))), i = 1, \dots, d \quad (13)$$

In which:

- X_i : The original data of variable i ;
- i : The variable/dimension index number and d is the total amount of variables/dimensions;
- F_i : Estimate of the marginal distribution function based on the data of variable i ;
- G : The distribution function of the standardised marginal distribution and G^{-1} its inverse;
- Y_i : The variable after being transformed into the chosen marginal distribution.

The specific probability integraltansform formula used to transform the GPD marginals into Laplace marginals is shown in equation 14 (Keef et al., 2013).

$$Y_i = \begin{cases} \log \{2F_i(X_i)\} & \text{for } X_i < F_i^{-1}(0.5) \\ -\log \{2[1 - F_i(X_i)]\} & \text{for } X_i \geq F_i^{-1}(0.5) \end{cases} \quad (14)$$

After fitting and transforming the marginal distributions the Heffernan & Tawn (2004) approach continues by conditioning variables on a chosen primary variable whilst it is above a certain threshold. This threshold can differ from the threshold(s) used during the marginal distribution fitting procedure. The conditioning is done via a regression type model which has been fitted to the transformed data. The choice of the regression model depends on the chosen distribution function G . The regression model for Laplace marginals as suggested by Keef et al. (2013) has been implemented in the `texmex` package and is shown in equation 15.

$$Y_{-i} = \alpha_{|i} Y_i + (Y_i)^{\beta_{|i}} Z_{|i} \quad (15)$$

In which:

- Y_{-i} : The marginal distributions of all secondary variables whilst being transformed to the Laplace distribution;
- Y_i : The marginal distribution of the primary variable whilst exceeding a picked threshold t and being in its Laplace form;
- $\alpha_{|i}$: A fitting parameter which expresses a positive dependency when positive and a negative dependency when negative $\in [-1, 1]^{d-1}$;
- $\beta_{|i}$: A fitting parameter $\in [-\infty, 1]^{d-1}$;
- $Z_{|i}$: A vector residual.

Note that the regression model does not use a parametric family of distributions to describe the distribution of the residual vector $Z_{|i}$. Instead $Z_{|i}$ is an empirical distribution resulting from the residuals after fitting the parameters $\alpha_{|i}$ and $\beta_{|i}$. This makes the Heffernan & Tawn (2004) dependence model semi-parametric.

One of the most straight forward ways of doing statistics on the dependence structure is by sampling data points from the model. This has also been implemented in the `texmex` package. In the case of one or multiple variables being dependent on one primary variable, an additional sampling threshold can be put on the primary variable.

B.3 Complete joint distribution sampling

In the previous paragraph (B.2) creating dependence structures via the Heffernan & Tawn (2004) approach based on a single primary variable has been summarised. The paper of Heffernan & Tawn (2004) also explains how to expand this method to a fully joint distribution of multiple dependent variables. The `texmex` package implements this method as well and their `texmexMultivariate` vignette clarifies their implementation in 6 steps (Southworth et al., 2020).

1. Create a Monte Carlo sample of the required size (without restrictions) from the original dataset on the original scale by uniform sampling with replacement.

2. Transform the Monte Carlo samples of step 1 into Laplace/Gumbel scale using a GPD fitted to the original data as explained in paragraph B.2.
3. Compare the data on the common Laplace scale and select the largest (least likeliest) values.
4. Select of the values obtained in step 3 the values that lie above the chosen dependence threshold. Then use these values to fit the regression model (equation 15 in the case Laplace marginals are used).
5. Create conditioning on each variable in turn a large sample of independent events, and use the dependence structures obtained in step 4 to find values for the dependent (not conditioned on) variables. These values are then transform back to the original variable scale.
6. Now replace the values identified by step 3 & 4 in the Monte Carlo sample of step 1 with the values obtained in step 5 from the appropriate conditional model.

This method can be used to simulate data in the upper tail end of an n dimensional dependent structure. Standard methods of data analysis can then be applied on this simulated data.

B.4 Creating scenarios using the conditional approach

B.4.1 Primary variables

In the case of a single variable one can create a traditional return level plot (value of the variable on the y-axis and the return period variable on the x-axis). However, when dealing with 2 or more variables such a simple and clear plot cannot be made. In the 2 dimensional case one can visualise the data in a similar way by plotting the return period contours. The `texmex` package can calculates such a method in the form of joint exceedance curves (Southworth et al., 2020). The concept behind this approach is to fix on one or more return periods, find all parameter combinations that lead to the chosen return period(s), and interpolate them (or more formally: equation 16). An example of a joint exceedance curve is shown in figure 39.

$$\{(x_{1,p}, \dots, x_{d,p}) : \Pr(X_1 > x_{1,p}, \dots, X_d > x_{d,p}) = p\} \quad (16)$$

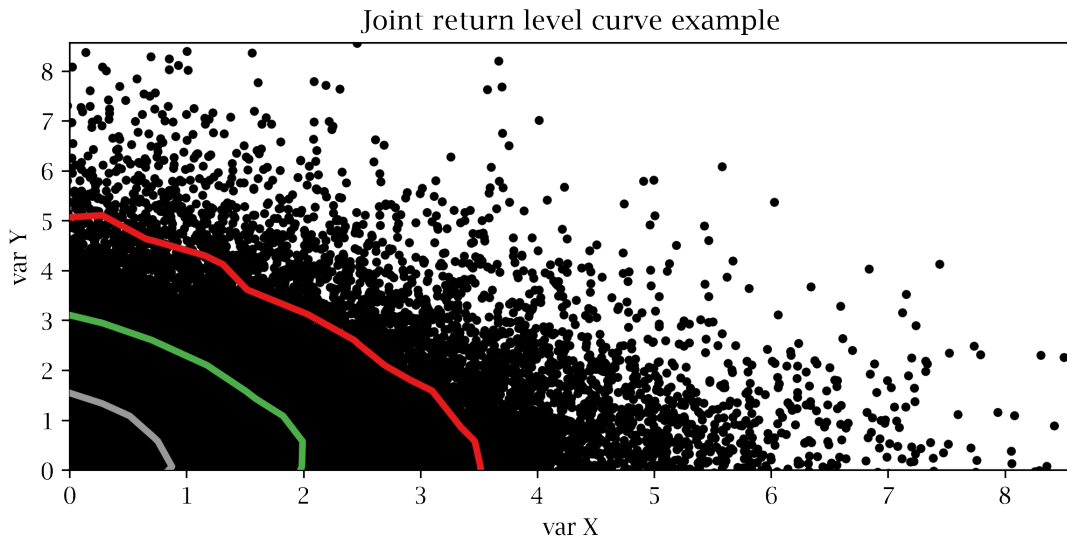


Figure 39: An illustration showing an example of joint exceedance curves. In which the return period of the grey curve is the smallest and the return period of the red curve is largest.

In order to find meaningful results on the importance of flood drivers, one can create multiple scenarios with the same return period. In the bivariate case this does thus mean that variable combinations should be chosen that share a contour line on the joint exceedance curve plot. The limits of these curves describe the original marginal distributions of the GPD.

B.4.2 Secondary variables

Not every imposed model variable should be used to base the scenarios on. This is because inclusion of many variables will decrease the probability of occurrence of an extreme event. These secondary variables should thus be chosen without impacting the overall probability of the scenario. Although it might not be specifically implemented, the `texmex` package can relatively easily be used to find the likeliest value of a dependent secondary variable, assuming that the primary variable has a value within a certain region.

The method as used in this research to find the likeliest value for the secondary values is relatively simple as is explained by the following steps.

1. Values of one or more secondary variables are simulated via the a dependence structure using either one or more primary variable(s) as explained in paragraph B.2 and B.3.
2. A value/values are chosen for the primary variable(s) together with a small deviation determined by the user.
3. All primary variable values outside the chosen value(s) + its deviation and their respective secondary variable values are disregarded.
4. The remaining secondary values are now representing a discrete PDF of the secondary variable given the primary variable has a certain value (+ a small deviation).
5. The value with the highest probability is found by maximising the discrete PDF (right illustration of figure 40).

A more visual way to interpret this, is to take a slice of a density plot of two variables and maximise it as is shown on the plots of figure 40. This method works especially well when using only one primary variable, since in this case one can create samples above a variable threshold. One simply pick a threshold close to the value of interested to create many relevant samples.

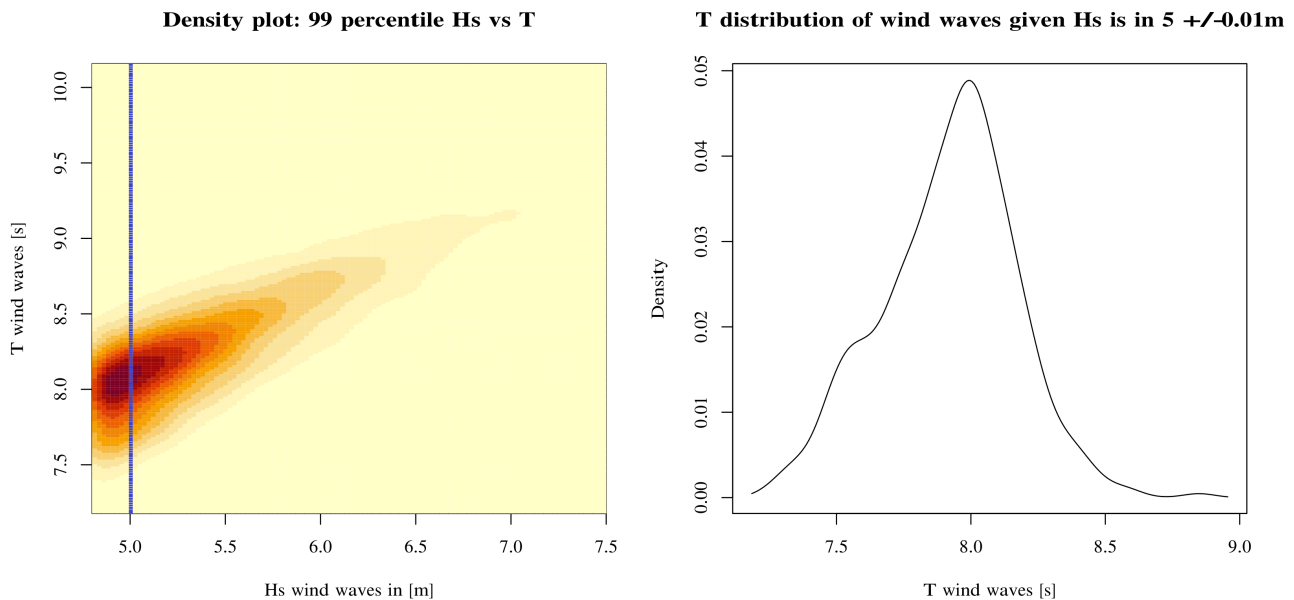


Figure 40: Finding the likeliest value of a secondary value based on a fixed primary variable value.

C Typical SWAN input file

```
$*****HEADING*****
$
PROJ 'Eastbourne' 'sc1'
$
$*****MODEL INPUT*****
$
SET LEVEL=3.232936697
MODE STATIONARY TwODimensional
COORDINATES SPHErical
$
CGRID UNSTRUCTured CIRCLE 72 0.03 0.6 31
READ UNSTRUCTURED ADCIRC
$
WIND 24.7287391 20
$
BOUN SHAPE JONswap 3.3 MEAN DSPR DEGRees
BOUN SIDE 1 UNIFORM PAR 8.0188854631365 9.6008068 19.68 30
$
FRICtion
DIFFRAC
NUMERIC STOPC STAT 100 0.01
$
$***** OUTPUT REQUESTS *****
FRAME 'FRAM1' 0.06 50.69490 0. 0.36 0.2251 500 340
TABLE 'FRAM1' HEAD '..\Output\Eastbourne_01_f1.tab' XP YP DEP HS WLEN WATLEV PDIR DISSIP
DISBOT DISSURF DISWCAP DISSWELL TPS TM01 DIR
$
CURVE 'LOC1' 0.2974939 50.771925 1220 0.42 50.694258
TABLE 'LOC1' HEAD '..\Output\Eastbourne_01_c1.tab' DIST DEP HS WLEN WATLEV PDIR DISSIP
DISBOT DISSURF DISWCAP DISSWELL TPS TM01 DIR XP YP BOTLEV
$
CURVE 'LOC2' 0.3263300 50.784963 1156 0.40839 50.69490
TABLE 'LOC2' HEAD '..\Output\Eastbourne_01_c2.tab' DIST DEP HS WLEN WATLEV PDIR DISSIP
DISBOT DISSURF DISWCAP DISSWELL TPS TM01 DIR XP YP BOTLEV
$
CURVE 'LOC3' 0.3344078 50.795129 676 0.42 50.767515
TABLE 'LOC3' HEAD '..\Output\Eastbourne_01_c3.tab' DIST DEP HS WLEN WATLEV PDIR DISSIP
DISBOT DISSURF DISWCAP DISSWELL TPS TM01 DIR XP YP BOTLEV
$
POINTS 'P_1' 0.301829 50.769175
TABLE 'P_1' HEAD '..\Output\Eastbourne_01_loc1.tab' XP YP DEP HS WLEN WATLEV PER DIR
TMM10
$
POINTS 'P_2' 0.3290068 50.782025
TABLE 'P_2' HEAD '..\Output\Eastbourne_01_loc2.tab' XP YP DEP HS WLEN WATLEV PER DIR
TMM10
$
POINTS 'P_3' 0.3393806 50.793523
TABLE 'P_3' HEAD '..\Output\Eastbourne_01_loc3.tab' XP YP DEP HS WLEN WATLEV PER DIR
TMM10
$
POINTS '1DCP1' 0.3175938 50.7592085
SPECout '1DCP1' SPEC1D ABS '..\..\SWASH\Input\1D_spec_1.bnd'
$
POINTS '1DCP2' 0.3405458 50.7693898
SPECout '1DCP2' SPEC1D ABS '..\..\SWASH\Input\1D_spec_2.bnd'
```

```
$
POINTS '1DCP3' 0.3597503 50.7869629
SPECout '1DCP3' SPEC1D ABS '..\..\SWASH\Input\1D_spec_3.bnd'
$
POINTS '2DCP1' 0.3175938 50.7592085
SPECout '2DCP1' SPEC2D ABS '..\..\SWASH\Input\2D_spec_1.bnd'
$
POINTS '2DCP2' 0.3405458 50.7693898
SPECout '2DCP2' SPEC2D ABS '..\..\SWASH\Input\2D_spec_2.bnd'
$
POINTS '2DCP3' 0.3597503 50.7869629
SPECout '2DCP3' SPEC2D ABS '..\..\SWASH\Input\2D_spec_3.bnd'
$
POINTS '1DP_1' 0.301829 50.769175
SPECout '1DP_1' SPEC1D ABS '..\..\SWASH\Input\1D_spec_Loc_1.tab'
$
TEST 1,0
COMPUTE
STOP
```

D Typical SWASH input file

```
!*****HEADING*****
!
PROJ 'EAST1D' '01'
!
! 1D Surfzone model
! with actual bathymetry
!
!*****MODEL INPUT*****
!
SET DEPMIN=0.005 maxerr=1 seed=34567890
MODE DYN ONEDimensional
!
CGRID 0. 0. 0. 2500. 0. 1249 0
!
VERT 3 33.3333333 33.3333333 33.3333333
!
INPGRID BOTTOM 0. 0. 0. 1249 0 2. 0.
READINP BOTTOM 1. './.././SWASH1D_loc1.bot' 1 0 FREE
!
INIT CONstant 3.2329
!
BOUndcond SIDE W UNIForm SPECFile '1D_spec_ref_1.bnd' 010000
BOUndcond SIDE E BTYPE WLEV CONstant 2.5
!
WIND -10.45081673 0
FRIC MANNING 0.019
VISC SMAG
BREAK 0.28 0.14
NONHYDrostatic STAN PREC ILU
!
DISCRET UPW MOM KOREN
BOTCel MIN
TIMEI METH EXPL 0.2 0.5
!
!***** OUTPUT REQUESTS *****
!
!CURVE'LINE' 0 0 1250 2500 0
!TABLE 'LINE' HEAD './Output/Eastbourne_1D_01_loc1_gr_break.tbl' TSEC WATL BOTLEV XP DEP
OUTPUT 001500.000 .5 SEC
!
POINTs 'OVERT' 2084 0
TABLE 'OVERT' HEAD './Output/Q_01_loc1.tbl' TSEC QMAG QDIR OUTPUT 001500.000 1 SEC
!
!POINTs 'WSIG' 1561 0
!TABLE 'WSIG' NOHEAD './Output/h_100m_no_ref_break_loc1.tbl' WATL OUTPUT 001500.000 .25
SEC TEST 1,0
COMPUTE 000000.000 0.02 SEC 021500.000
STOP
```

E Figures

E.1 Correlation matrix

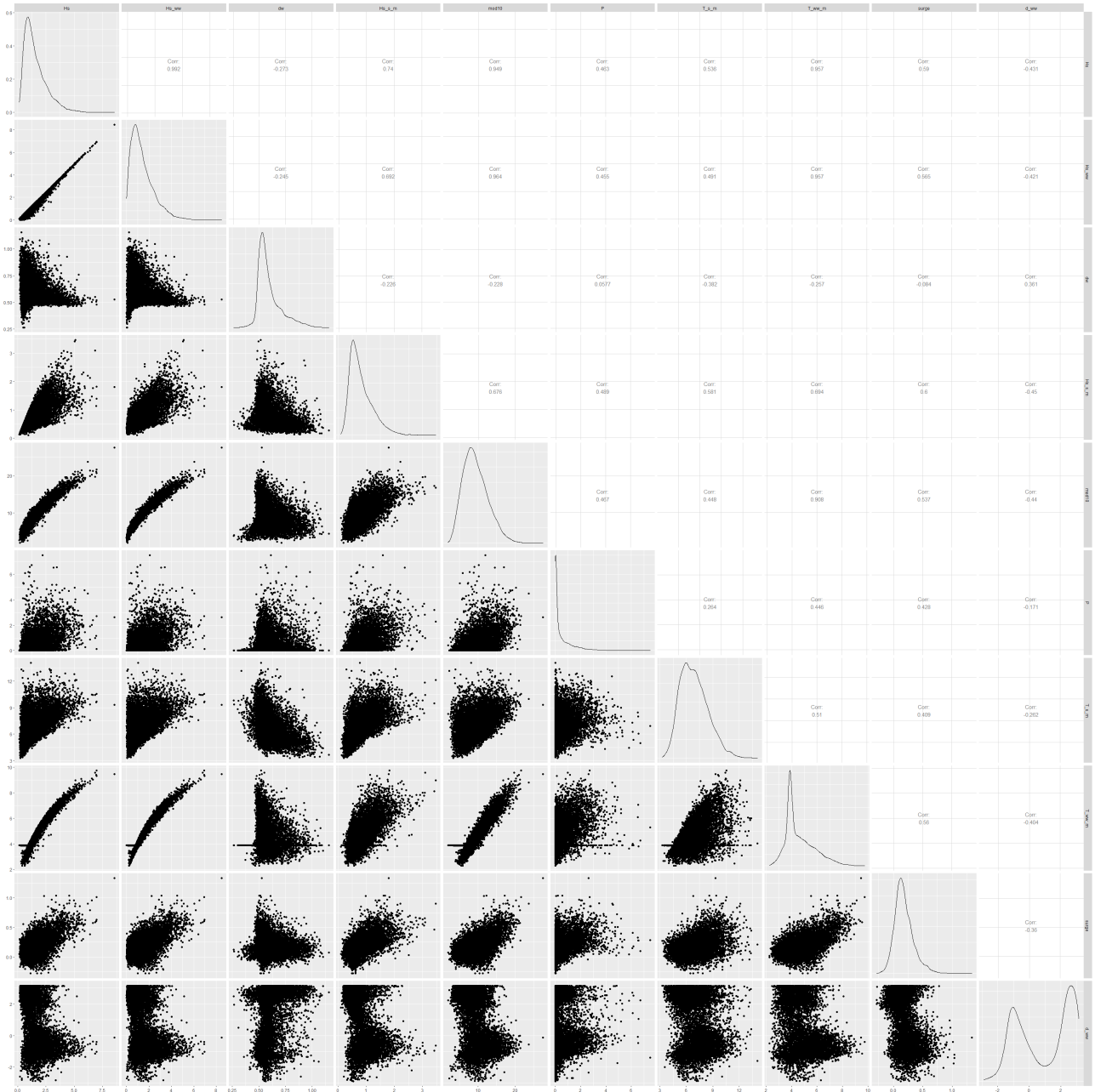


Figure 41: Full correlation matrix with correlation coefficients. Hs: significant waveheight [m], Hs_ww: significant wave height of wind waves [m], dw: directional width [°], Hs_s_m: significant wave height of swell [m], mod10: average wind speed 10m above MSL [m/s], P: precipitation intensity [mm/h], T_s_m: mean swell period [t], T_ww_m: mean wind wave period [t], surge: Storm surge estimation based on Utide analysis [m], d_ww: wind wave direction.

Note: There is a bias in the wave direction due to an error in the data handling, a correct directional plot is visible in section 3.1.1 figure 18.

E.2 Refraction coefficients

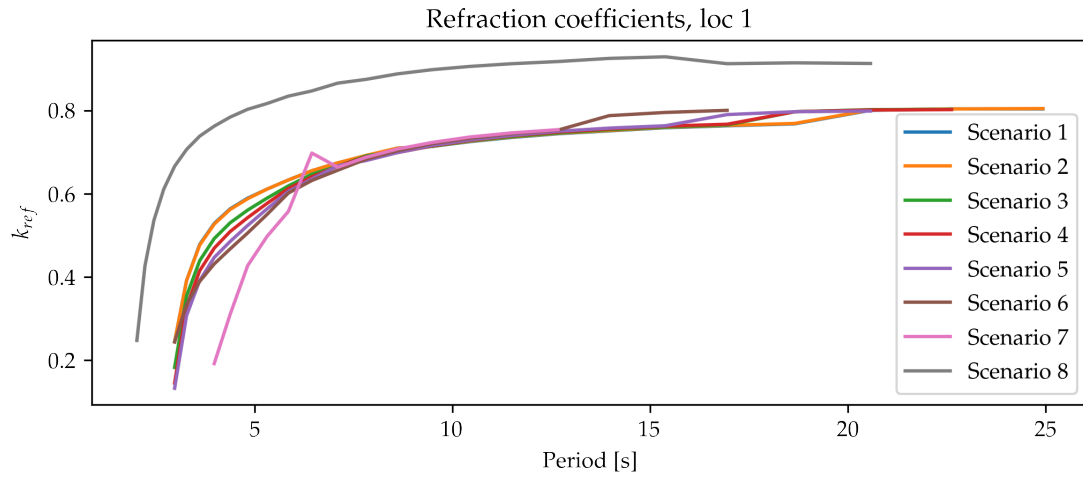


Figure 42: Period varying refraction coefficients for all scenarios at location 1

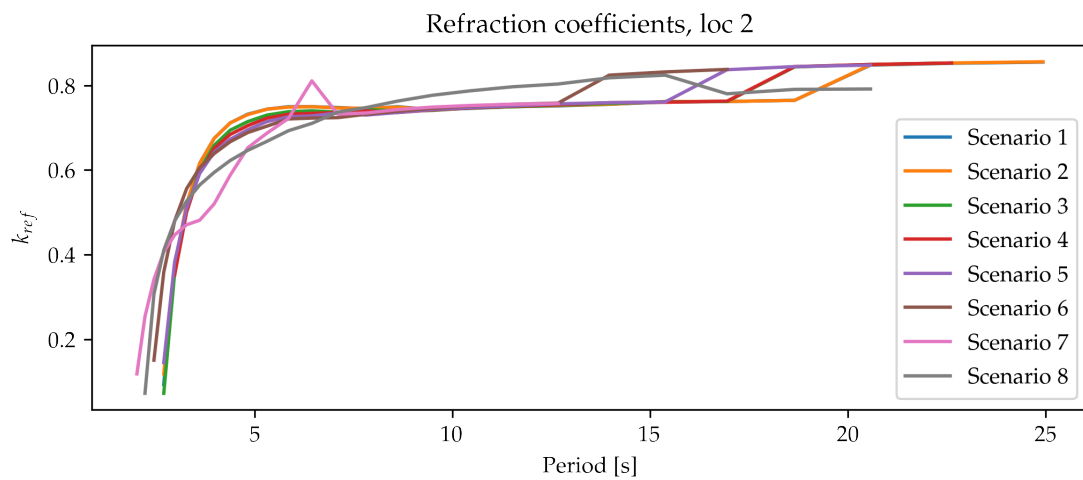


Figure 43: Period varying refraction coefficients for all scenarios at location 2

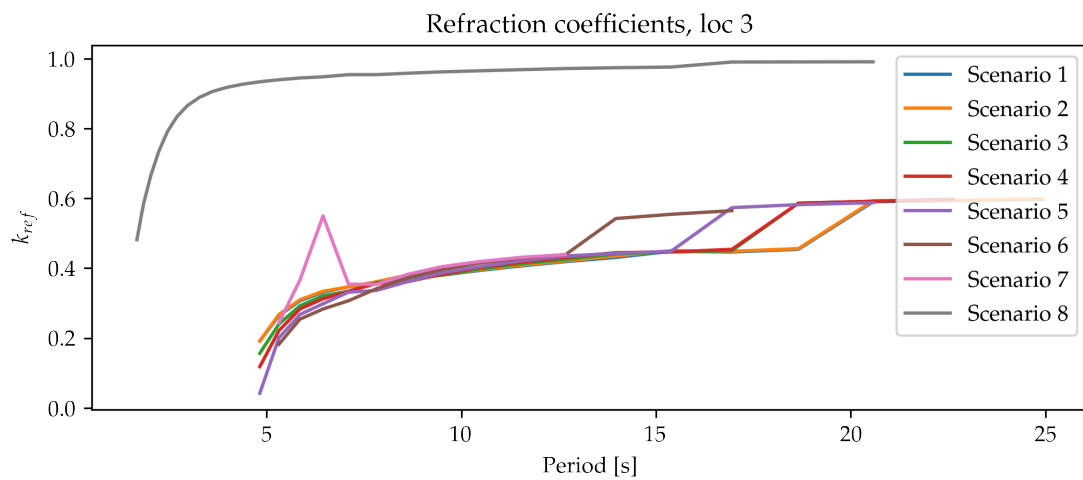


Figure 44: Period varying refraction coefficients for all scenarios at location 3

E.3 Surf zone cross sections

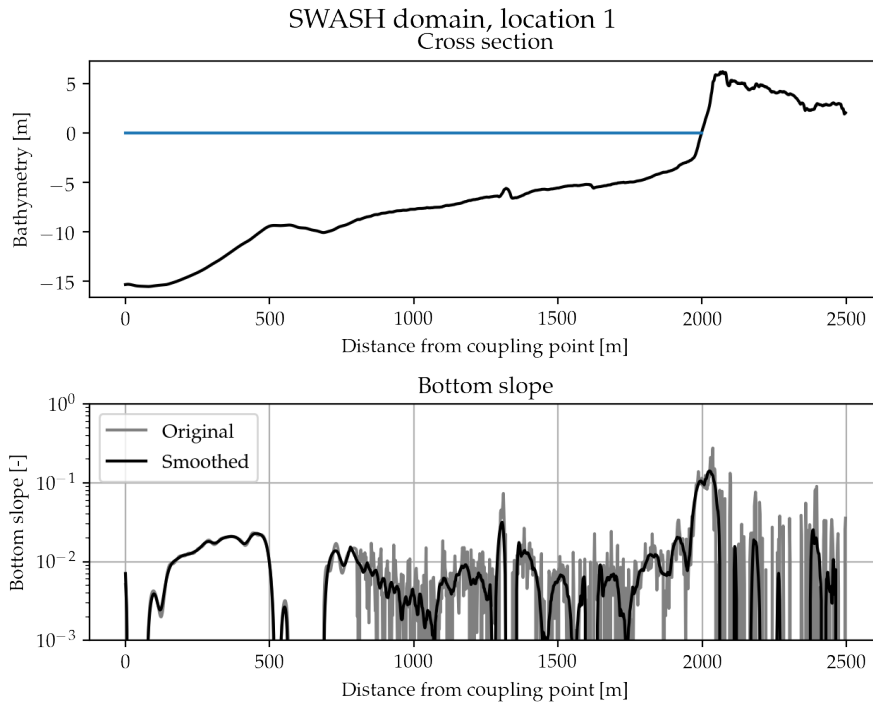


Figure 45: Shore normal bathymetry cross section and slope at location 1

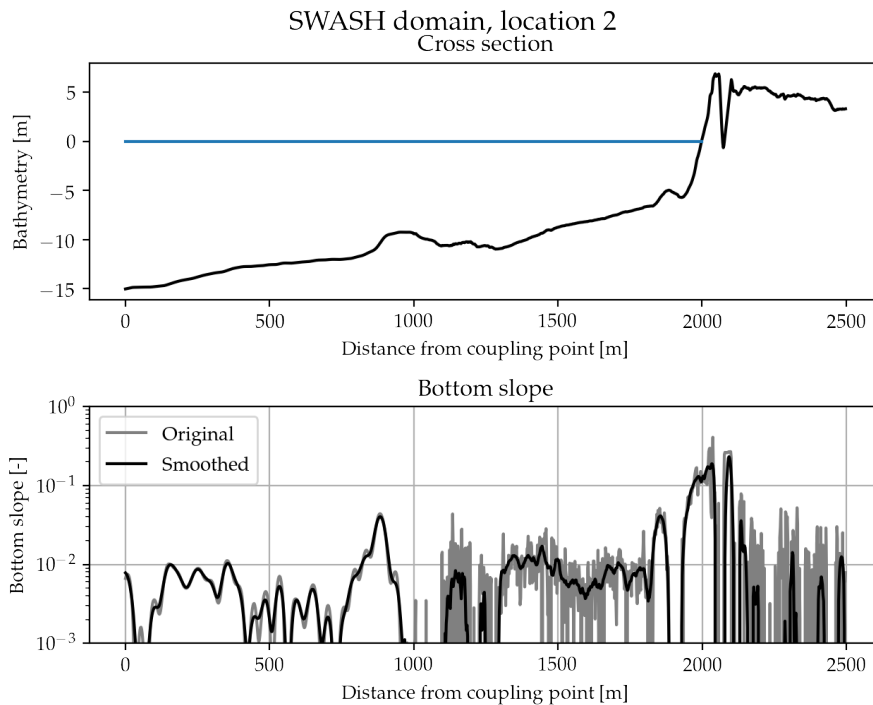


Figure 46: Shore normal bathymetry cross section and slope at location 2

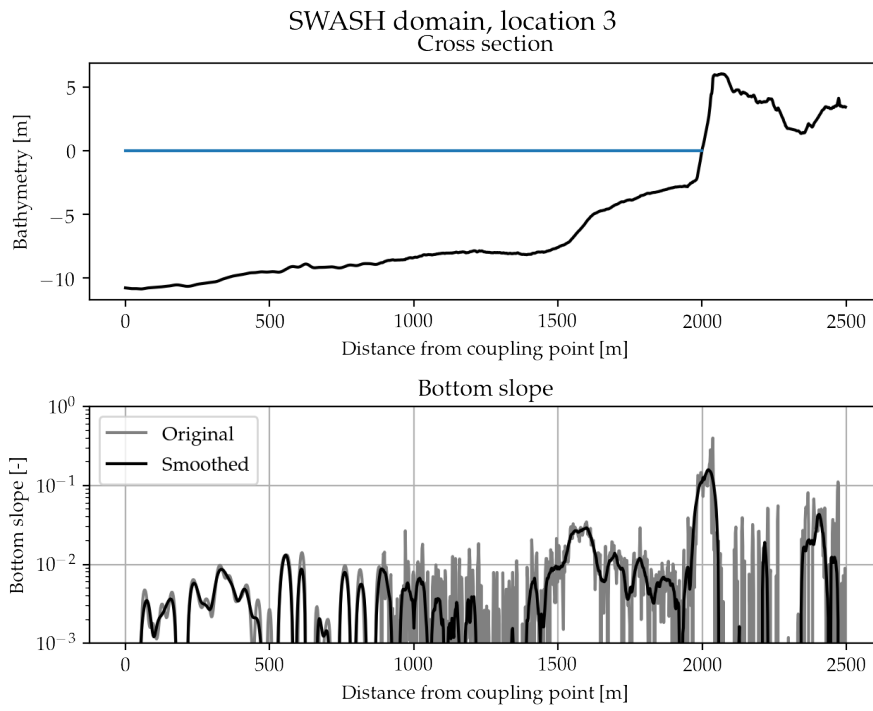
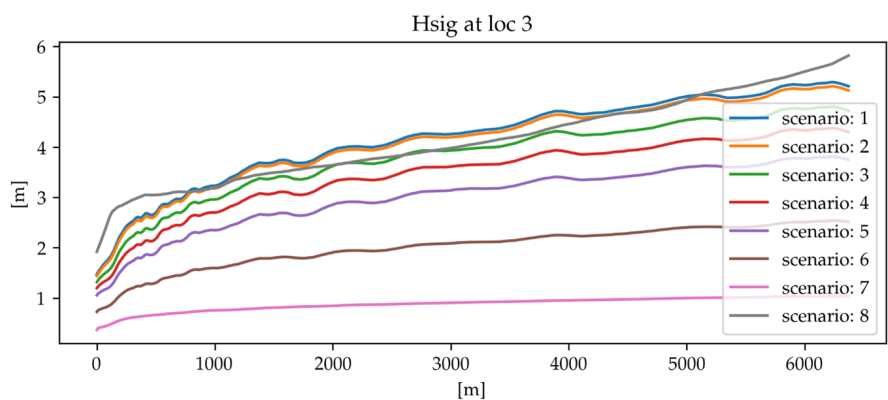
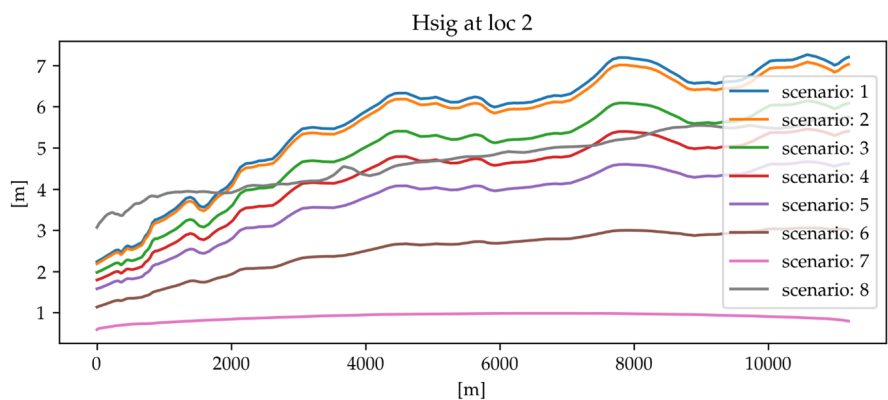
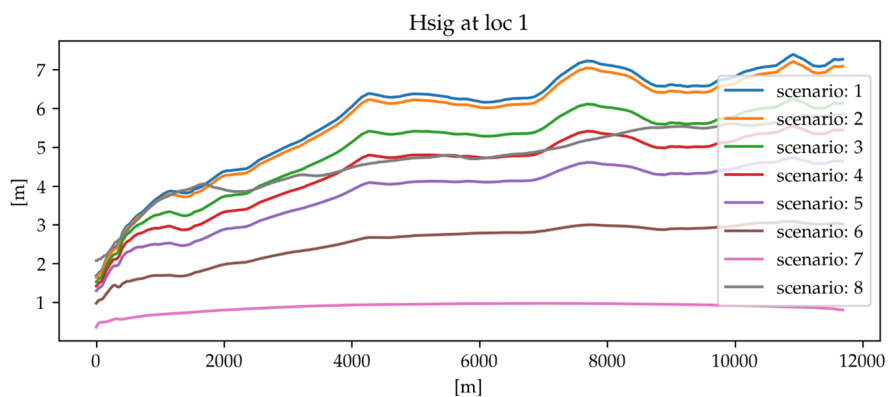


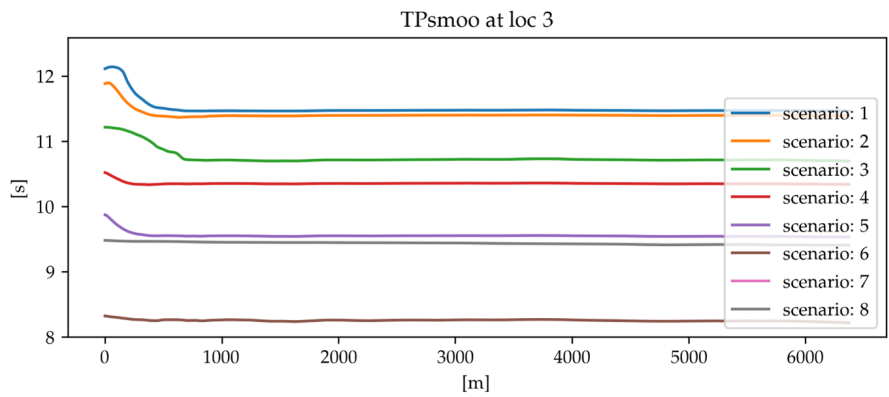
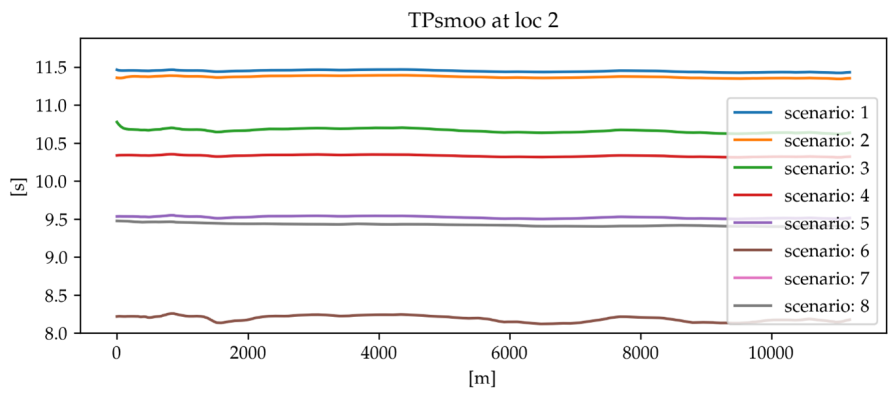
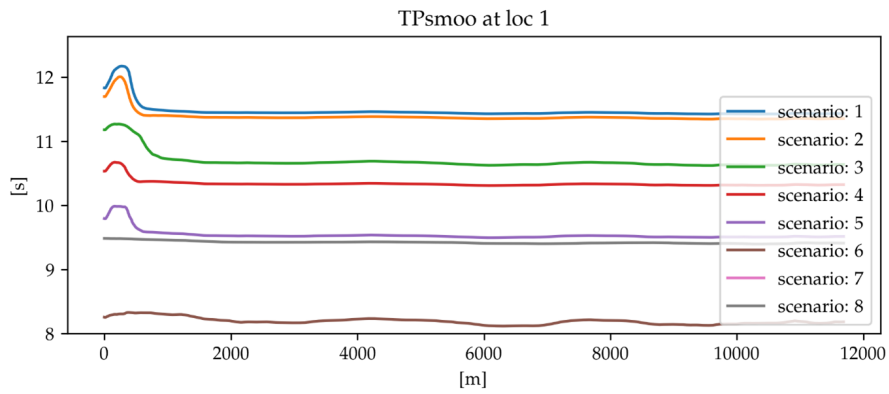
Figure 47: Shore normal bathymetry cross section and slope at location 3

E.4 SWAN output: Shore normal cross sections

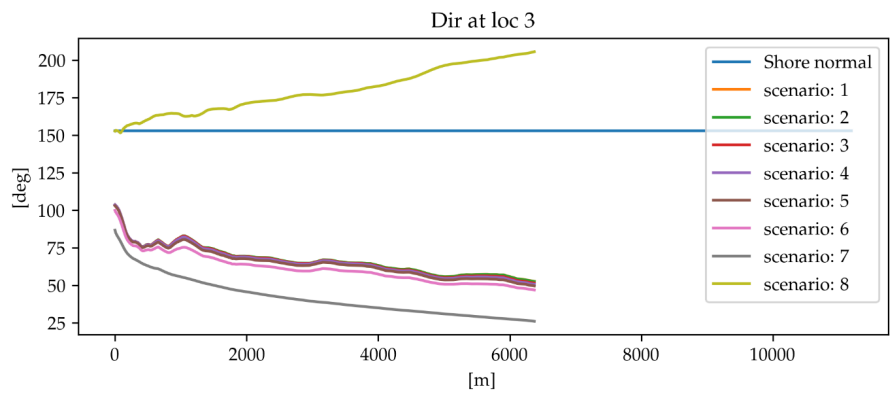
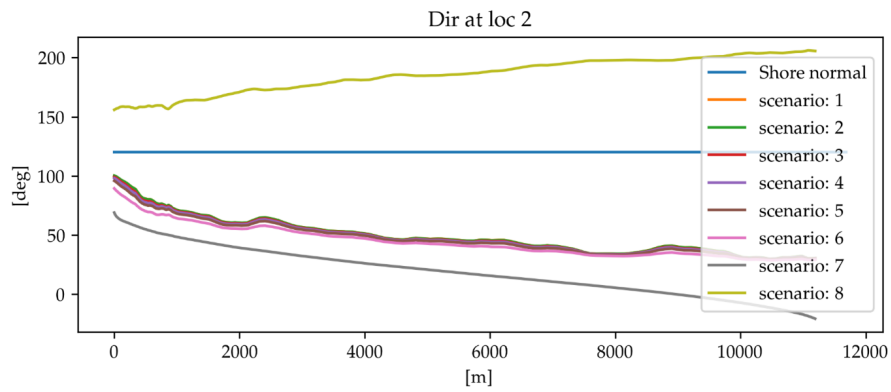
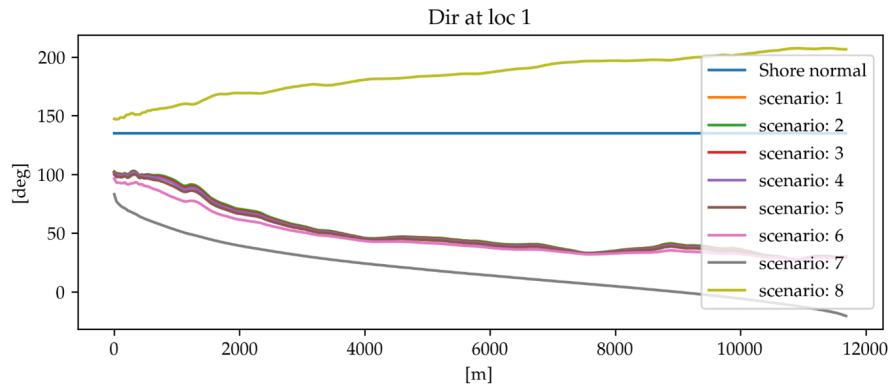
Significant wave height



Peak period

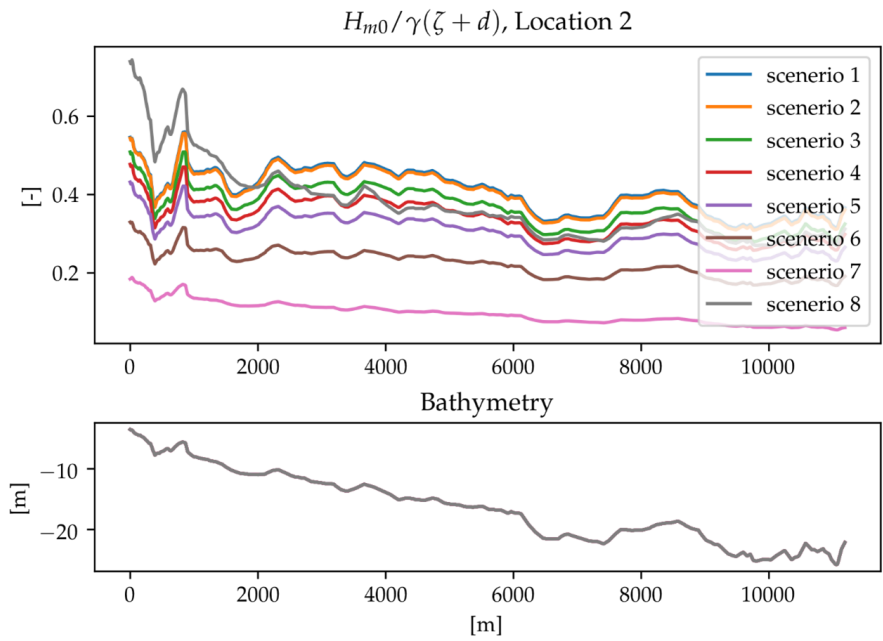
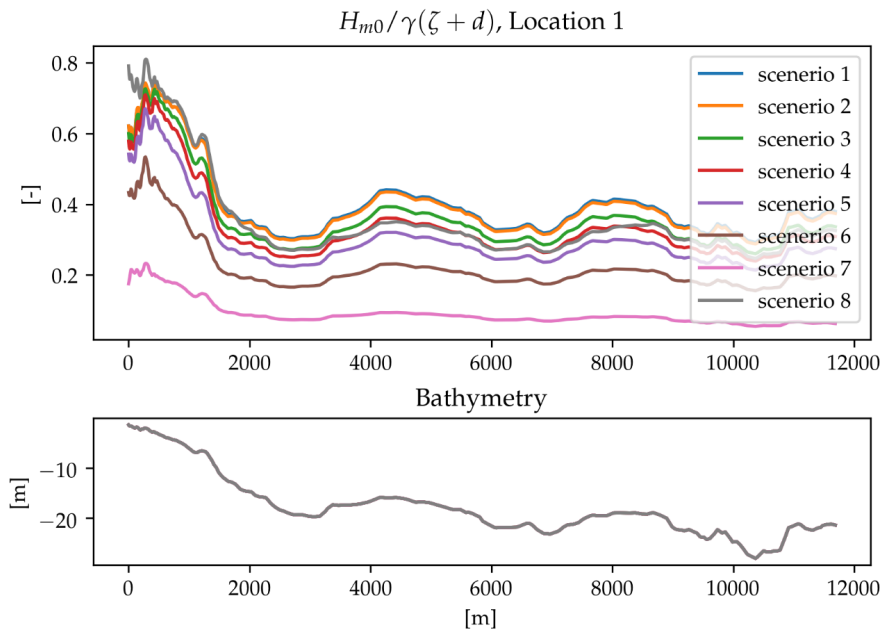


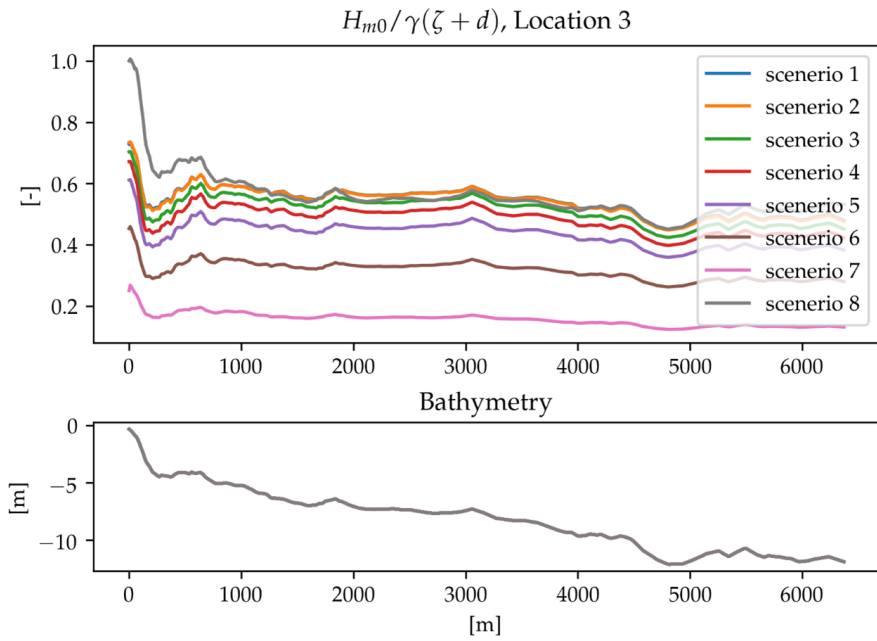
Mean wave direction



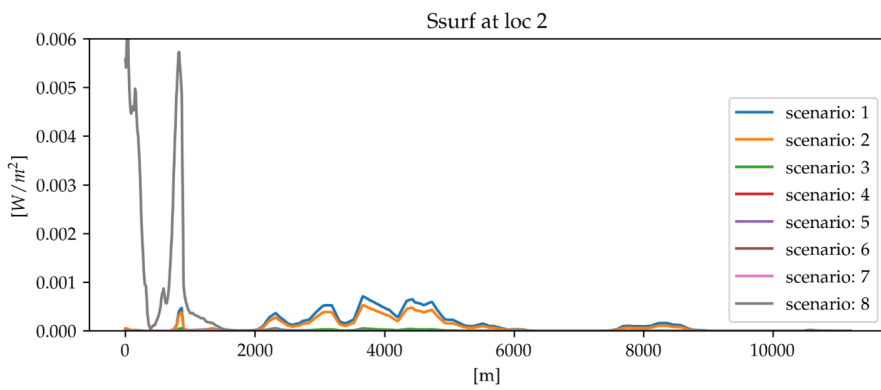
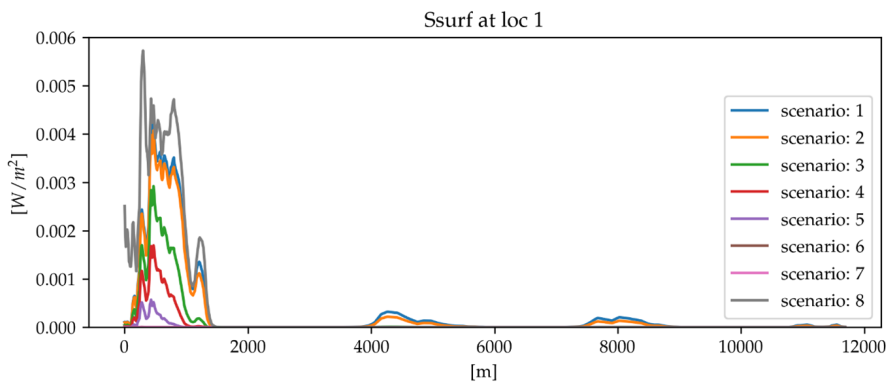
Breaking parameter

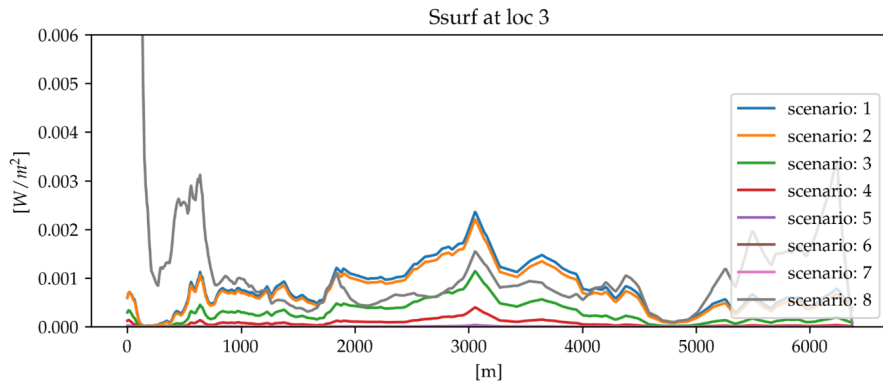
Breaking parameter via [Battjes & Stive \(1985\)](#) as described by [Holthuijsen \(2007\)](#).





Surfbreaking dissipation as calculated by SWAN





E.5 SWAN output: SWASH wave spectrum input

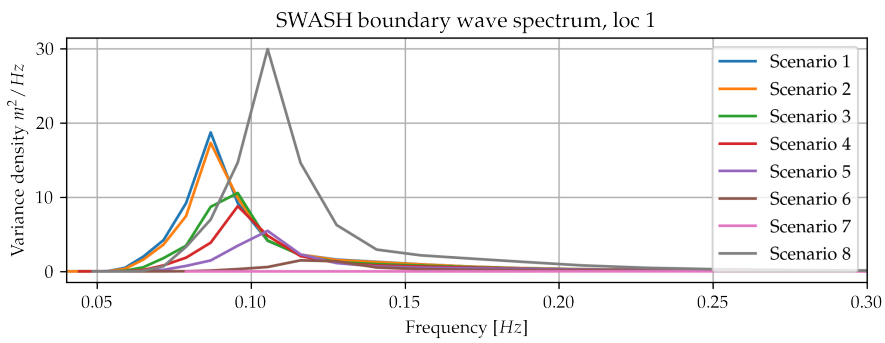


Figure 48: SWASH wave spectrum input, location 1

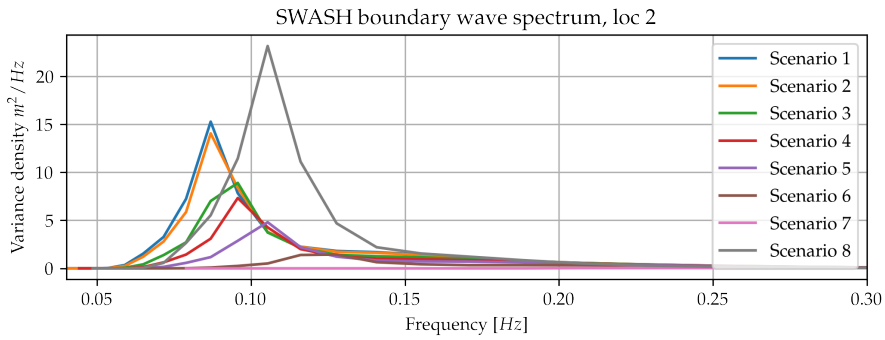


Figure 49: SWASH wave spectrum input, location 2

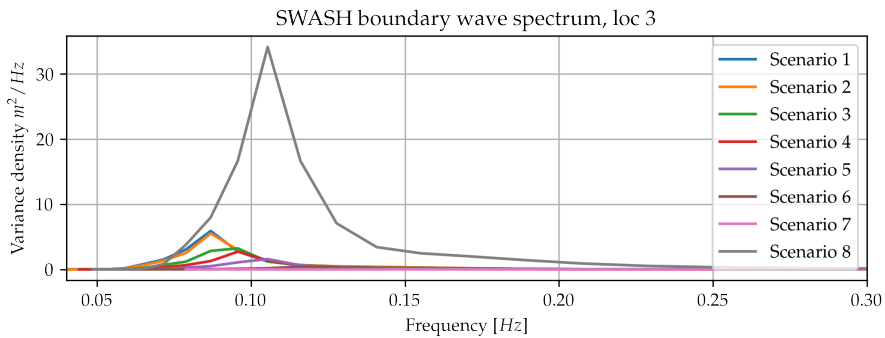


Figure 50: SWASH wave spectrum input, location 3

E.6 Maps of Eastbourne

Elevation of Eastbourne

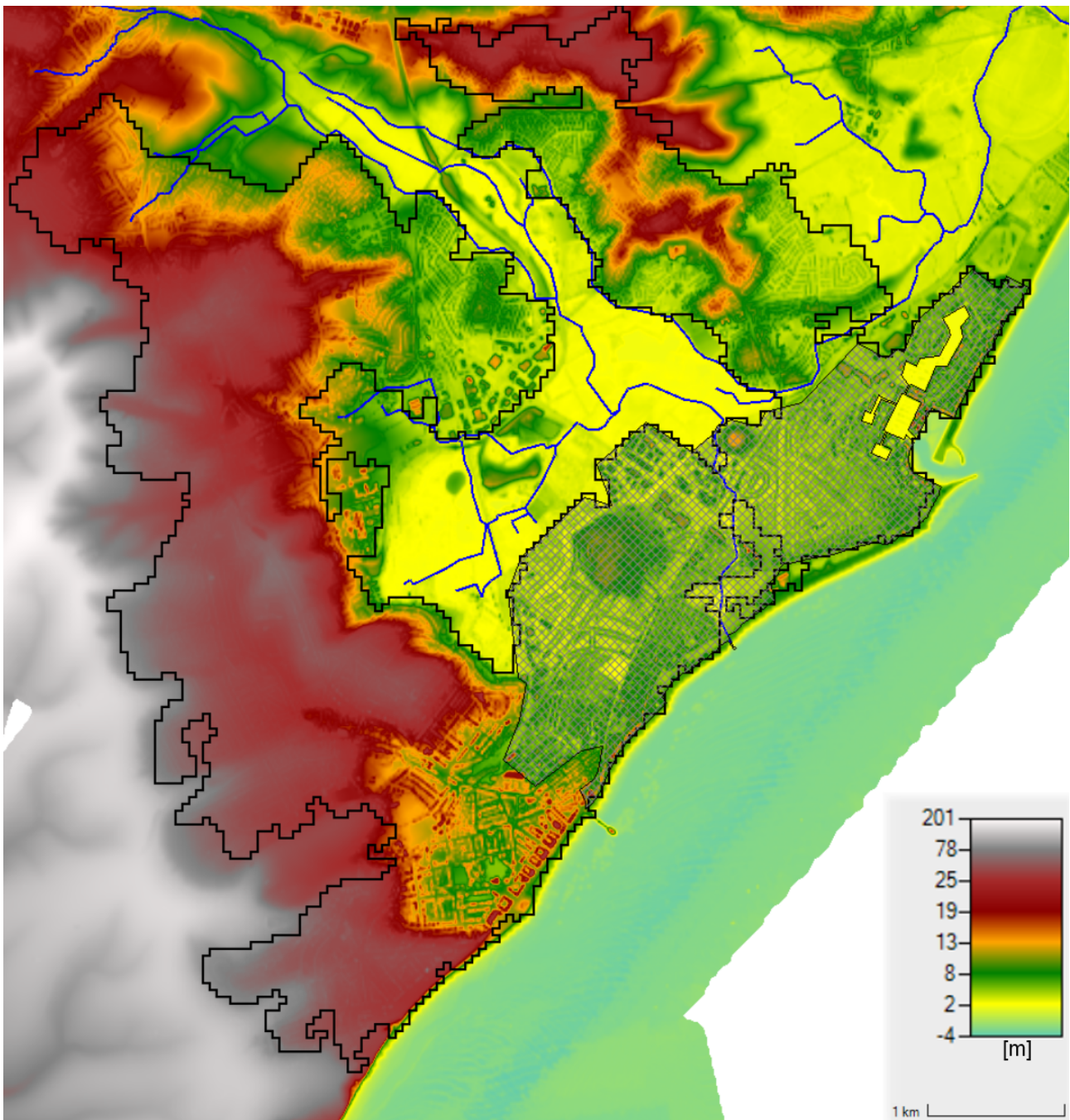


Figure 51: Elevation map of Eastbound showing the inundation domain (hashed part)

Land Cover of Eastbourne

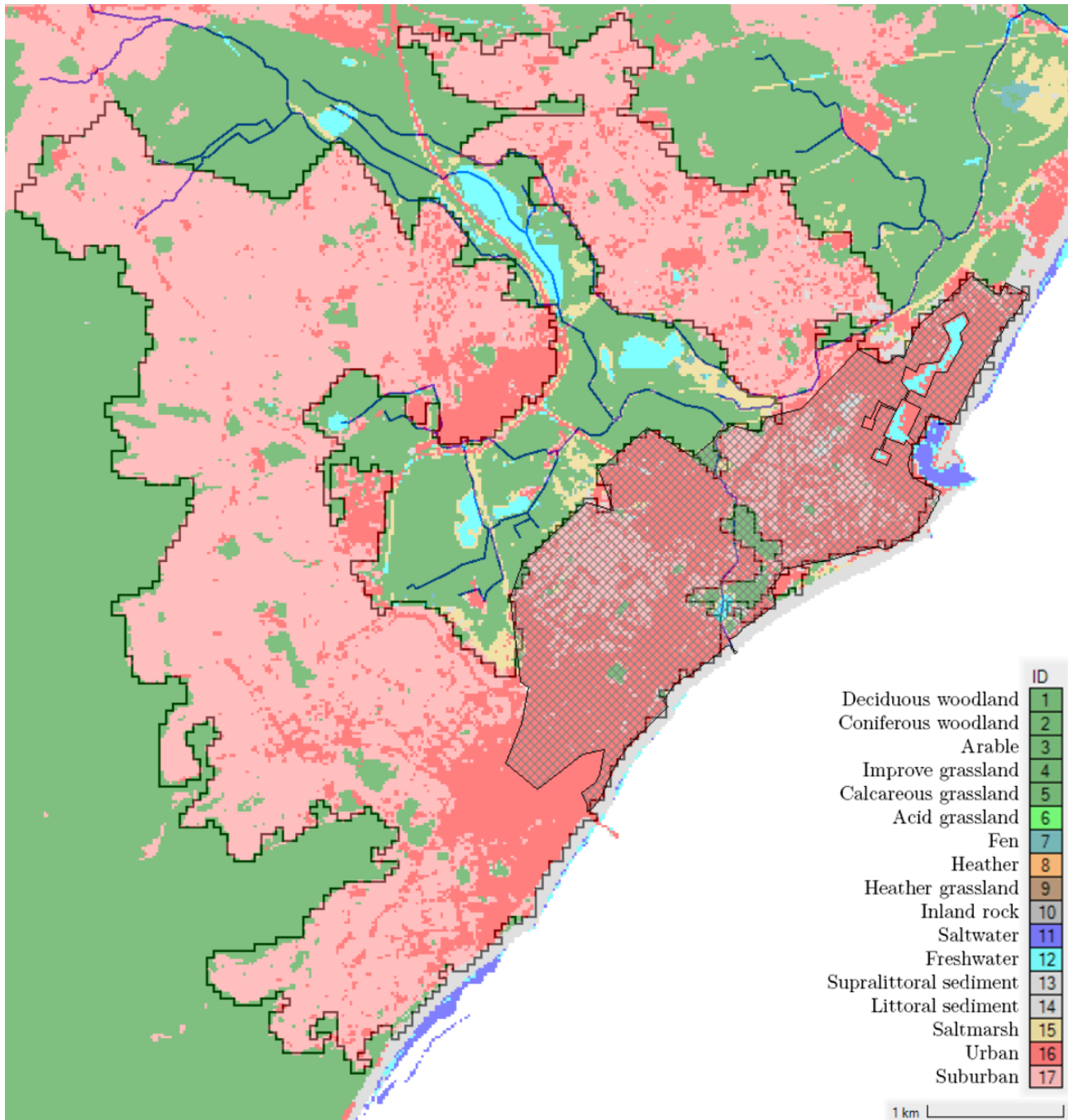
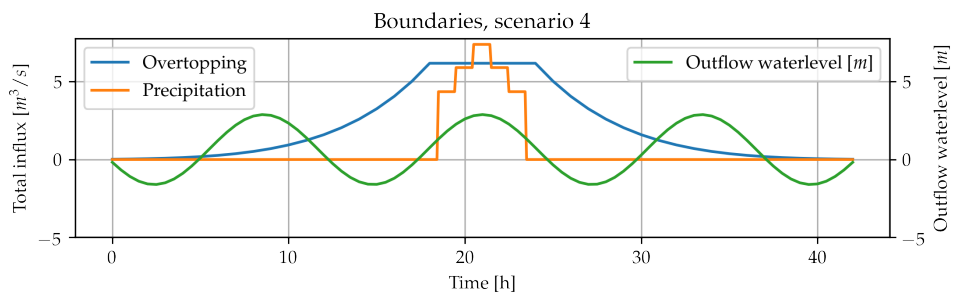
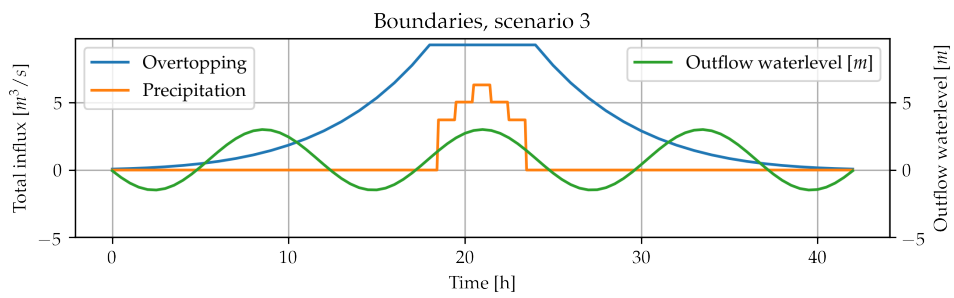
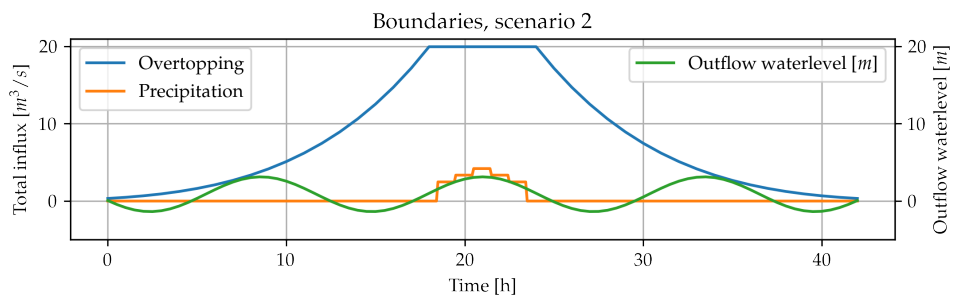
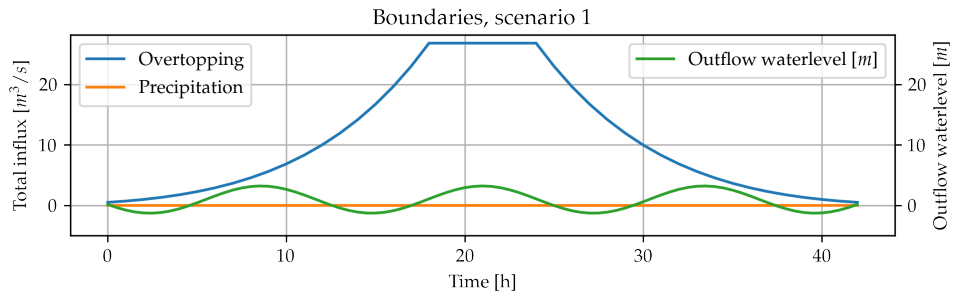
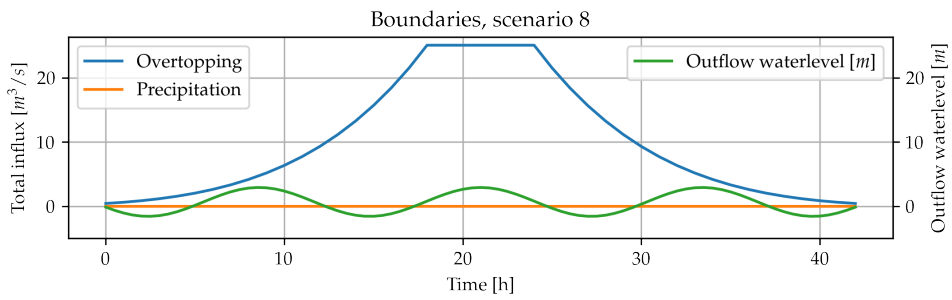
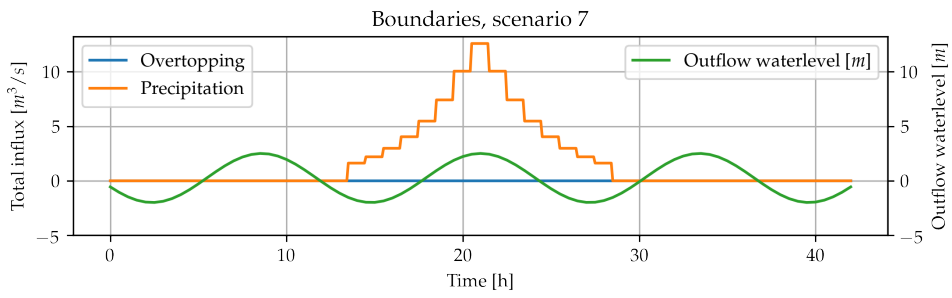
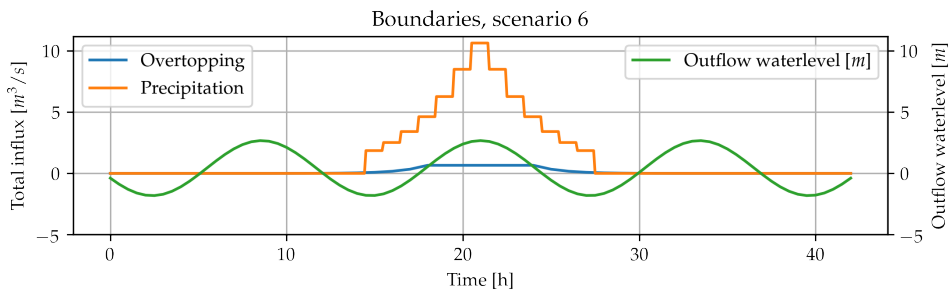
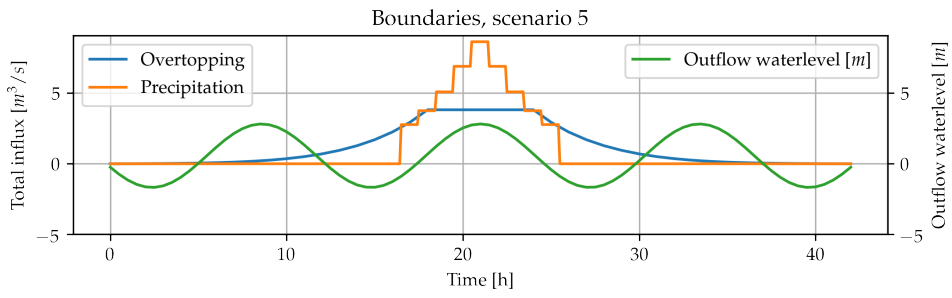


Figure 52: Land cover map of Eastbound showing the inundation domain (hashed part)

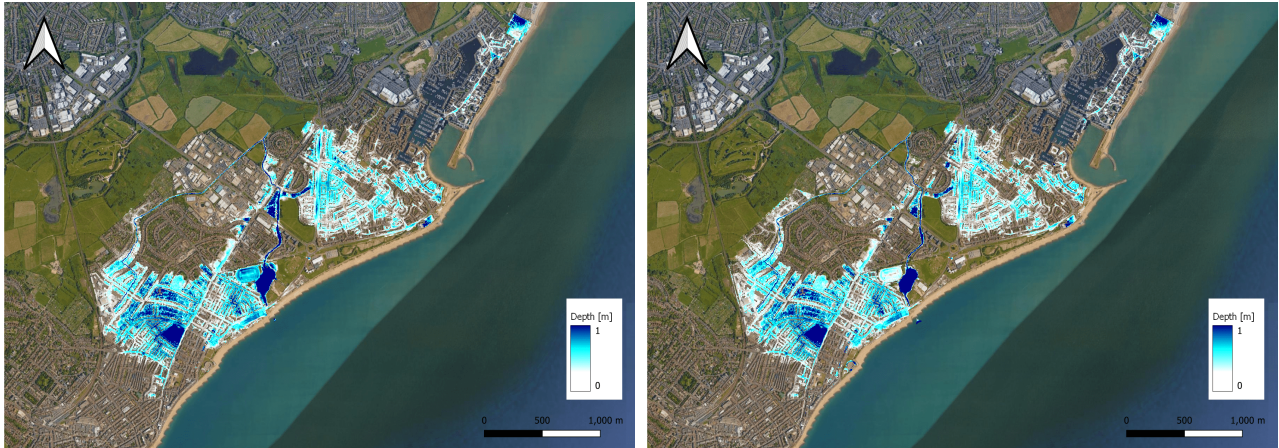
E.7 Boundary summary plots

The following plots give a summary view of the time varying boundary conditions per scenario.





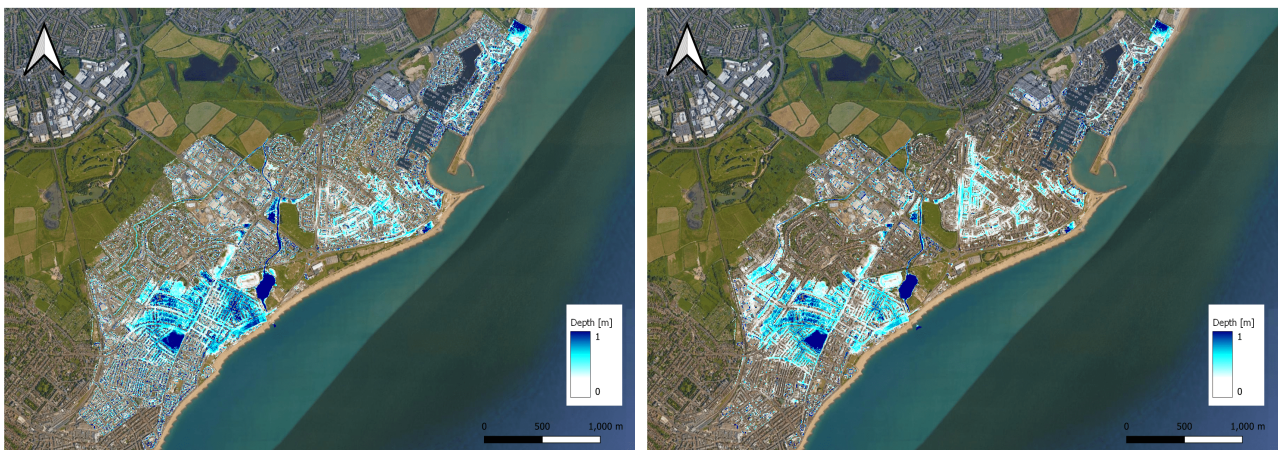
E.8 Inundation maps of Eastbourne



(a) Scenario 1 using DSW

(b) Scenario 1 using SWE

Figure 53: SWE & DSW inundation comparison, scenario 1



(a) Scenario 2 using DSW

(b) Scenario 2 using SWE

Figure 54: SWE & DSW inundation comparison, scenario 2



(a) Scenario 3 using DSW

(b) Scenario 3 using SWE

Figure 55: SWE & DSW inundation comparison, scenario 3



(a) Scenario 4 using DSW



(b) Scenario 4 using SWE

Figure 56: SWE & DSW inundation comparison, scenario 4



(a) Scenario 5 using DSW



(b) Scenario 5 using SWE

Figure 57: SWE & DSW inundation comparison, scenario 5



(a) Scenario 6 using DSW



(b) Scenario 6 using SWE

Figure 58: SWE & DSW inundation comparison, scenario 6



(a) Scenario 7 using DSW



(b) Scenario 7 using SWE

Figure 59: SWE & DSW inundation comparison, scenario 7



(a) Scenario 8 using DSW



(b) Scenario 8 using SWE

Figure 60: SWE & DSW inundation comparison, scenario 8